Studies of Molecular Beam Epitaxial Growth of III-V Semiconductor on Nonplanar Substrates

(段差基板上での III-V 族半導体の分子線
エピタキシャル成長に関する研究)

A Thesis Presented to
the Graduate School of the University of Tokyo
in Partial Fulfillment of the Requirements for
the Degree of Doctor of Engineering

by

Xu-Qiang SHEN

Dissertation Supervisor

Professor Tatau NISHINAGA

Abstract

This thesis concerns the molecular beam epitaxial (MBE) growth of III-V semiconductor on nonplanar (NP) substrates. The contents are divided mainly into two parts. Part one is the study of the growth mechanism on such substrates. Part two relates to the fabrication and the characterization of quantum-wire (QWR) structures at the bottom of V-grooves, which is based on the results of part one.

Efforts were made in order to understand the growth mechanism of III-V semiconductor, especially the surface diffusion phenomena on NP substrates during the MBE growth. At the bottom of the V-groove, the resharpening effect of AlAs was firstly pointed out, which gives the lightening future to MBE for fabricating QWR structures. On the other hand, the surface diffusion phenomena were investigated in detail using microprobe RHEED/SEM MBE system. It was found that the diffusion length of incorporation of Ga (In) depends strongly on the arsenic pressure and the growth temperature, while it is almost independent of Ga (In) flux itself. These experimental results give deep insight into the understanding of growth mechanism on atomic level, such as the adatom stoichiometry entering the step edges and so on. Based on the one-dimensional surface diffusion equation, a growth model, which can explain the experimental phenomena very well, was proposed. With the model and the experimental data, the ratio of the diffusion coefficients on (111)B and (001) surfaces was obtained to be 140 for the first time, although the absolute value of the diffusion coefficient can not be measured in the experiments.

Fabrications of multiple and single GaAs/AlAs QWR structures at the bottom of V-grooves were carried out by MBE, using the surface diffusion results described above. Very narrow crescent-shaped QWR structures were successfully formed at the bottom of V-grooves by cross sectional observations of high-resolution scanning electron microscopy (RHSEM) and transmission electron microscopy (TEM). Cathodoluminescence (CL) and photoluminescence (PL) were also performed to characterize the QWR structures and very good luminescence properties of the QWR were obtained. The narrowest QWR until now in MBE growth was obtained, which had the size of 42 Å x 70 Å. This fabricating technique gives a new field to MBE to the applications for the future low-dimensional quantum devices.

Acknowledgments

This thesis is based on the work carried out under the supervision of Prof. Tatau Nishinaga, at the Department of Electronic Engineering, Faculty of Engineering, the University of Tokyo, between April 1990 to march 1995. Most of the work in this thesis was done during my doctor course from April 1992 to march 1995, although some parts (sections 2.3 and 5.3.2) are included, which were done at the end of my master course study, in order to fulfill this thesis.

At first, I should express my deep gratitude to my dissertation supervisor, Prof. Tatau Nishinaga for his guidance and moral support during my study in his laboratory. It is impossible to finish this thesis without his continuous encouragement and enlightening comments. I learned from him not only the way of researching, but also the attitude of mind to work and life. I believe these will affect me greatly in my future life. Furthermore, I would like to thank him and his wife for taking care of my family during these years.

I am indebted to Prof. Nai-Beng Ming, Nanjing University, P.R.China, who helped and recommended me to study at the University of Tokyo, which has excellent equipments and a free academic atmosphere.

I would like to thank Dr. Masaaki Tanaka, associate professor in this laboratory, for his interesting discussions and help throughout this work. It was him who introduced me to this modern and competitive research field.

I also wish to pay my respect to Ms. Masako Washiyama for her constant support and help during these years. I have benefited a great deal from a number of my colleagues at this laboratory. Special thanks are to Dr. Takashi Suzuki, Dr. Wu-yih Uen, Messrs. Eiji Morifuji and Daisuke Kishimoto for their useful discussions and help in carrying out this work.

I would like to thank Prof. K.Onabe and Mr. Wu-Gen Pan, Department of Applied Physics, the University of Tokyo, for their helps to prepare fine V-grooved substrates. I also

like to pay my gratitude to Prof. H.Sakaki and Mr. T.Noda of Institute of Industrial Science of the University of Tokyo for their helps and advises to conduct low-temperature photoluminescence (PL) measurements of quantum-wire (QWR) structures.

Thanks are also paid to Dr. K.Wada of LSI laboratories, Nippon Telegraph and Telephone Corporation for the low-temperature cathodoluminescence (CL) measurements of QWR structures. I am grateful to Ms. Mine Nakagawa of Hitachi Instrument Engineering, Messrs. Etsuo Sei and Mitsuru Nomura of Nissei Sangyo for their helps in the cross sectional high-resolution scanning electron microscope (HRSEM) observations.

I also like to thank Dr. Kyoung-Ik Cho and Dr. Sahn Nahm, semiconductor Technology Division, Electronics and Telecommunications Research and Technology, Korea, for their helps and advises in the transmission electron microscopy (TEM) observations of QWR structures.

It is my great pleasure to make acquaintance of some guest researchers in the laboratory during these years. Among them, I would like to thank Mr. Hong-Jun Chen and Dr. Hong-Wen Ren for their useful discussions and helps in the fabrication and characterization of QWR structures.

I have to express sincere gratitude to my relatives and friends of Chinese, Japanese and other countries for their lasting friendships, who gave me and my family great help and pleasures during these years, although it is impossible to list their names here.

I would like to thank the government of P.R.of China for providing me the opportunity to study abroad. I also wish to thank the Ministry of Education, Science and Culture, Japan, for financial support during my study in the University of Tokyo.

Finally, I owe considerable debts to my parents who fostered and encouraged me throughout these years. My deepest thank is to my dear wife, Jin-Ping He, for her continuing supports and encouragement. My pretty son also gave me a lot of pleasure during the period of fulfilling the thesis.

Abbreviations

MBE	Molecular Beam Epitaxy
MOCVD (OMCVD)	Metalorganic Chemical Vapor Deposition
MEE	Migration Enhanced Epitaxy
RHEED	Reflection High-Energy Electron Diffraction
SEM	Scanning Electron Microscopy
RHSEM	High-Resolution Scanning Electron Microscopy
TEM	Transmission Electron Microscopy
μ-RHEED/SEM MBE	Microprobe RHEED/SEM MBE
SREM	Scanning Reflection Electron Microscopy
STM	Scanning Tunneling Microscopy
AFM	Atomic Force Microscopy
CL	Cathodoluminescence
PL	Photoluminescence
0D	Zero-Dimensional
1D	One-Dimensional
2D	Two-Dimensional
QW	Quantum Well
QWR	Quantum-Wire
QD	Quantum Dot
SL	Superlattice
HEMT	High-Electron Mobility Transistor
RAD	Resonant Tunneling Diode
$\lambda_{inc.}$	Surface Diffusion Length of Incorporation
$\tau_{inc.}$	Lifetime of Atoms of Incorporation
D	Surface Diffusion Coefficient
NP	Nonplanar Substrate
UHV	Ultrahigh Vacuum
K-Cell	Knudsen Cell
PBN	Pyrolitic Boron Nitride
LN2	Liquid Nitrogen

TABLE of CONTENTS

Chapter 1 Introduction

Modern optoelectronic materials and microwave devices require new types of semiconductor materials and structures. Especially, high-speed and high-efficiency quantum effect structures with low-dimensions are attracting a great deal of interests for the future applications. In order to obtain high quality thin crystal films and layered structures, molecular beam epitaxy (MBE) is regarded at present as one of the most competitive growth methods, together with other kinds of growth techniques such as metalorganic chemical vapor deposition (MOCVD) etc.

MBE is an epitaxial growth process, which let thermal atoms or molecules grow on a clean crystalline surface under ultra-high vacuum (UHV) conditions. Therefore, MBE itself has several important advantages for getting high-quality thin film comparing with other growth methods. Since the growth is carried out under UHV conditions, substrate surfaces can be kept clean and the impurity level is quite low in the growth chamber, which is very important for the device fabrications. On the other hand, UHV makes it possible to equip an electron gun or other kinds of characterization units in the chamber for getting information from the surface during the growth, such as reflection high-energy electron diffraction (RHEED). Furthermore, the growth rate can be controlled accurately and the flux of sources can be easily shut on and off. Therefore, the designed structures can be precisely obtained by MBE.

The present thesis concerns the growth of III-V semiconductor on nonplanar (NP) substrates by MBE. The contents are divided mainly into two parts. Part one is the study of the growth mechanism on such NP substrates. Part two relates to the fabrication and the characterization of quantum-wire (QWR) structures at the bottom of V-grooves, which is based on the results of part one. In the experiments, the conventional MBE and microprobe RHEED/SEM MBE (μ-RHEED/SEM MBE) systems were employed for the study of the growth mechanism and the fabrications of QWR structures. The details will be described in each chapter.

§1.1 Historical Background

Since the MBE technique was introduced, it has been used as one of the most powerful tools for the thin film growth together with MOCVD etc. Pioneering works on the epitaxial growth of GaAs at the early development of MBE were mainly contributed by Cho(1969), Arthur (1968), Foxon (1974) an Harris (1981), which concerned the epitaxial growth conditions, surface chemical processes and reflection high-energy electron diffraction (RHEED) oscillation. The excellent uniformity and control of thickness, composition and doping on a monatomic-layer level allow growth of multi-layer structures of various material parameters, including the energy gap, built-in electric and magnetic fields and refractive index. The 1D quantum confinement, superlattice (SL) formation and tunneling phenomena, which give deep insight information to physics, were realized by the growth technique. Also, a number of new device concepts, such as the high-electron mobility transistor (HEMT), the quantum well (QW) semiconductor laser and the resonant tunneling diode (RTD), were made.

As a natural extension of the 1D modulated structures, the present new challenges for fabricating 2D and 3D quantum confinement structures have been carried out by a various of methods. Of particular interest are quantum-wire (QWR) and quantum-dot (QD) heterostructures, in which the quasi-1D or 0D nature of carriers leads to enhancement of various of material properties such as carrier mobility (Sakaki,1980) and optical absorption and gain (Arakawa et al.,1986). These properties meet the development of electric and optoelectronic circuits which requires high packing density and reduced power dissipation. Using NP substrates and growing on them are regarded now as one of the most hopeful and powerful ways to fabricate the 1D and 0D structures, which can be defect and contamination free. Therefore, this field has attracted a great deal of interest and many modern growth techniques such as MBE and MOCVD have been applied to fabricate the structures, together with the study of the growth mechanism.

Since the NP substrates , which are formed mainly by lithography and etching techniques, are quite different from the conventional plane substrates, the growth behaviors should be much complicated on such substrates. In MBE growth, the surface diffusion phenomenon is the most important process. The surface diffusion length of Ga on the GaAs (001) surface was first investigated to be shorter than 20 nm (Nagata et al., 1977) under the As rich condition, which is consistent with the results by the disappearance of RHEED oscillations

(Neave et al., 1985) by use of vicinal GaAs substrates. On the other hand, surface diffusion length for several group III adatoms have been measured for MBE growth on NP substrates. Surprisingly, the results showed that the diffusion length is in micrometer order, which is nearly 100 times longer than that using plane substrates (Smith et al.1985; Kapon et al.1988; Meier et al.1989; Guha et al.1990; Arent et al.1990; Nilsson et al.1989; Hata et al.1990; Isu et al.1991). This gives a new research topic which should be studied carefully in an atomic scale. There are a lot of another interesting phenomena on NP substrates, such as quasi-periodic composition modulation of Al on (111)A sidewalls (Hoenk et al.1989), facet formations during the growth (Smith et al.1985; Kapon et al.1987; Takebe et al.1993) and p-n doping properties on different surfaces (Fujii et al.1991). Also, theoretical studies were carried out, which simulated the growth behaviors on NP substrates by computers (Ohtsuka et al.1988; Ratsch et al.1991; Haider et al.1993). But, no clear answers have been obtained until now, which concerns the difference of the surface diffusion length between conventional plane substrates and NP substrates as mentioned above. This problem may relate to the growth kinetics at the step edges (Nishinaga et al.1991) and the chemical reaction processes on surfaces (Foxon et al.1974,1975), which should be studied systematically.

Another important purpose, where a great deal of interest has been attracted, is to fabricate low-dimensional semiconductor quantum structures such as QWR and QD on NP substrates for the future devices. Many efforts have been made by use of various kinds of growth techniques. The material system was also widely chosen for different purposes, such as GaAs/AlGaAs (Kapon et al.1989,1992), InGaAs/AlGaAs (Arakawa et al.1993), InP/InGaAsP (Bhat et al.1990; Komori et al.1992), SiGe/Si (Usami et al.1994), and AlGaAs/GaAs on Si substrates (Hasegawa et al.1993). Nowadays, MOCVD is mainly used for the QWR fabrications (Kapon et al.1989; Ismail et al.1991; Tuskamoto et al.1992,1993; Colas et al.1990; Lee et al.1993; Karam et al.1991; Bertram et al.1994), because the self-ordering effect of AlGaAs gives the great advantage for such fabrications. The narrowest width of QWR until now was nearly or less than 10 nm by MOCVD (Tsukamoto et al.1993) and the QWR semiconductor laser fabrication was succeeded with a threshold current of 4.3 mA (Kapon et al.1989). The properties of the fabricated QWR structures were also studied both in experimental and theoretical ways in order to understand the physics in the QWR (McInlyre et al.1992; Nagamune et al.1992; Christen et al.1992; Walther et al.1992).

MBE, on the other hand, is also applied to the fabrications of QWR structures. Most of the work were held on the ridge patterned substrates. Therefore, ridge QWR (Eberl et al.1993; Koshiba et al.1994; Lopez et al.1993; Saito et al.1993) and edge QWR (Nakamura et al.1991) structures were fabricated by MBE, which were characterized by SEM, TEM, PL, CL. But, the V-grooved NP substrates, which were mainly used in MOCVD, were fairly used for the QWR fabrications in MBE. This may be because it is difficult to control the surface diffusion during the MBE growth and no self-ordering effect of AlGaAs occurs in MBE. As a result, QWR structures only with wide width at the bottom of V-grooves has been obtained (Kojima et al.1990; Turco et al.1990). This kind of difficulties in the MBE growth demands the hurry understanding of the growth mechanism, especially the surface diffusion on NP substrates in MBE which can give the guidance to the QWR fabrications. Since MBE has many advantages over other growth techniques, the nearly ideal 1D and 0D structures with excellent properties are under expectation.

§1.2 Motivations of the Present Work

As mentioned in §1.1, understanding of the growth mechanism on NP substrates in MBE is very important both for the basic study of crystal growth and the actual applications to the QWR fabrications. Especially, the growth on the NP substrates provides many new and interesting phenomena which can not be obtained on the usual plane substrates. It is well known that surface diffusion is one of the most important processes in MBE. NP substrates give a chance to study such phenomena in much more complicated conditions, because inter-surface diffusion phenomenon occurs between the adjacent surfaces. The intrinsic growth behaviors on NP substrates, such as surface supersaturation of atoms and the adatom stoichiometry entering the steps, are quite different from the case using the conventional plane substrates. Unfortunately, the growth mechanism on NP substrates has not been fully understood yet on an atomic level, although many interesting phenomena have been found by researchers.

On the other hand, fabrications of low-dimensional structures such as QWR and QD are attracting many scientists, because this field has potential physical interests and future applications. However MBE, as one of the most powerful growth techniques in many fields, is

not widely used at present for the QWR fabrications on V-grooved NP substrates because of the difficulty in controlling the surface diffusion of atoms on NP substrates.

According to such kinds of situation, it is necessary to make the growth mechanism on NP substrates clear first. Then, by controlling the surface diffusion on the NP substrates, fabrications of QWR structures with small size and good properties should be challenged by MBE. The above two points are the motivations of the present study.

Chapter 2 MBE Growth and SEM Characterizations of III-V Semiconductor on V-grooved GaAs Substrates

§2.1 Introduction

Epitaxial growth on patterned substrates has generated a great deal of interest over the past few years primarily motivated by the fabrication of laser structures and other functional optical devices (Arakawa et al.1986; Kapon et al.1987). Much effort in this field has recently been devoted to understanding the MBE growth mechanism of III-V semiconductors on such patterned substrates, since the understanding and the control of the growth are essential for the applications to the fabrication of low dimensional microstructures and devices without any process damages (Meier et al.1989; Takebe et al.1993; Hoenk et al.1989; Turco et al.1990; Nilsson et al.1989; Hata et al.1990; Isu et al.1992). For instance, Hoenk et al. reported the orientation dependence of Al concentration in AlGaAs epitaxial layers grown by MBE on NP substrates and suggested a possibility of growing lateral heterostructures. Nilsson et al. and Hata et al. observed that the increase in the growth rates of GaAs on the (001) surface near the edge of the (311)A or (111)A sidewall followed as an exponential function of the distance from the edge, which is ascribed to the lateral flux of Ga atoms migrating from the sidewalls to the (001) surface. From the experimental observations, they deduced that the migration length of Ga on the (001) GaAs surfaces is in micrometer order. Turco et al. studied the migration effects on the growth of (Ga,Al)As on submicron-period patterned substrates and pointed out that significant surface migration of Ga during the growth of GaAs leads to a fast filling in of the V-groove by creating a new (001) surface. However, the growth of AlAs and AlGaAs are similar, which better preserves the shape of the grating.

In this chapter, detailed and systematic study done on the growth of (Al,Ga)As and (In,Ga)As on V-grooved substrates by MBE is described by investigating the morphology and surface diffusions of Ga, Al and In atoms on such patterned substrates. The cross-sectional observations of the (Al,Ga)As and (In,Ga)As layered structures by scanning electron microscopy (SEM) show very different growth behaviors for each material near the edge of the

(001) surface and at the bottom of V-groove. The growth mechanisms on V-grooved NP substrates are also discussed according to the experimental results.

§2.2 Experimental Methods

2.2.1 MBE Equipment

The MBE system used in the experiments was made by ULVAC company and named MBC-508, which consists of preparation chamber and growth chamber. Fig.2.1 shows the schematic figure of the equipment. The system is prepumped around 10^{-8} Toor by rotary and turbomolecular pumps. A combination of ion pump and titanium gettering pump with cryopanel is used to achieve UHV pressure in the growth chamber. The vacuum level of background usually is lower than 10^{-10} Torr and several Knudsen cells for various sources (Ga, Al, In, As, Mn, Si, and Be) are equipped. Reflection high-energy electron diffraction (RHEED) is installed in the growth chamber to monitor and control the growth.

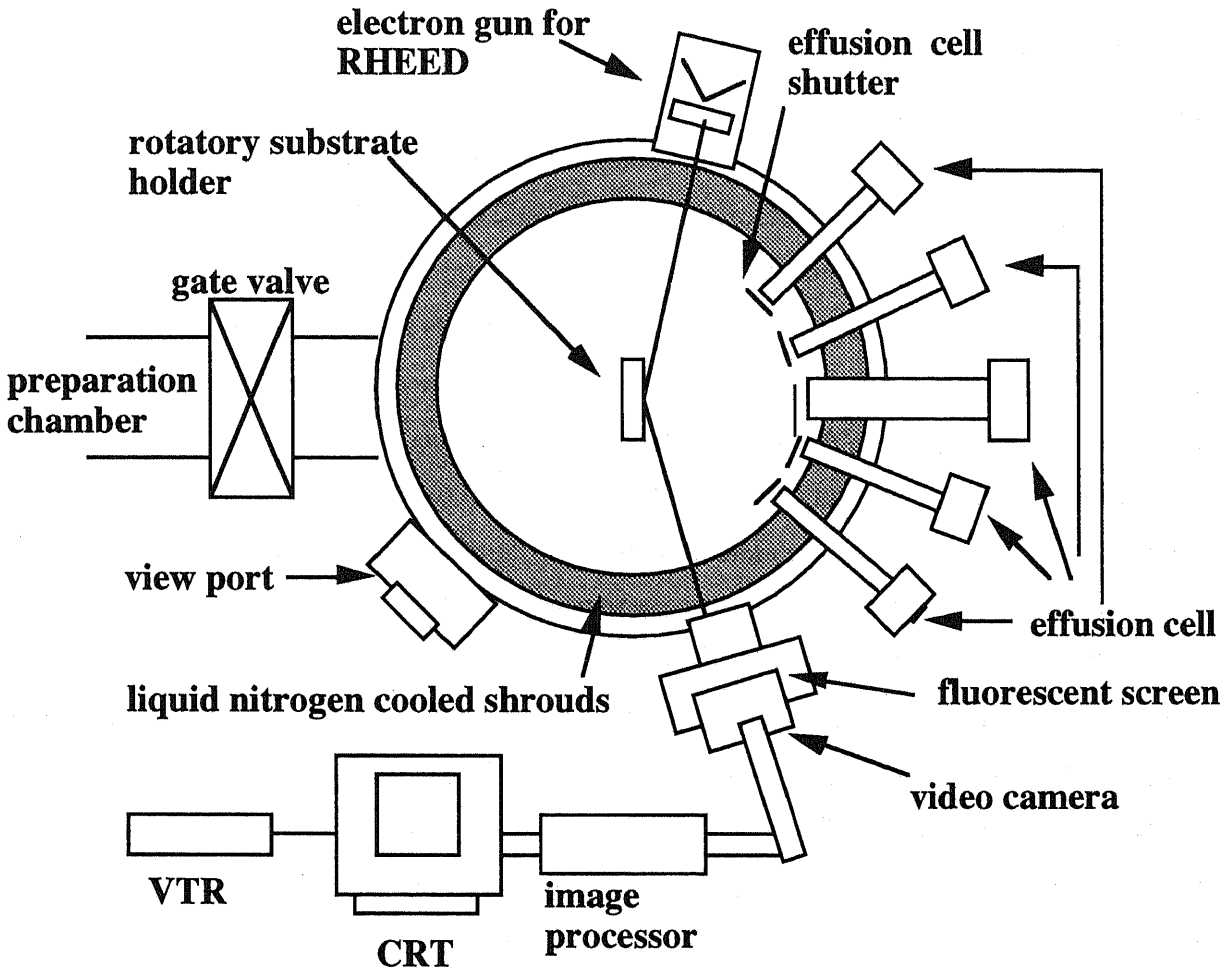

Figure 2.1. Schematic illustration of the equipment of MBC-508

2.2.2 Preparations of V-grooved Substrates and MBE Growth

Samples were prepared firstly by making V-grooves on (001) semi-insulating GaAs substrates using conventional photolithography and wet chemical etching methods in $NH_4OH:H_2O_2:H_2O$ (1:1:5 by volume) at 2 °C for about 15 minutes. The grooves, nearly 14 μm wide and 9 μm deep, were aligned along the $[\bar{1}10]$ direction and have V-shaped profiles with (111)A sidewalls due to the anisotropic etchings as shown in Fig.2.2. After degreasing treatments, the V-grooved substrates were introduced into the MBE chamber.

GaAs/AlAs and GaAs/$Al_{0.45}Ga_{0.55}As$ heterostructures were grown at 580°C with GaAs, AlAs and AlGaAs growth rates of 0.85, 0.7 and 1.55 μm/hr, respectively. During the growth, the V/III ratio was kept at about 4 and the rotation speed of the substrates was 4 rpm. Schematic illustrations of the sample structures are shown in Fig.2.3(a) (sample A) and Fig.2.3(b) (sample B). On the substrates, 0.5 μm-thick AlAs ($Al_{0.45}Ga_{0.55}As$), 0.3 μm-thick GaAs, 0.3 μm-thick AlAs ($Al_{0.45}Ga_{0.55}As$), and finally a 20 nm-thick GaAs caplayer were successively grown in sample A (sample B). The thickness of each layer is calibrated on the (001) surface. Note here that unlike the usual MBE-grown heterostructures with GaAs buffer layers, sample A and sample B have 0.5 μm-thick AlAs and 0.5 μm-thick AlGaAs, respectively, as the first epitaxial layer on the V grooved substrates. In order to observe the shape of each epitaxial layer by cross sectional SEM, the samples were cleaved and then stain etched in $NH_4OH:H_2O_2$ (1:30 by volume). In §2.3, two different parts of the (Ga,Al)As heterostructures on the V-grooved substrates, which correspond to the edge between the (001) surface and the (111)A sidewall and the bottom of the V-grooves respectively, were observed by SEM.

The temperature dependence of the morphology in GaAs/AlAs heteroepitaxy at the bottom of the V-grooves were also investigated. The growth rate of GaAs and AlAs were chosen same as described above. The growth temperatures were varied from 450-630°C for GaAs/AlAs heterostructures. The details of the growth and sample structures will be described in section 2.3.3.

The growth of (In,Ga)As/AlAs heterostructures were carried out in order to study the surface diffusion of In adatoms. The details will be described in §2.4.

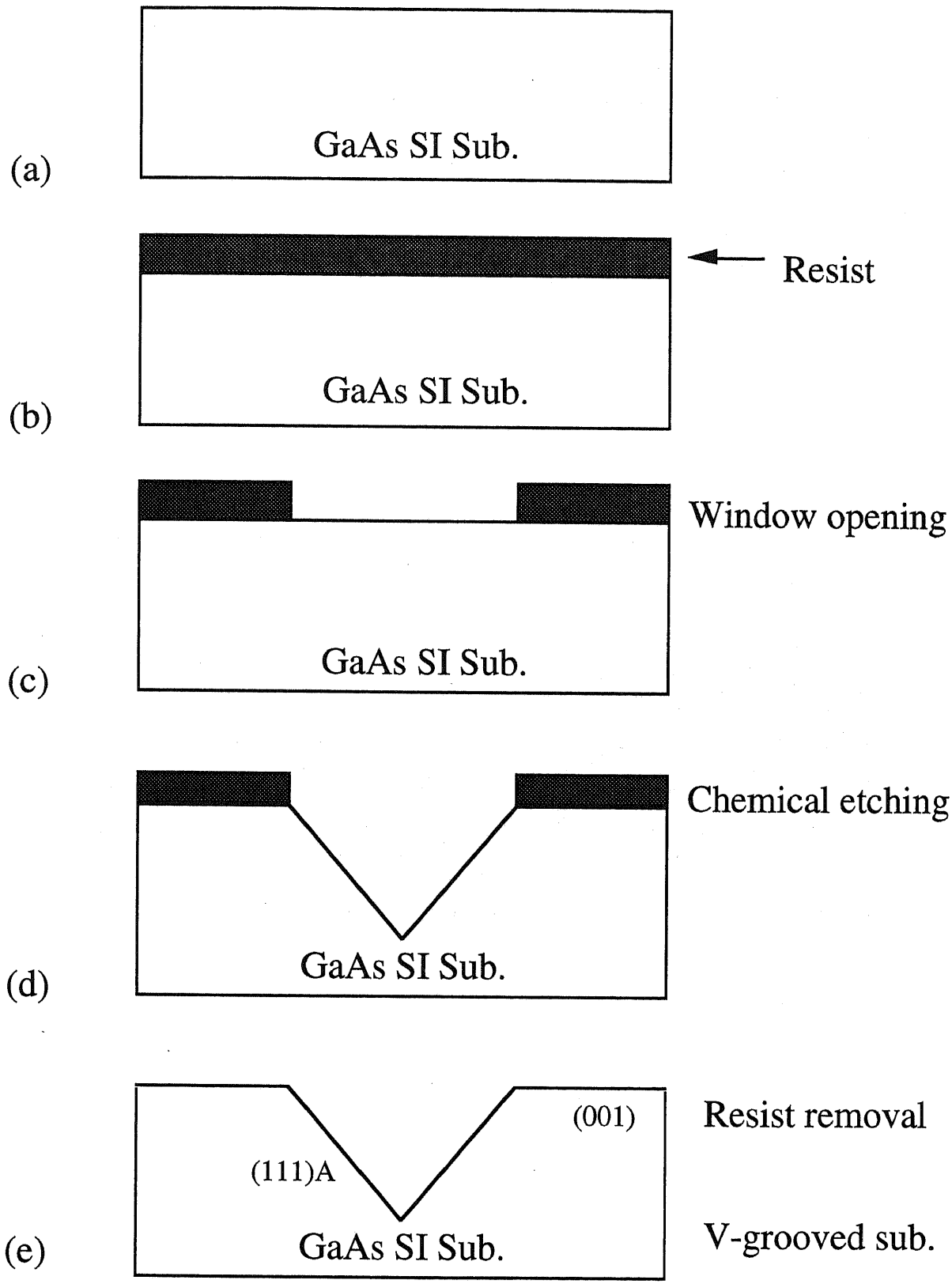

Figure 2.2. Fabrication processes of the V-grooved substrates. (a) (001) SI GaAs substrate, (b) resist deposition, (c) window opening, (d) chemical etching, (e) resist removal

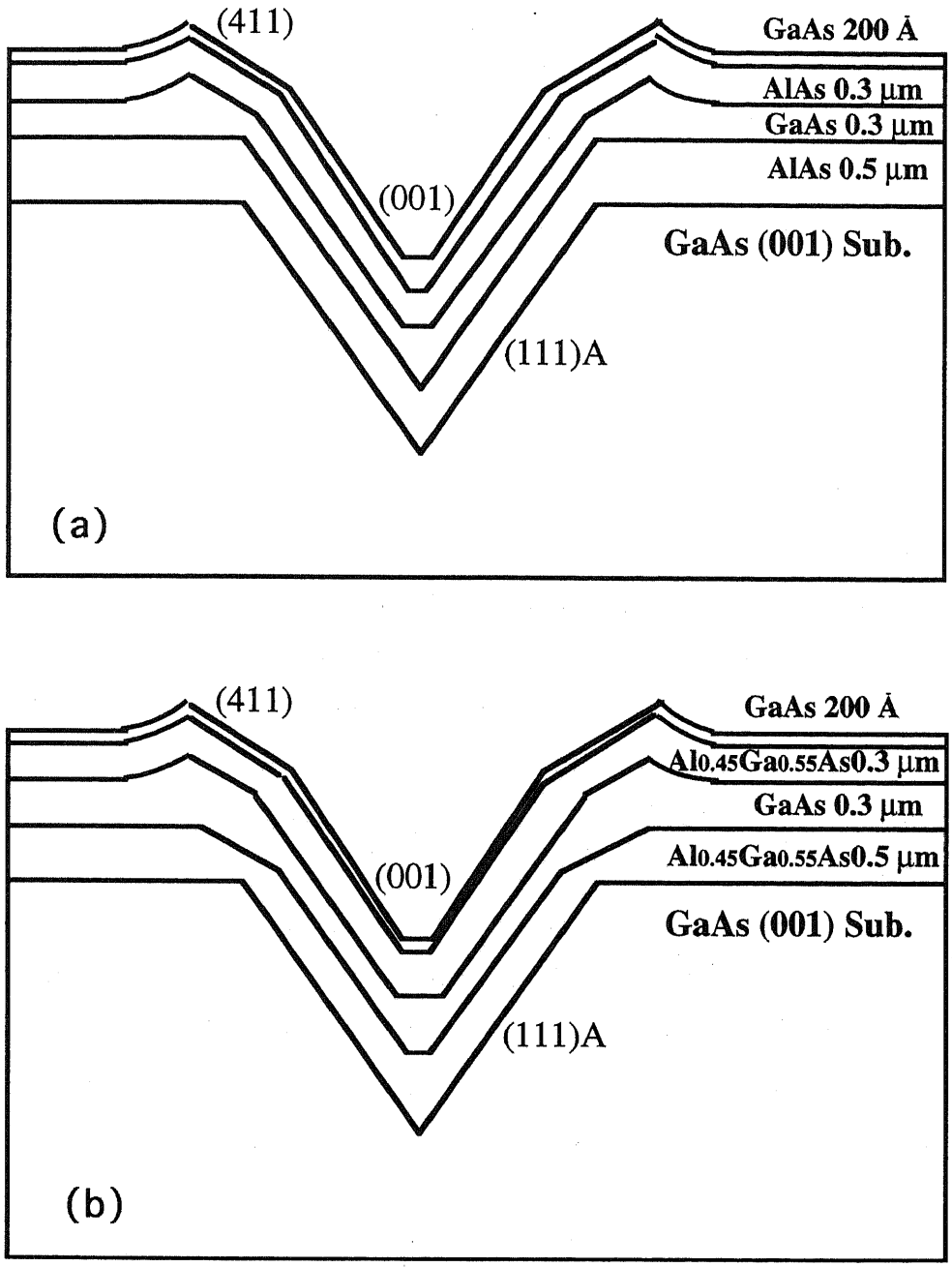

Figure 2.3. Sample structures (a) sample A: AlAs was grown as the first layer on the substrates. (b) sample B: AlGaAs was grown as the first layer on the substrates.

§2.3 Cross Sectional Observations of the (Ga, Al)As Hetero-structures by SEM

Two different parts of MBE-grown layers on the V-grooves in sample A and B are observed by SEM, which correspond to the edge between the (001) surface and the (111)A sidewall and the bottom of the V-grooves, respectively. Material dependent growth behavior is described in these different positions on the V-grooved substrates as follows.

2.3.1 Al Composition Dependence of the Cross-Sectional Growth Morphology

2.3.1.a At the Edge Between the (001) and the (111)A surfaces

Cross sectional SEM pictures of sample A and sample B at the edge between the (001) surface and the (111)A sidewall are shown in Fig.2.4(a) and (b), respectively. The first epitaxial layers grown on the V-grooved substrates, the AlAs in sample A and $Al_{0.45}Ga_{0.55}As$ in sample B, show no thickness change on the (001) surface near the edge of the (111)A sidewall, while GaAs layers grown over them do. Furthermore, the growth of AlAs does not show facet growing but preserves the shape of the original substrate, while the growth of $Al_{0.45}Ga_{0.55}As$ leads to the appearance of a (411) facet between the (001) surface and the (111)A sidewall, where the angle between the facet and the (001) surface was measured to be nearly 20° which agrees quite well with the angle of 19.47° between the (411) facet and the (001) surface. The GaAs layer grown on the first $Al_{0.45}Ga_{0.55}As$ layer leads to the broadening of the (411) facet. It should be noted that even when the Al composition of the first AlGaAs layer is as low as 0.2, the results are almost the same as the case of $Al_{0.45}Ga_{0.55}As$ as described above.

As reported by Nilsson et al. and Hata et al., the exponential thickness change of the GaAs layer grown on the (001) surface near the edge of the (311)A or (111)A sidewalls is due to the lateral flux of Ga migrating from the sidewalls to the (001) surface. However, since the surface diffusivity of Al atoms is much smaller (Koshiba et al.1992), almost no lateral flux migrates from the (111)A sidewall to the (001) surface. Therefore, the shape of the substrate is maintained, during the growth of AlAs. The growth of AlGaAs is more complex because both Al and Ga atoms are involved in the surface diffusion and atom incorporation process on the (001), (411)A and (111)A surfaces. A possible mechanism will be discussed in section 2.3.2.

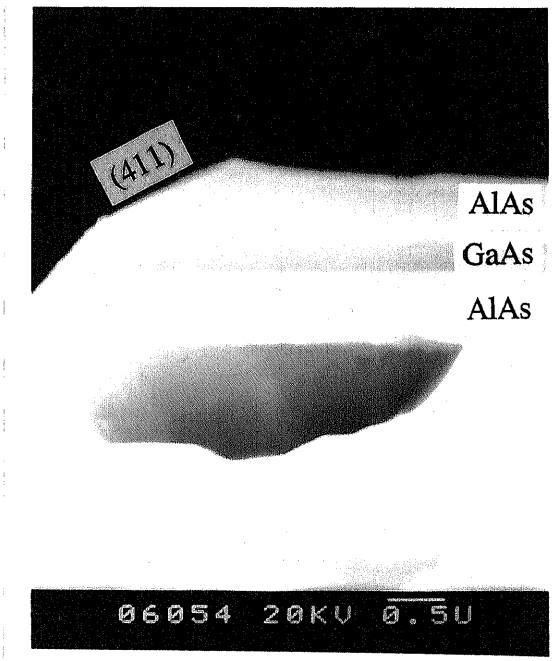

(a)

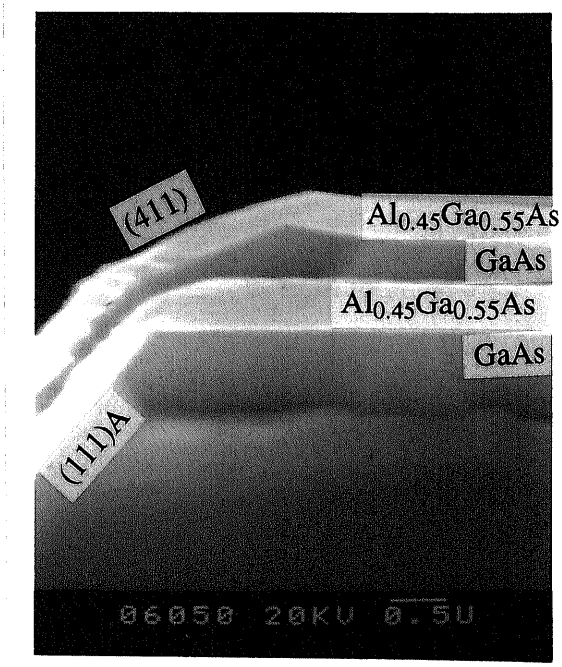

(b)

Figure 2.4. SEM cross-sections of the MBE-grown layers at the edge between the (001) surface and the (111)A sidewall on the V-grooved substrates.
(a) sample A (b) sample B.

2.3.1.b At the Bottom of the V-grooves

At the bottom the of V-grooves, the morphology of AlAs, $Al_{0.45}Ga_{0.55}As$, and GaAs layers are also very different. As shown in Fig.2.5, the bottom of the chemically etched V-grooved substrates have a rounded shape before MBE growth. After the growth of the first 0.5 μm-thick AlAs, the growth layer of AlAs on the (111)A sidewall is very flat and the shape of the bottom of the V-groove is found to become extremely sharp (**resharpening effect of AlAs**) as illustrated in Fig.2.5(a). This is similar to the AlGaAs growth in MOCVD (Kapon et al.1992). The drastic sharpening effect by the growth of AlAs is caused by the difference in the growth rate between on the (111)A surface and on other surfaces.

In contrast, the growth of 0.5 μm-thick AlGaAs on the V-grooves results in the appearance of a new (001) surface with the width of about 0.3 μm as shown in Fig. 2.5(b). Further growth of GaAs on this AlGaAs leads to the broadening of the (001) face. This indicates that GaAs shows a faster planarization of the groove than AlGaAs by creating a wider (001) surface at the bottom of the V-grooves, resulting from the significant migration of Ga atom on (111)A sidewalls. Furthermore, the corrugation of the growth layer of AlGaAs on the (111)A sidewall is observed , in the contrast to the growth of AlAs as described above.

According to the above observations, AlGaAs shows an intermediate growth behavior between GaAs and AlAs. This material-dependent growth behavior at the bottom of the V-grooves gives a possibility to fabricate GaAs/AlAs quantum-wire structures at the bottom of the V-grooves by MBE.

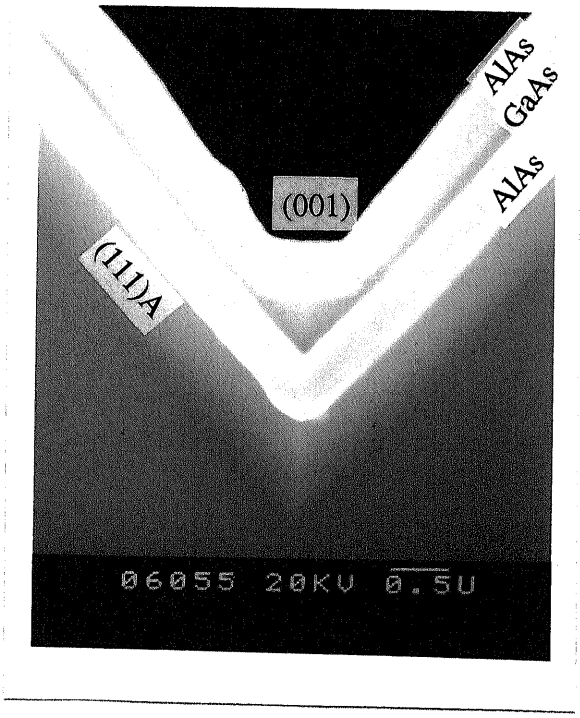

(a)

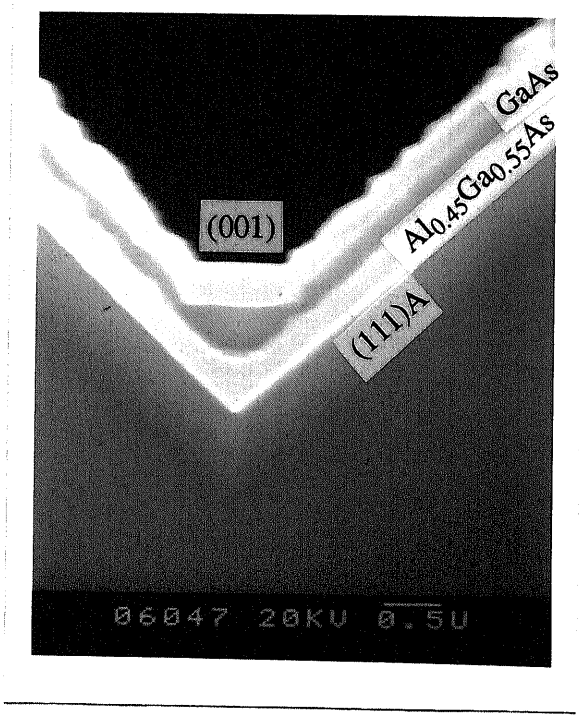

(b)

Figure 2.5. SEM cross-sections of the MBE-grown layers at the bottom of V-grooves .
(a) sample A, (b) sample B

2.3.2 Discussions

When GaAs layers are grown on the V-grooved substrates, an exponential-shaped layers of the GaAs on the (001) surface near the edge of the (111)A sidewall can be observed, while the AlAs and $Al_{0.45}Ga_{0.55}As$ layers show no such exponential shapes at the same place even when the Al concentration is as low as 0.2. This phenomenon can be explained as follows. When GaAs is grown on the V-grooves, the probability of Ga atom incorporation on the (111)A surface is relatively low because the (111)A surface is an a Ga-stabilized surface. Therefore, the concentration of Ga atoms on the (111)A surface would become higher than the neighboring (001) surface and some of the Ga atoms unincorporated on the (111)A sidewalls will migrate easily from the sidewalls to the (001) surface. This inter-surface migration of Ga atoms results in the increase of the GaAs thickness on the (001) surface near the edge. In contrast, in the case of AlAs, since the diffusivity of Al atoms is much smaller and atom incorporation, i.e. growth rate of AlAs, is greater on (111)A surfaces, the inter-surface migration is small and no exponential shape was observed. When AlGaAs is grown, the AlGaAs layer shows the roughening on the (111)A sidewalls, where there are a great number of steps and kinks. Thus most of the Ga atoms in the AlGaAs on the (111)A surface can be incorporated into such steps and kinks easily, resulting in a great reduction of Ga lateral flux from the (111)A sidewall to the (001) surface. Therefore, the exponential shape of the AlGaAs layers on the (001) surface near the edge of the (111)A sidewall can not be observed.

It is found that AlAs can be grown with very smooth surface on the (111)A sidewalls and makes the concave part of V-grooves become very sharp. The fact means that the growth rate of AlAs on the (111)A surface is faster than on the (001) surface, considering the difference of the arriving fluxes on each surface. This is probably because, under the current growth conditions, Al atoms can be incorporated into the (111)A surfaces very easily, while they are much more difficult to be incorporated into (001) and other surfaces. Hence, the concave shaped bottom of the V-grooves consisting of two flat (111)A surfaces becomes very sharp.

2.3.3 Temperature Dependence of GaAs/AlAs Heterostructure at V-grooves

From the results described in section 2.3.1b, the MBE growth of AlAs was found to have a resharpening effect while the growth of GaAs showed a fast filling at the bottom of the V-groove. In order to use the difference growth behavior and try to fabricate multiple quantum-wires at the bottom of the V-groove, GaAs/AlAs multiple quantum-well structures were grown by MBE. The sample structures are described as follows: first, a 0.5 μm AlAs buffer layer was grown on the V-grooved substrate in order to make the concave part of V-groove sharp. Then four 80 Å-thick GaAs quantum wells were grown with 1000 Å-thick AlAs barrier layers. The 1000 Å-thick AlAs barrier layers are expected to have the effect of resharpening the concave part of the V-grooves. Finally, a 200 Å-thick GaAs cap layer was grown. The thickness of each layer described here is the same as on the (001) surface. In these growth runs, to investigate the temperature dependence of the surface diffusion and morphology of the grown heterostructures, the growth temperature was varied from 450°C to 630°C, while other growth parameters were fixed. During the growth, the V/III ratio was kept at about 4 and the rotation speed of the substrate was 4 rpm.

Fig.2.6 shows the cross-sectional photographs of the samples grown at various temperatures, which were taken without stain etching in the reflected electron mode of a high-resolution scanning electron microscope (RHSEM ; Hitachi S-5000). Note here that the bright and dark regions are GaAs and AlAs, respectively, where the contrast is reversed against the pictures of Fig.2.4-Fig.2.5 due to the use of the reflected electron mode. At the growth temperature of 450°C, the AlAs can not be grown in a layered structure on the (111)A sidewalls as shown in Fig.2.6(a) when the thickness exceeds 0.1 μm. Also, during the growth at high temperature (630°C), the GaAs/AlAs heterostructures can not be formed uniformly as shown in Fig.2.6(c). This might be because interdiffusion between the GaAs and AlAs takes place at this high temperature and the interfaces between each epitaxial layer are broadened. Only at the proper growth temperature (580°C) as shown in Fig.2.6(b), can the growth be successfully carried out and well-defined GaAs/AlAs quantum wells with smooth interface are formed.

From the above results, it is clear that fabrication of QWR structures at the bottom of V-grooves is possible by MBE under the usual growth conditions. This gives a new challenge topic for MBE. The detailed fabrication and characterization results will be described in chapter 5.

(a)

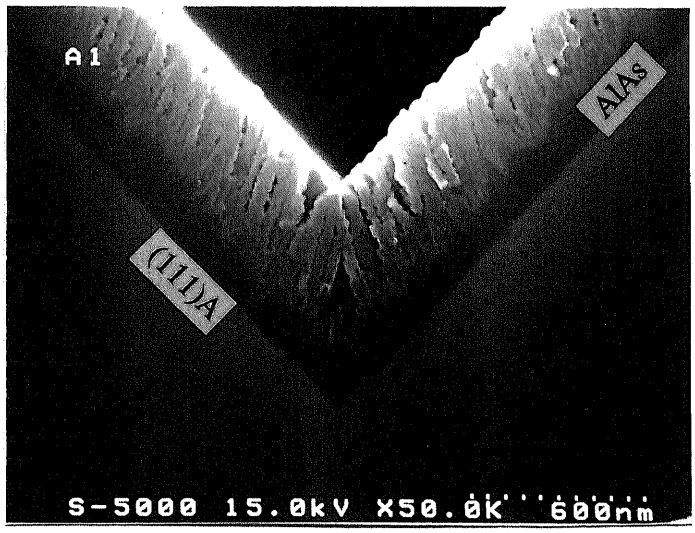

(b)

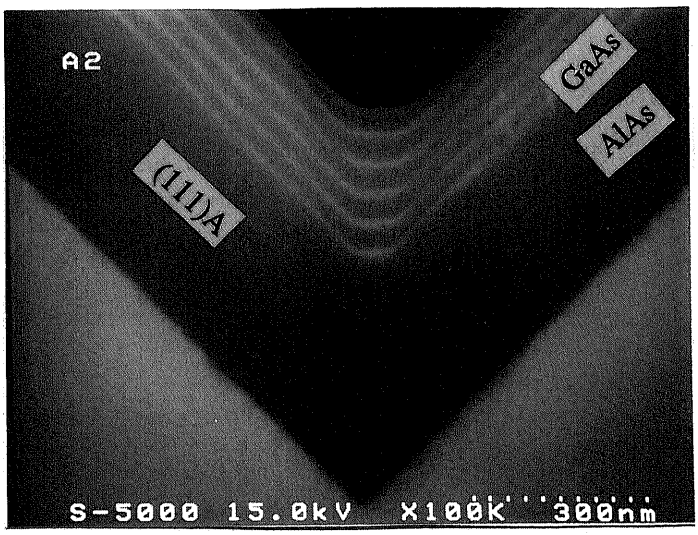

(c)

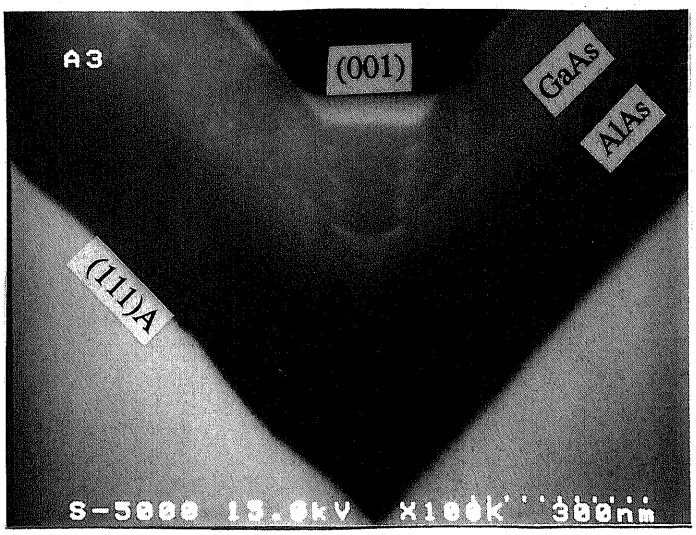

Figure 2.6. High-resolution SEM images of the GaAs/AlAs heterostructures at the bottom of the V-grooves under various growth temperatures Ts. The bright lines are the GaAs layers and the dark regions are the AlAs.(a) Ts=450°C, (b) Ts=580°C, (c) Ts=630°C.

§2.4 The Growth of (In, Ga)As Heterostructures at V-grooves

There is a strong interest in the growth of lattice mismatched system such as (In,Ga)As/GaAs heterostructures because of the large energy gap difference and high electron mobility. Therefore, it is necessary to understand the In surface diffusion during the MBE growth.

To study the surface diffusion in the growth of InGaAs/AlAs and InAs/AlAs heterostructures on V-grooved substrates, and also to ascertain the possibility of fabricating quantum-wires in lattice mismatched materials, the following structures were grown: First 0.5 μm AlAs buffer layer was grown on V-grooved substrates to make the V-grooves become sharp. Then, three 100Å thick InGaAs and InAs quantum wells with 1000Å AlAs barrier layers were grown on the buffer layer. The growth temperatures were 400°C and 500°C for (In,Ga)As and 580°C for AlAs. After the growth of InGaAs and InAs at low temperatures, only a few monolayers of AlAs were grown firstly at the same temperatures in order to preserve the grown InGaAs and InAs layers. Then, the growth temperature was raised to 580°C and the AlAs layers were grown at the temperature. At last, GaAs cap layer was grown at 580°C. The growth rate of AlAs and InGaAs were 0.70 μm/hr and 1.0 μm/hr, respectively. The In composition in InGaAs was 0.15.

2.4.1 HRSEM Observations of $In_{0.15}Ga_{0.85}As$/AlAs Heterostructures

The cross-sectional images of RHSEM of InGaAs/AlAs epilayers without stain etching in reflected electron mode are illustrated in Fig.2.7. It can be seen that the InGaAs epilayers grow very smoothly on (111)A sidewalls both at 400°C and 500°C. But, at the bottom of V-grooves, the growth layer of InGaAs shows different growth behaviors at each growth temperature. When growth temperature of InGaAs is 400°C, the InGaAs layers almost preserve the shape of the substrate and growth layer of InGaAs at the bottom is very sharp. Instead, the shape of InGaAs becomes sharper and sharper at the bottom of V-grooves with the growth of AlAs as shown in Fig.2.7(a). This phenomenon can be understood by considering that almost no Ga migrate from (111)A sidewalls to the bottom of V-grooves at such a low growth temperature and the In composition in the InGaAs is quite low (0.15). When InGaAs was grown at 500°C, the shape of InGaAs layers at the bottom is different from that described

above. At the bottom of V-groove, the crescent-shaped InGaAs layer is observed with the width of about 1200Å as shown in Fig.2.7(b). This is attributed to the surface migration of In and Ga atoms from (111)A sidewalls to the bottom of V-grooves. But the new (001) surface is too wide to be resharpened although 1000Å AlAs barrier layers were grown.

Since the surface diffusion of In atoms is faster than that of Ga atoms , it can be easily understood that the size of crescent shape of InGaAs epilayer is larger than that of GaAs at the same growth temperature. At the very low growth temperature (400°C), since the surface diffusion of Ga atoms is very slow and the In composition in the InGaAs is quite low (0.15), no crescent-shaped layer of InGaAs at the bottom can be formed, while at 500°C it can be. From the results obtained, it is suggested that the fabrication of multiple InGaAs/AlAs quantum-wires at the bottom of V-grooves by MBE is possible if the proper growth conditions are chosen although the temperature range is narrow.

2.4.2 HRSEM Observations of InAs/AlAs Heterostructures

Fig.2.8 shows the cross sectional picture of InAs/AlAs heterostructures by RHSEM in reflected electron mode. White and black regions in the figure denote the parts of InAs and AlAs, respectively. The growth temperature was chosen as 400°C and the growth rate of InAs on the flat surface was 0.15 μm/hr. It is very interesting to see the shape of InAs growth layers at the bottom of the V-grooves. Almost no InAs was grown on the (111)A sidewall and most of the In atoms migrated from the sidewall to the bottom. This means that the In adatom can diffuse much longer on the GaAs substrate than Ga does at such a low growth temperature (400°C) comparing the results of InGaAs growth described in the above section. Furthermore, the InAs layer at the bottom shows the formation of (311)A facet which is different from the case of GaAs in which (001) surface is formed. This (311)A InAs facet is often observed during the initial stage of the InAs growth on the (001) planar GaAs substrate by RHEED patterns.

Almost no growth of InAs on the (111)A sidewall illustrates that the surface diffusion of In atom is very large on GaAs surfaces as reported by Arent et al. From the results obtained, it is suggested that the fabrication of single InAs/AlAs quantum-wires at the bottom of V-grooves by MBE might be also possible and strong lateral confinement is expected.

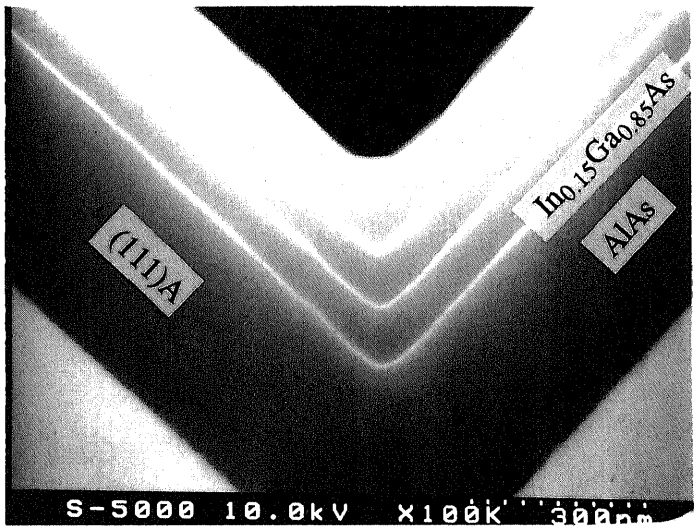

(a)

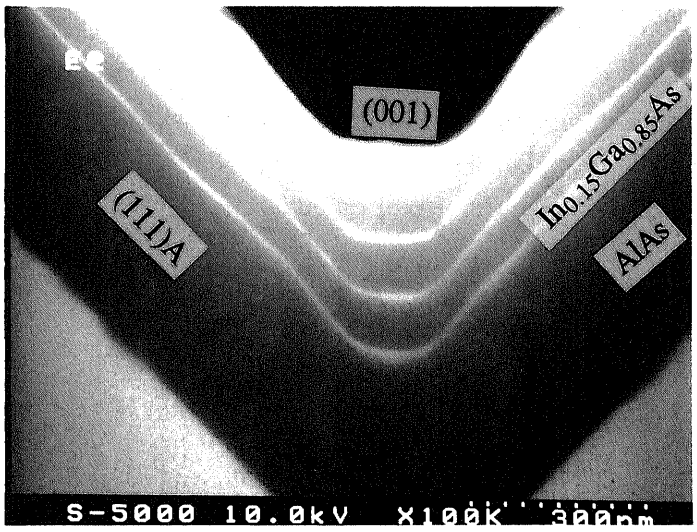

(b)

Figure 2.7. HRSEM Observations of InGaAs/AlAs Heterostructures.
(a) Ts=400°C, (b) Ts=500°C

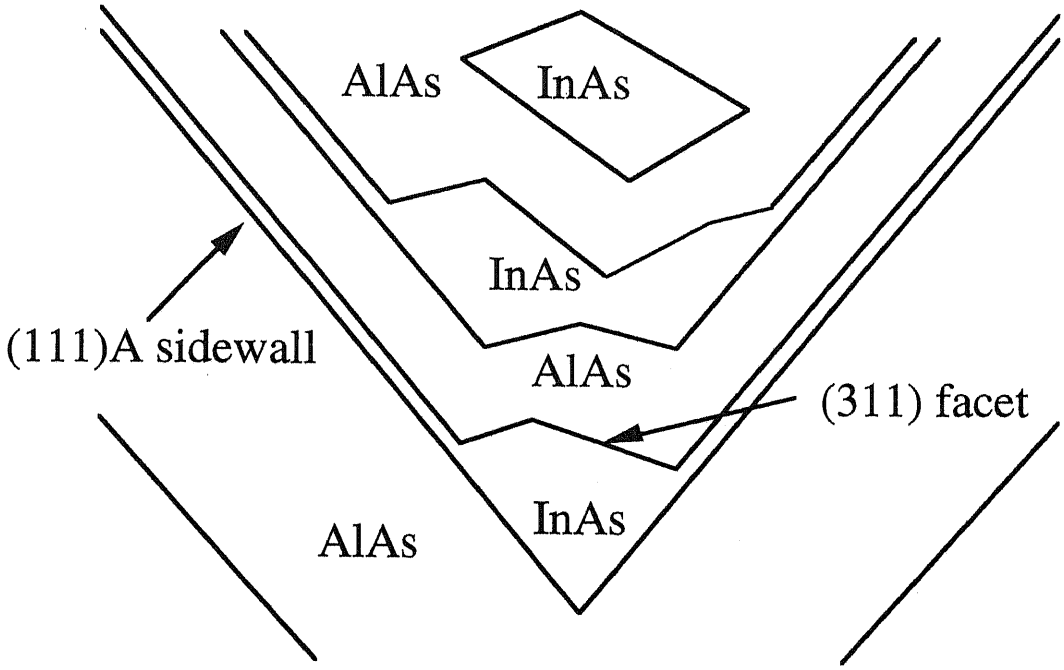

(a)

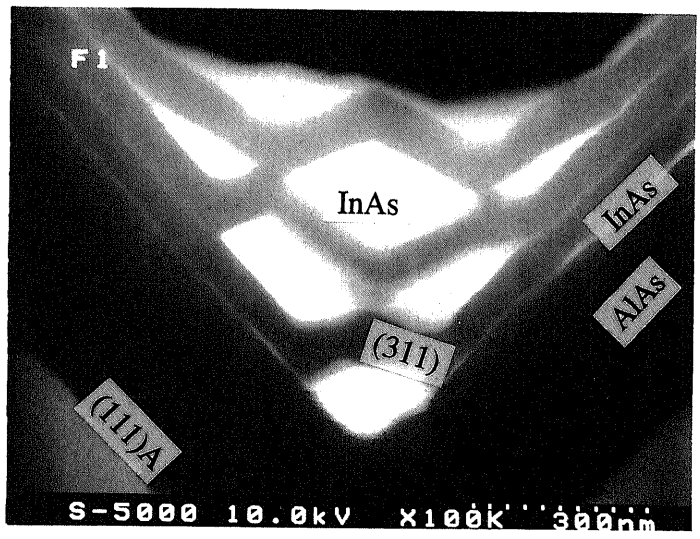

(b)

Figure 2.8. (a) Schematical illustration and (b) HRSEM Observations of InAs/AlAs Heterostructures. The white parts are InAs and the black ones are AlAs. Ts=400°C

§2.5 Summary

The MBE growth of (Al,Ga)As and (In,Ga)As heterostructures on V-grooved substrates were carried out. By the cross sectional SEM observations of the grown layers on the various parts of the V-grooved substrates, the surface diffusion phenomena of adatoms (Ga, Al, In) were studied and diffusion length of incorporation is compared each other.

Facet formations and the growth thickness change on the (001) surface near the edge are observed, which relate to the inter-surface diffusion of Ga between the (111)A sidewall and the (001) surface. It is shown, in particular, that the growth of AlAs leads to a drastic sharpening at the bottom of the V-grooves (**resharpening effect of AlAs**). AlGaAs, however, has no such phenomena. Instead, it grows roughly on the (111)A surfaces and makes a new (001) surface at the bottoms as GaAs does.

Comparing the shape of the InGaAs grown at the bottom of V-grooves, it is found that the diffusion length of In adatom depends strongly on the growth temperature. Almost no growth of InAs on the (111)A sidewall shows the large diffusion length of In on the (111)A GaAs sidewall. Furthermore, the InAs layer at the bottom shows the formation of (311)A facet which is different from the case of GaAs forming (001) surfaces.

By using the different growth behaviors of each material at the bottom of the V-grooves, it is pointed out that fabrication of multiple GaAs/AlAs and (In,Ga)As/AlAs quantum-wires structures at the bottom of the V-grooves by MBE is possible.

Chapter 3 Surface Diffusion of Ga (In) Adatoms on the (001) Surface Using (n11)A-(001) NP Substrates by μ-RHEED/SEM MBE

§3.1 Introduction

Recently, the surface diffusion phenomena during epitaxial growth on mesa-etched substrates have generated a great deal of interest because of its importance not only in the study of the growth mechanism but also in the fabrication of low dimensional microstructures and devices. With the development of the modern characterization techniques, such as STM, AFM etc., the surface has been carefully studied in an atomic scale. But these are not the powerful methods for *in situ* observations during the crystal growth. MBE equipped with microprobe RHEED (μ-RHEED) or scanning electron microscope (SEM) makes it possible to observe the surface image in real time (Ichikawa et al.1982, Isu et al.1988; Inoue et al.1991). By this method, Inoue et al. succeeded in observing the monolayer steps on the GaAs (001) vicinal surfaces. Furthermore, Hata et al.(1990) developed a new measuring method for the *in situ* measurements of the growth rate distribution on the NP substrates by using *in situ* scanning microprobe reflection high-energy electron diffraction (μ-RHEED) MBE. It was observed by them that the growth rate of GaAs on the (001) surface near the edge between the (001) surface and the (111)A sidewall decreases exponentially as a function of the distance from the edge, which results from the migration of Ga adatoms from the (111)A sidewall to the (001) surface on the (111)A-(001) mesa-etched substrates. In their studies, the surface diffusion lengths of Ga incorporation on the (001) GaAs surface in the [110] direction was estimated to be about 1 μm at 560°C. Also, it was reported by them that on (111)A-(001) mesa-etched GaAs substrates, the surface diffusion length in the [110] direction depends on the growth temperatures and the surface reconstructions. However there have been no systematic studies concerning the arsenic pressure dependence of surface diffusion of Ga and In on nonplanar substrates until now. This kind of study is very important both for the study of the growth mechanism and for the fabrications of the future devices.

In this chapter, detailed experimental results, which concern the As_4 and Ga (In) pressure dependence of surface diffusion phenomena on the (n11)A-(001) GaAs (InAs) NP substrates by the method developed by Hata et al., are reported. First, a simple model based on the surface diffusion theory is proposed. The lifetime of the Ga adatom until incorporation into the crystal on each surface is introduced in the model. Then the surface diffusion length of incorporation and the migration direction of Ga (In) adatoms are investigated under various As_4 and Ga (In) pressures by measuring the distributions of the growth rates on the (001) surface near the edge of sidewalls, from the images of μ-RHEED. At last, the step kinetics and the surface reaction process of As_4 are discussed.

§3.2 Experimental Methods

3.2.1 μ-RHEED/SEM MBE System

The growth apparatus of the μ-RHEED/SEM MBE system used in the present work was described elsewhere (Suzuki et al.1994). Fig.3.1 shows the present MBE system schematically. An electron gun for SEM and μ-RHEED is installed in the specially designed MBE(ULVAC), which is equipped with solid source K-cells. Diffraction patterns from the substrate are observed on a fluorescent screen. By selecting a particular diffraction spot and using an optical lens, the intensity can be measured by a photomultiplier. The images of scanning reflection high-energy electron diffraction (SREM) is produced from this intensity by scanning the electron beam.

3.2.2 Methods for Measurements

MBE growth was carried out on (001) GaAs and InAs substrates with grooves cut in the [110] direction where the sidewall is (n11)A surfaces. The NP substrates were prepared as described in chapter 2 for GaAs growth and the preparation of InAs NP substrates will be described in §3.6.

In the present work, exactly the same technique which was developed by Hata et al. was employed to measure the growth rate distributions near the edge. The images of SREM were obtained using the intensity of the specular beam spot of the RHEED pattern on the (001) surface. The incident electron beam was in the [$\bar{1}$10] direction at a glancing angle about 1°. The distribution of the growth rate on the (001) surface near the edge of the (n11)A sidewalls can be derived by measuring the intervals of the stripes, i.e. the periods of the RHEED oscillations, using the image processor. Fig.3.2 show a typical image of SREM during the MBE growth on the (001) surface near the edge of (111)A sidewalls in the experiment. From Fig.3.2, it can be seen that horizontal stripes due to the RHEED intensity oscillations appear in the image of the upper (001) surface after the start of the MBE growth and the intervals between the stripes near the edge become narrower than that far from the edge, which means that the growth rate near the edge is faster than that far from the edge. By this method, the distribution of the growth rate can be measured easily.

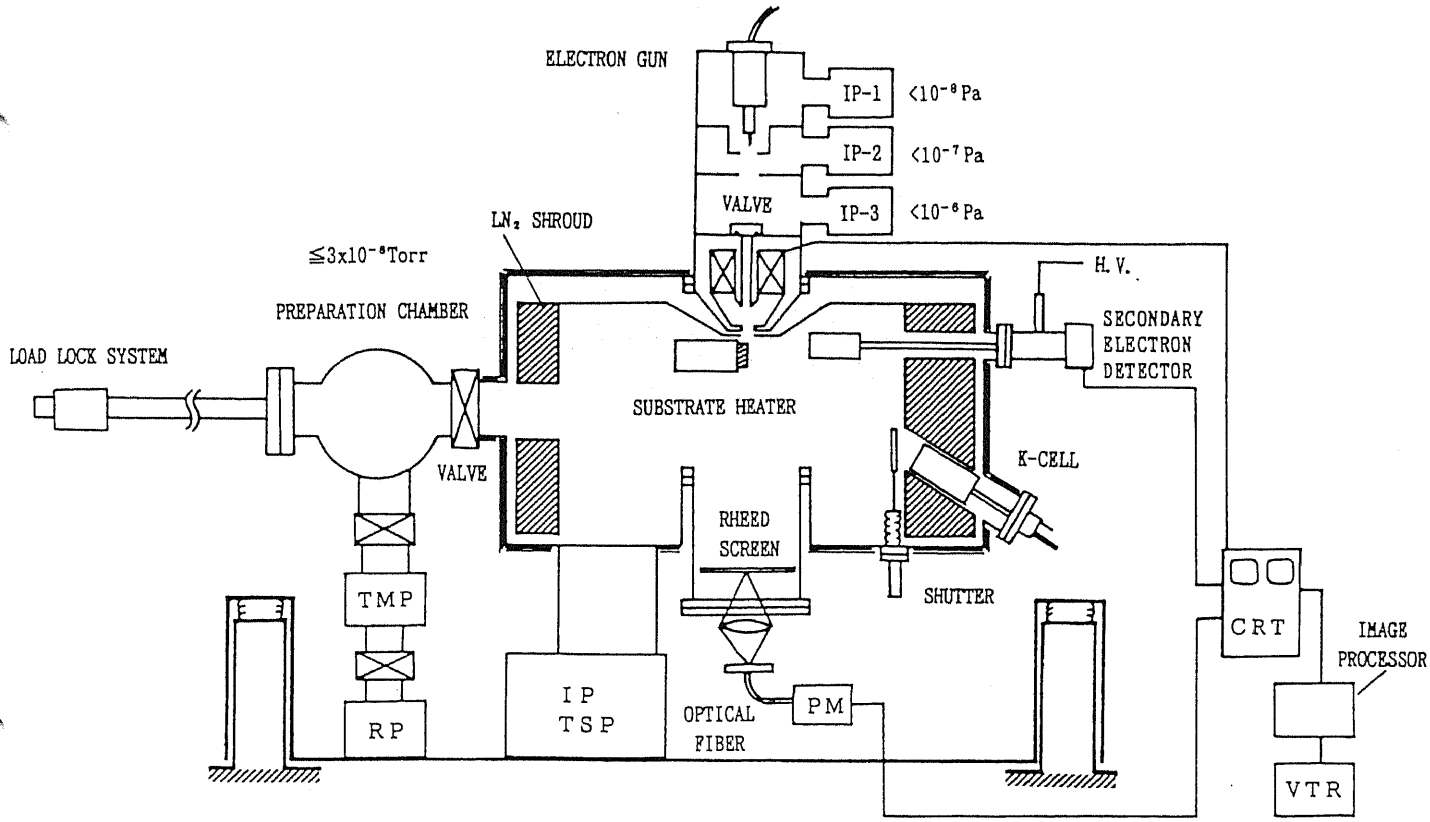

Figure 3.1. Schematic illustration of μ-RHEED/SEM MBE system. In the figure, IP, TSP, TMP and RP denote an ion pump, a titan sublimation pump, a turbo-molecular pump and a rotary pump, respectively.

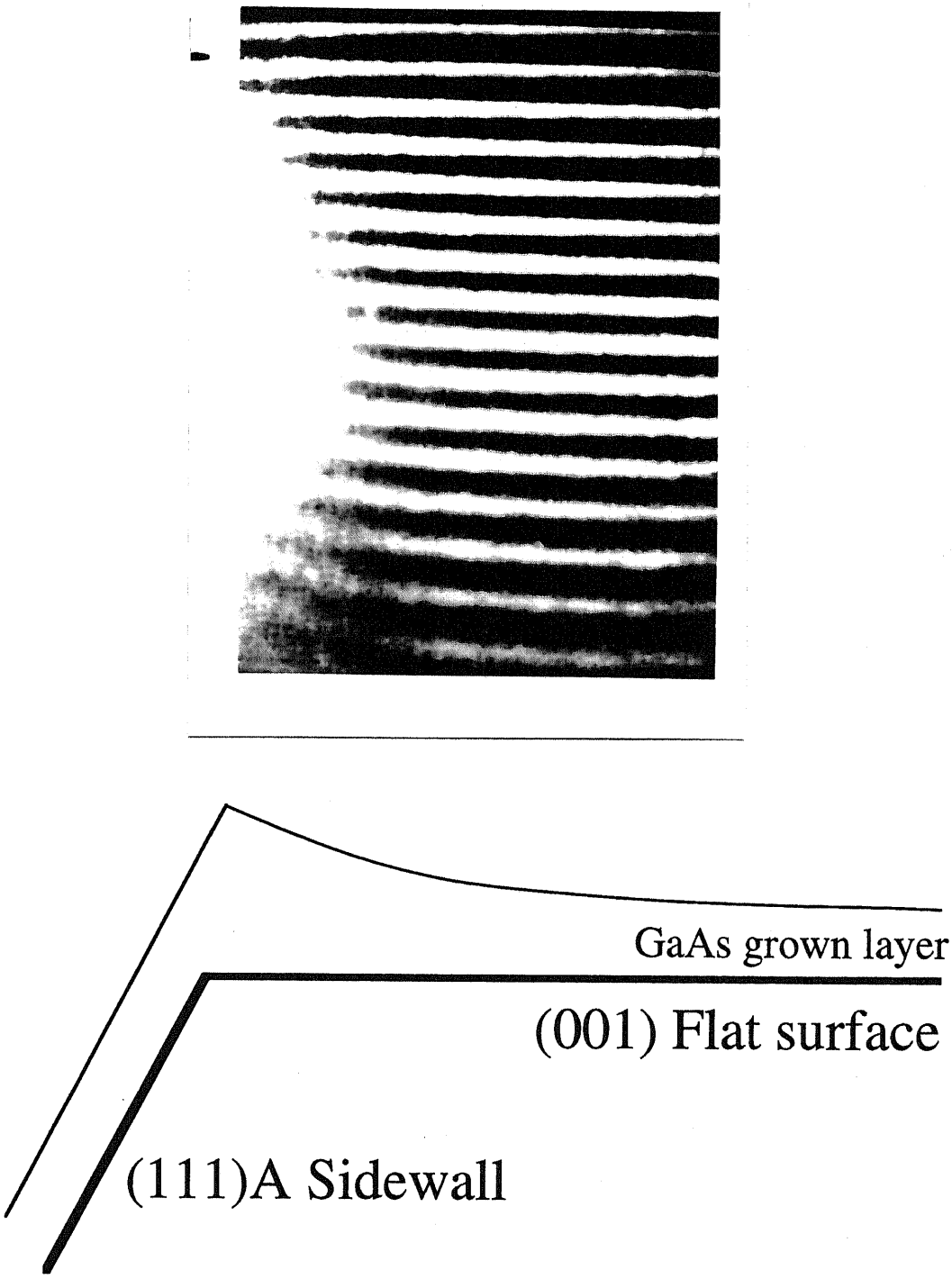

Figure 3.2. Typical images of SREM during the MBE growth on the (001) surface near the edge between the (001) surface and the (111)A sidewall

§3.3 Model

The spatial distribution of the growth rate $R_p(x)$ on the (001) surface near the edge of the (n11)A sidewall is composed of two terms and is given by

$$R_p(x)=R_V+R_L(x) \tag{3.1}$$

where x denotes the distance on the (001) surface from the edge, $R_L(x)$ is the growth rate by a lateral flux and R_V is the growth rate by a direct flux from the K-cell. As shown in Fig.3.3(a), $R_L(x)$ can take positive and negative values depending on the direction of lateral flux migrating from or to the sidewall.

In the following, a simple model based on the one-dimensional surface diffusion equation is proposed. Here, GaAs growth on the (111)A-(001) GaAs NP substrates is taken as an example. In this model, the lifetime τ of Ga adatoms until incorporation into crystals on each surface is introduced. Fig.3.3(b) shows this model schematically. Here, parameters on the (001) planar surface and the (111)A sidewall are symbolized as "p" (plane) and "s" (sidewall) in the suffix of each variable, respectively. Therefore, the equations from the surface diffusion theory can be given as

$$D_p \frac{d^2N_p}{dx^2} - \frac{N_p}{\tau_p} + J_{Ga} = 0 \tag{3.2}$$

and

$$D_s \frac{d^2N_s}{dy^2} - \frac{N_s}{\tau_s} + J'_{Ga} = 0 , \tag{3.3}$$

where N, τ, D, x and y are defined as the surface density of Ga adatoms, the lifetime of Ga adatoms until incorporation into the crystal, the surface diffusion coefficient, and the distance from the edge between the (001) surface and the (111)A sidewall on each surface, respectively. $J'_{Ga}=J_{Ga}\cos\theta$, where θ is the angle between the (001) and (111)A surfaces and J_{Ga} is the flux of Ga from the K-cell.

In the present model, the boundary conditions at the edge are given as

$$N_p(0) = N_s(0) \tag{3.4}$$

and

$$D_p\left(\frac{dN_p}{dx}\right)_{x=0} + D_s\left(\frac{dN_s}{dy}\right)_{y=0} = 0 , \qquad (3.5)$$

where eq. (3.4) implies that the surface densities of Ga adatoms on the (001) surface and the (111)A sidewall are equal at the edge. Equation (3.5) indicates that the lateral flux of Ga adatoms at the edge is continuous because the edge is not an absorbing source.

From the above equations, the growth rate $R_p(x)$ on the (001) surface near the edge can be obtained as

$$R_p(x) = \frac{N_p(x)}{\tau_p} = J_{Ga} + \frac{J_{Ga} D_s \lambda_p (\tau_s \cos\theta - \tau_p)}{(D_s\lambda_p + D_p\lambda_s)\tau_p} \exp\left(-\frac{x}{\lambda_p}\right) \qquad (3.6)$$

In the eq. (3.6), the first term in the right-hand side stands for R_V and the second one for $R_L(x)$. It is clear that $R_L(x)$ changes exponentially with the distance from the edge and the gradient of the $\log R_L(x)$ corresponds to the reverse of the surface diffusion length.

The above treatments are also valid if the sidewall is another kinds of surfaces and the growth materials are different from GaAs. Therefore, the proposed model is thought to be suitable for describing the MBE growth on NP substrates.

On (111)A-(001) NP substrates, according to the experimental results of GaAs growth described in chapter 2, $R_L(x)$ takes a positive value and decreases exponentially with the distance from the edge. This indicates that the lifetime of Ga adatoms until incorporation into the crystal on the (111)A sidewall is longer than that on the (001) surface. Also, the surface diffusion length of Ga on the (001) surface can be derived to be in the micrometer order from the gradient of the $\log R_L(x)$ according to the model.

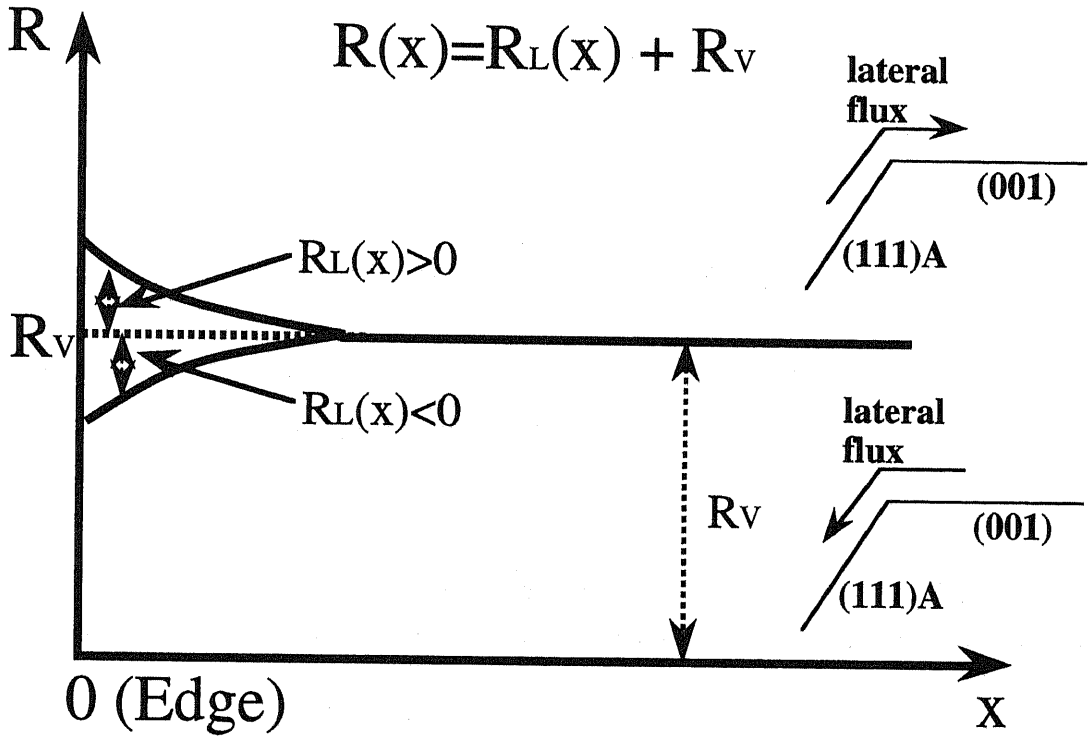
R
R(x)=RL(x) + RV
lateral
flux
(001)
(111)A
RL(x)>0
RV
RL(x)<0
lateral
flux
RV
(001)
(111)A
0 (Edge)
X

(a)

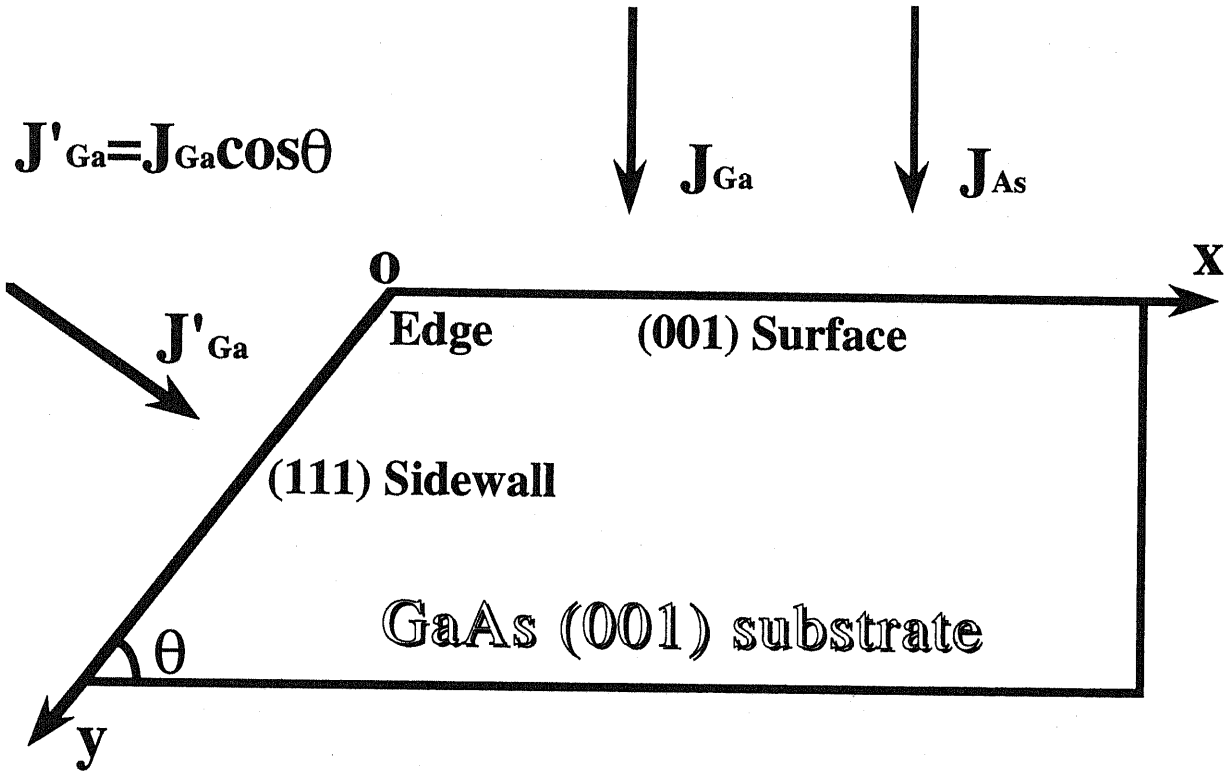

(b)

Figure 3.3. Schematic illustrations of (a) growth rate distributions near the edge; (b) the model.

§3.4 Arsenic Pressure Dependence of Surface Diffusion Length of Ga on (n11)A-(001) GaAs NP Substrates

The results of the surface diffusion length of Ga on the (001) GaAs surface measured on the NP substrates (Hata et al.1990; Isu et al.1992) show a great difference from what was calculated by measuring the critical temperature of the disappearance of RHEED oscillations (Neave et al.1985). In the conventional case, the arsenic flux entering the step is much larger than that of Ga, since the growth is usually carried out under the arsenic rich condition. However, in the case of NP substrates, the Ga flux flowing into the steps on the (001) surface might be much lager than that of As, because the lateral flux from the (n11)A sidewall is about 40 times larger than the surface flux entering the steps due to the direct molecular beam from the K-cell (Nishinaga et al.1991). Therefore, the migrating Ga adatoms will not be absorbed into the steps, unless sufficient As atoms arrive at these steps to fix them. This assumption requires detailed studies concerning the arsenic pressure and Ga flux dependence of the surface diffusion length.

3.4.1 Diffusion Length on (001) GaAs Surface Along the [110] Direction With (111)A Sidewalls

Using the methods described in section 3.2.2, the measurements of the growth rate distributions $R_L(x)$ near the edge between the (001) and the (111)A surfaces were carried out. In order to investigate the arsenic pressure dependence of the surface diffusion length of incorporation, the arsenic pressures were varied from 3.3×10^{-4} Pa to 1.5×10^{-3} Pa and the surface reconstruction was kept under (2x4) conditions showing the arsenic stabilized surfaces. During the growth, the growth temperatures and the growth rate were set at 610°C and 1.5 Å/s, respectively.

Experimentally obtained $R_L(x)$ is shown in Fig.3.4. From the figure, it can be seen that $R_L(x)$ decreases exponentially with the distance from the edge, as described by Hata et al. The gradient of $\log R_L(x)$, which corresponds to the reverse of the diffusion length of incorporation from the proposed model, is different under various arsenic pressures. This means that the surface diffusion length of Ga adatoms on the (001) surface is affected by the arsenic pressure. Furthermore, $R_L(x)$ itself also depends strongly on the arsenic pressure. This

indicates that the amount of Ga lateral flux from the (111)A sidewall is very sensitive to the arsenic pressure which so far has not been fully understood.

From the gradient of $\log R_L(x)$, the surface diffusion length of Ga adatoms of incorporation on the (001) surface can be calculated. Fig.3.5 shows the dependence of the surface diffusion length of Ga adatoms on the arsenic pressures at 610°C. It can be seen that the diffusion length of Ga adatoms is in the order of micrometers and decreases with the increase of arsenic pressures under (2x4) reconstruction conditions. Arsenic pressures were calculated by measuring the RHEED oscillation of As incorporation in the experiments. It can be seen that the diffusion lengths are almost proportional to the reverse of arsenic pressures within the experimental errors, where the reason will be explained in §3.7. The above results give a direct evidence to the assumption about the growth process at the step edge on NP substrates, where the Ga flux flowing into the steps on the (001) surface is thought to be much lager than that of As. The details will be discussed later, together with the results of the dependence of the diffusion length on Ga fluxes.

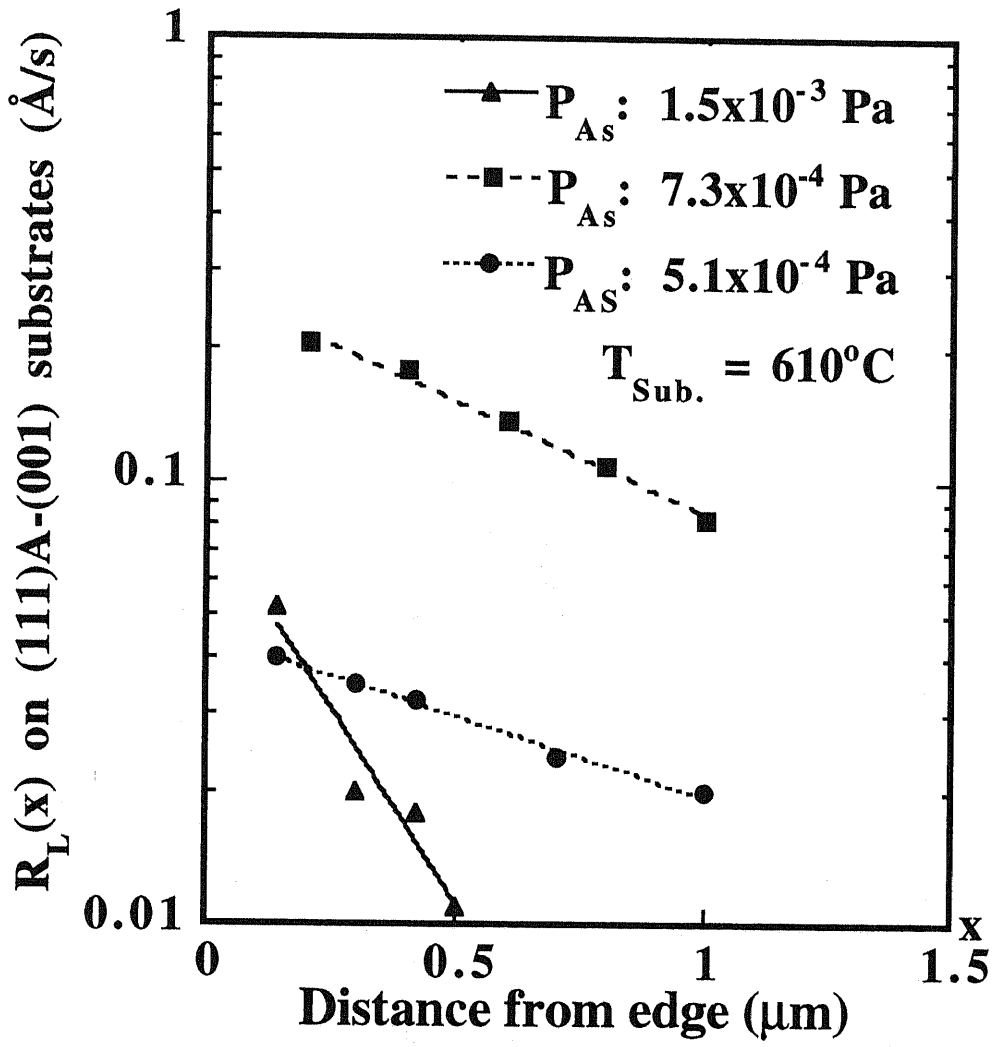

Figure 3.4. The distributions of the growth rate of GaAs near the edge.

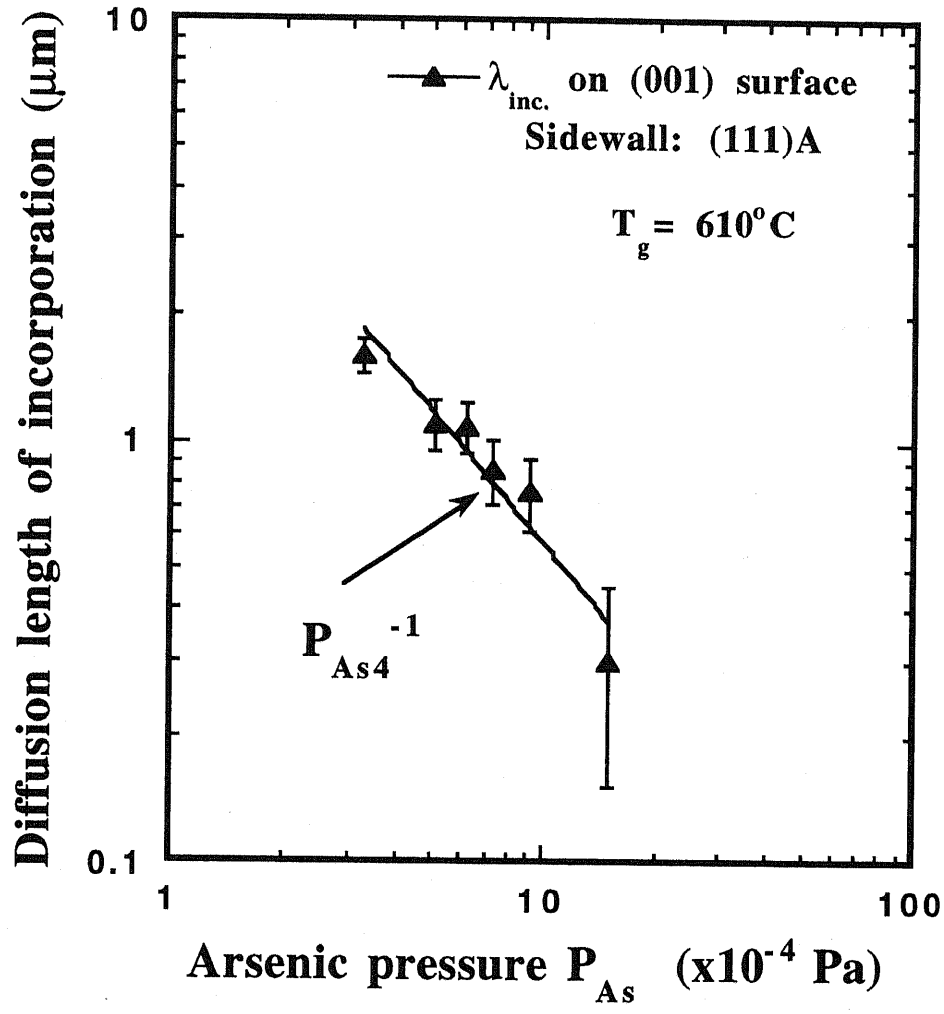

Figure 3.5. The arsenic pressure dependence of the surface diffusion length of Ga on the (001) GaAs surface with (111)A sidewalls.

3.4.2 Diffusion Length on (001) GaAs Surface Along the [110] Direction With (411)A Sidewalls

As described in §2.3, during the MBE growth of GaAs on NP substrates, (411)A facets always appear between the (001) surface and the (111)A sidewall. In order to investigate the influence of the (411)A facet on the surface diffusion of Ga on the (001) surface, the (411)A-(001) NP substrates were used for the experiments. Such kind of substrates were prepared by the same methods described in §2.2, except for the using of the etchant ($HF:H_2O_2:H_2O=1:2:40$.)

The experiments were carried out with the same methods as that of (111)A-(001) NP substrates. From the SREM images, the surface diffusion length was derived. Both the growth temperature and the arsenic pressure dependence of the Ga diffusion length on the (001) surface were investigated. The growth rate at the flat place was set at 1.5 Å/s and the surface reconstruction was always kept at (2x4). The growth temperatures were varied from 550 °C to 610°C for the measurements of the growth temperature dependence, while the arsenic pressures were changed from $3.1\text{x}10^{-4}$ Pa to $1.2\text{x}10^{-3}$ Pa in order to study the arsenic pressure dependence of the diffusion length.

Fig.3.6 illustrates the growth temperature dependence of the Ga diffusion length on the (001) surface with the (411)A sidewall. It can be seen that the Ga diffusion length depends on the growth temperature exponentially. The activation energy for the surface diffusion is calculated to be 0.67 eV from the dependence, which is almost the same result as that on the (111)A-(001) NP substrates (Hata et al.1990).

Fig.3.7(a) shows some results of the growth rate distributions on the (001) surface near the edge of (411)A sidewall under various arsenic pressures. It can be seen that the gradients of the $\log R_L(x)$ change with the the arsenic pressure, which means that the surface diffusion lengths of Ga incorporation depend on the arsenic pressure. Fig.3.7(b) shows the dependence of the surface diffusion length on the arsenic pressure. The results are almost the same as that of (111)A-(001) NP substrates described in section 3.4.1 within the same arsenic pressure region. These indicate that surface diffusion lengths on the (001) surface only depend on the growth conditions and the surface condition itself, while they are independent of the kind of the sidewalls.

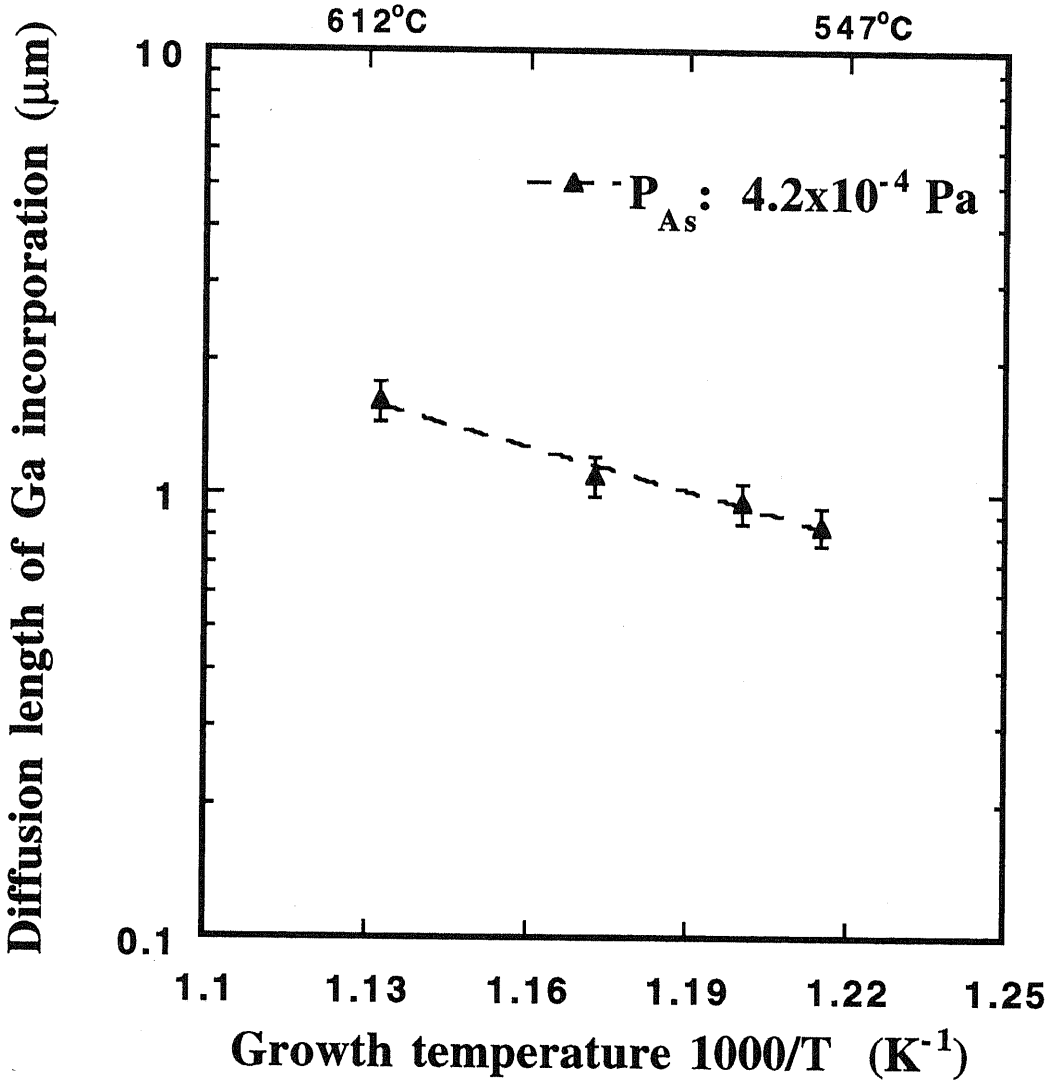

Figure 3.6. The growth temperature dependence of the surface diffusion length of Ga on the (001) GaAs surface with (411)A sidewalls.

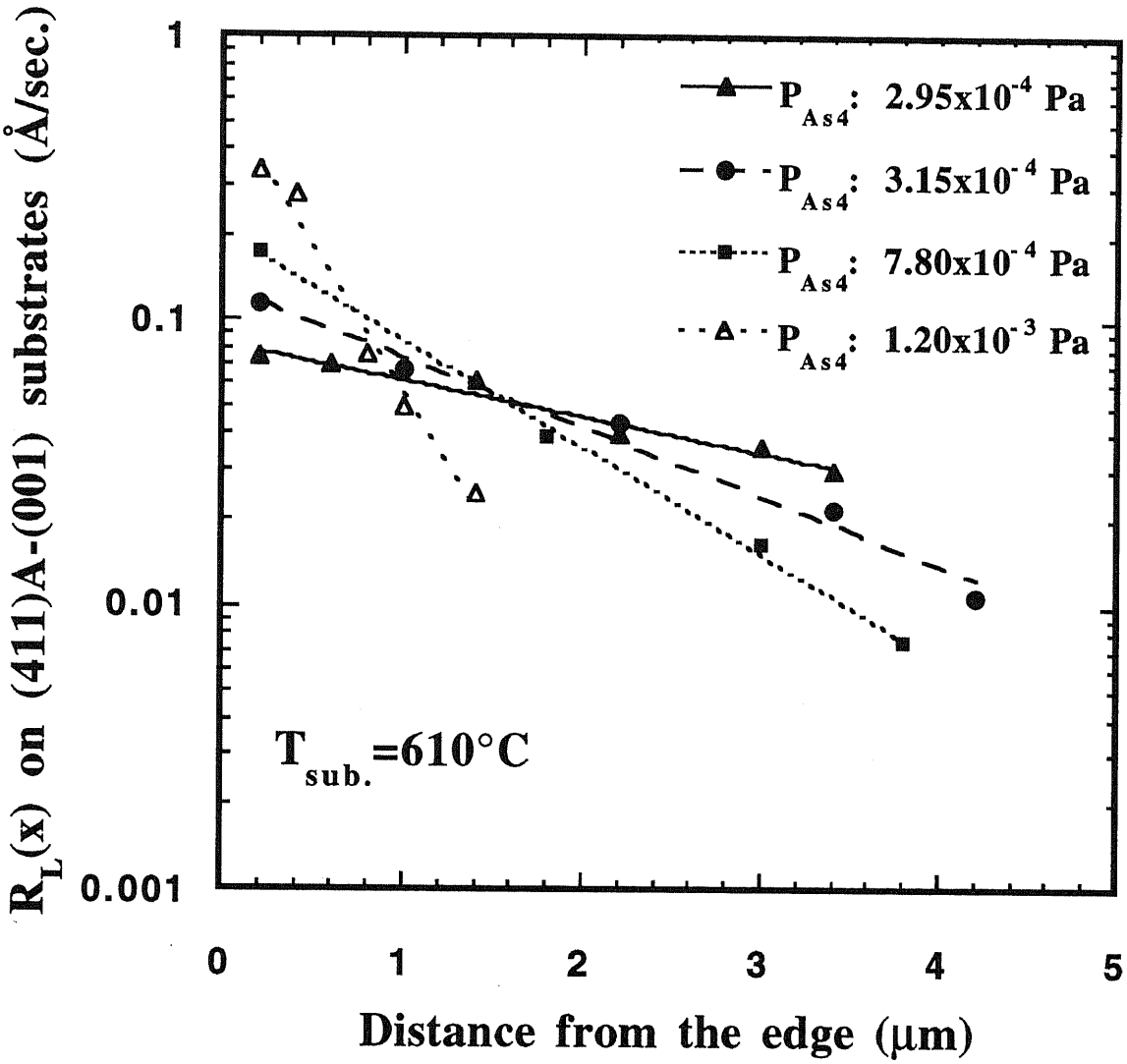
$R_L(x)$ on (411)A-(001) substrates (Å/sec.)
1
0.1
0.01
0.001
0
1
2
3
4
5
Distance from the edge (μm)
P_{As4}: 2.95x10^{-4} Pa
P_{As4}: 3.15x10^{-4} Pa
P_{As4}: 7.80x10^{-4} Pa
P_{As4}: 1.20x10^{-3} Pa
$T_{sub.}$=610°C

(a)

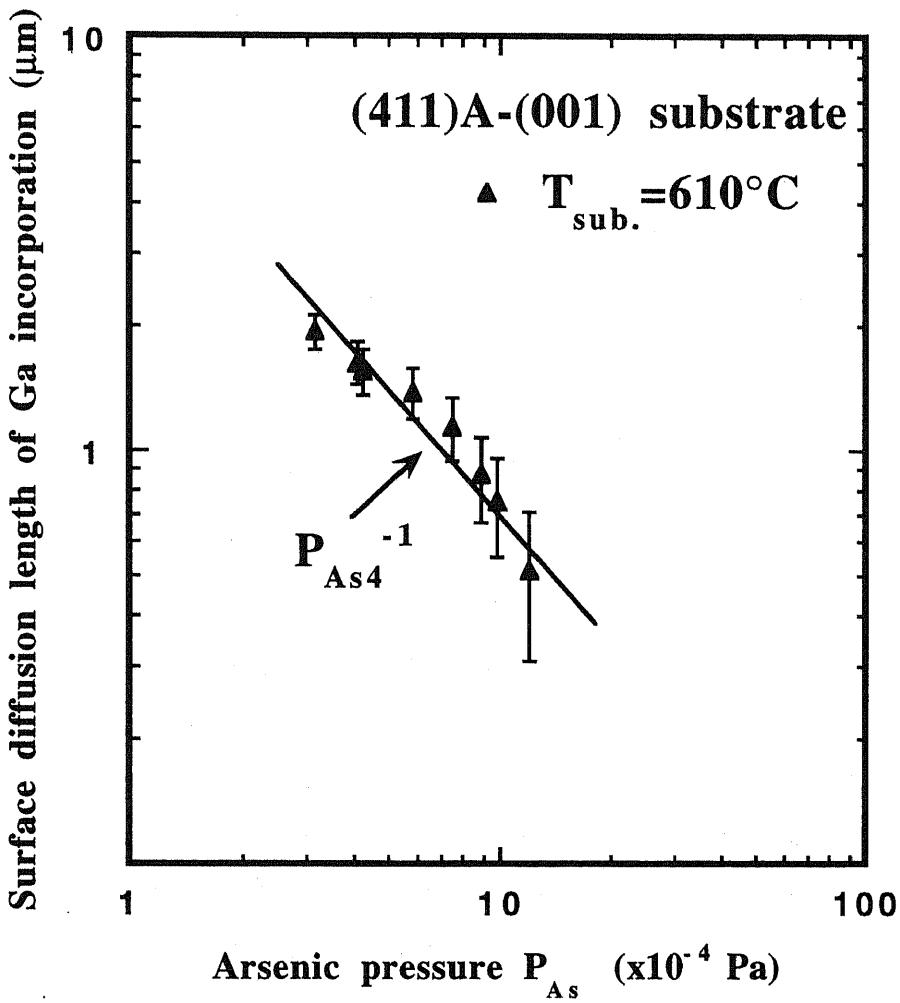

(b)

Figure 3.7. (a) The growth rate distributions and (b) the arsenic pressure dependence of the surface diffusion length of Ga on the (001) GaAs surface with (411)A sidewalls.

§3.5 Ga Flux Dependence of Diffusion Length of Ga on the (001) GaAs Surface

As described in §3.4, the arsenic pressure dependence of the surface diffusion length has been systematically studied. The results show that the surface diffusion length depends strongly on the arsenic pressure. On the other hand, it has been found that the diffusion length is independent of the kind of sidewalls, although the lateral flux of Ga from the (111)A sidewall should be different from that from the (411)A sidewall. In order to completely understand the growth behavior at the step edge, it is also necessary to investigate the Ga flux dependence of the diffusion length.

The lateral flux intensity of Ga can be easily calculated by the use of the distribution of the growth rate and the diffusion length. According to the proposed model, the intensity of the lateral flux at the edge can be expressed by the integration of the growth rate distribution $R_L(x)$ by the distance x from the edge as follows:

$$I = \int_0^\infty \frac{N_0}{d} R_L(x)dx = \frac{N_0 R_L(0)\lambda_{inc.}}{d} \qquad (3.7)$$

where I, $R_L(0)$, $\lambda_{inc.}$, N_0 and d are the intensity of the lateral flux at the edge, growth rate change at the edge, diffusion length on the (001) surface, site density of the (001) GaAs surface and the height of one monolayer of GaAs, respectively.

By use of the eq.(3.7), the intensities of the lateral flux at the edge are calculated based on the experimental data and Fig.3.8 shows the arsenic pressure dependence of the lateral flux intensities of Ga adatoms from the sidewalls of (111)A and (411)A to the (001) surfaces. It is clear that the lateral flux intensity from the (411)A sidewall is nearly two times larger than that from the (111)A sidewall. But, comparing the results of the diffusion length of Ga on the (001) GaAs surface with (111)A and (411)A sidewalls, it is surprised that the diffusion lengths of Ga are almost the same within the experimental error as shown in Fig.3.9. This means that the diffusion lengths of Ga are independent of the Ga lateral flux.

In order to verify this phenomenon, the flux of Ga from the K-cell was varied in the experiments to see how the diffusion length of Ga changes. Fig.3.10 shows the experimental

results. The same as what is described above, the surface diffusion length of Ga on the (001) GaAs surface is also independent of the Ga flux from the K-cell.

Summarizing the above results, it can be said that the surface diffusion length of Ga on the (001) GaAs surface is independent of the Ga flux. This means that the surface diffusion length depends only on the arsenic pressure, not the V/III ratio of the fluxes in the case of NP substrates. This phenomenon is very important for the understanding of the growth mechanism which will be described in the §3.7.

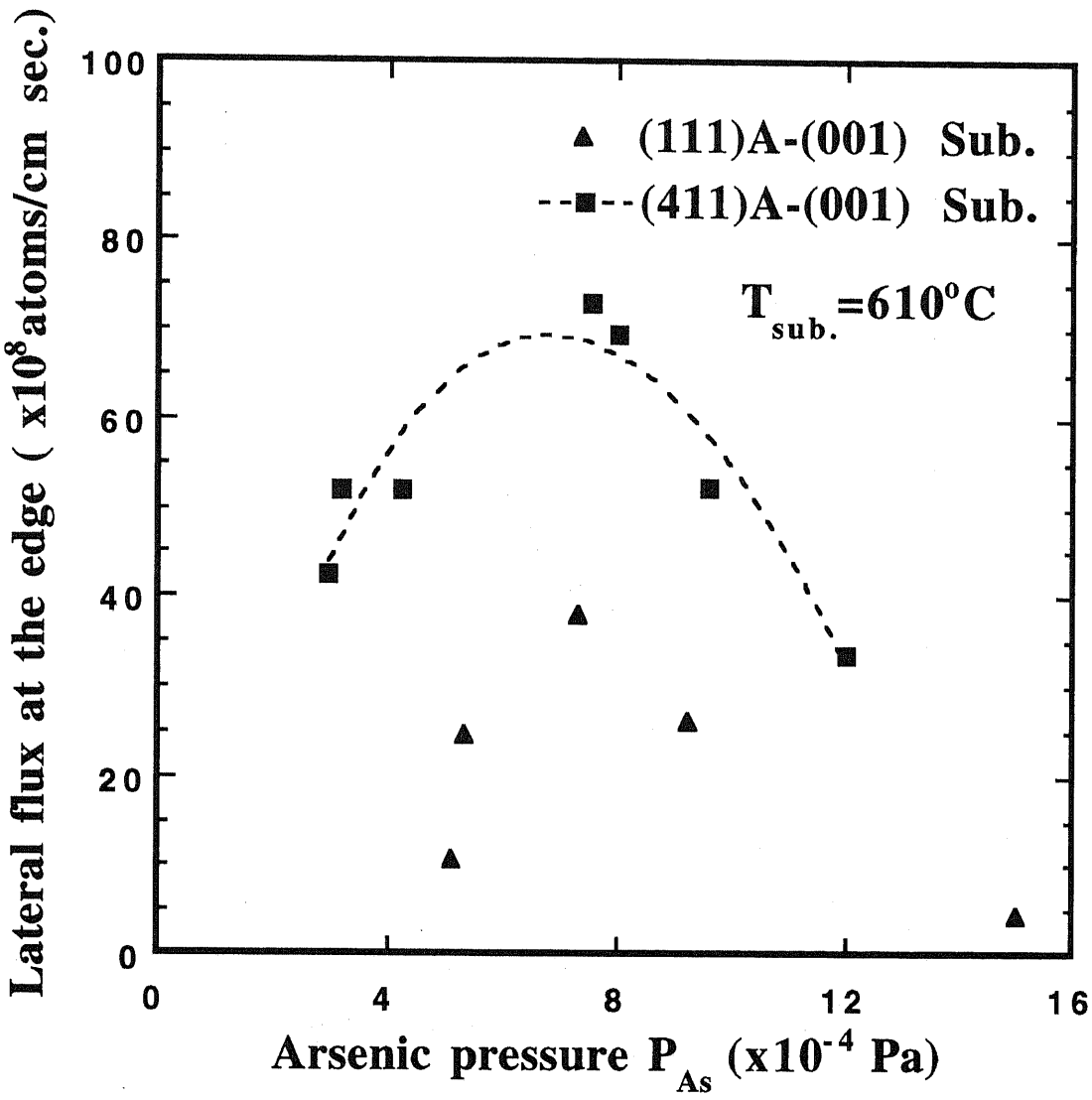

Figure 3.8. Arsenic pressure dependence of the lateral flux intensities of Ga adatoms from the sidewalls of (111)A and (411)A to the (001) surfaces.

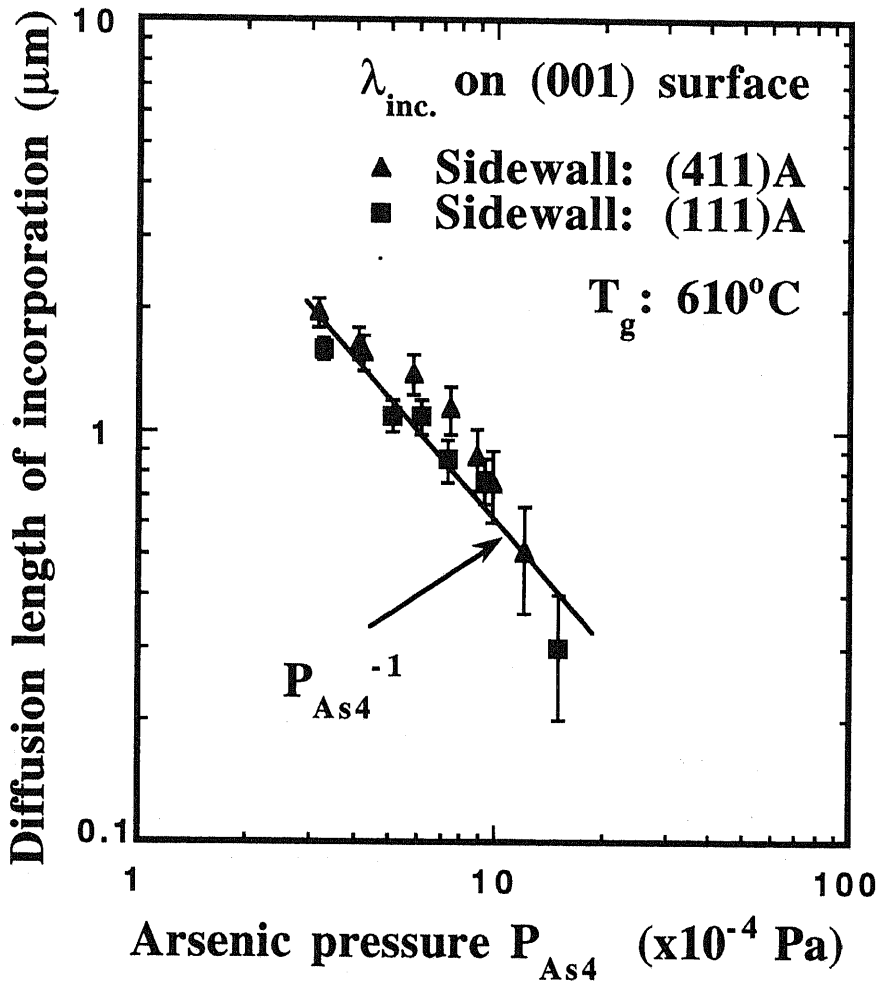

Figure 3.9. The arsenic pressure dependence of the surface diffusion length of Ga on the (001) GaAs surface with (111)A and (411)A sidewalls.

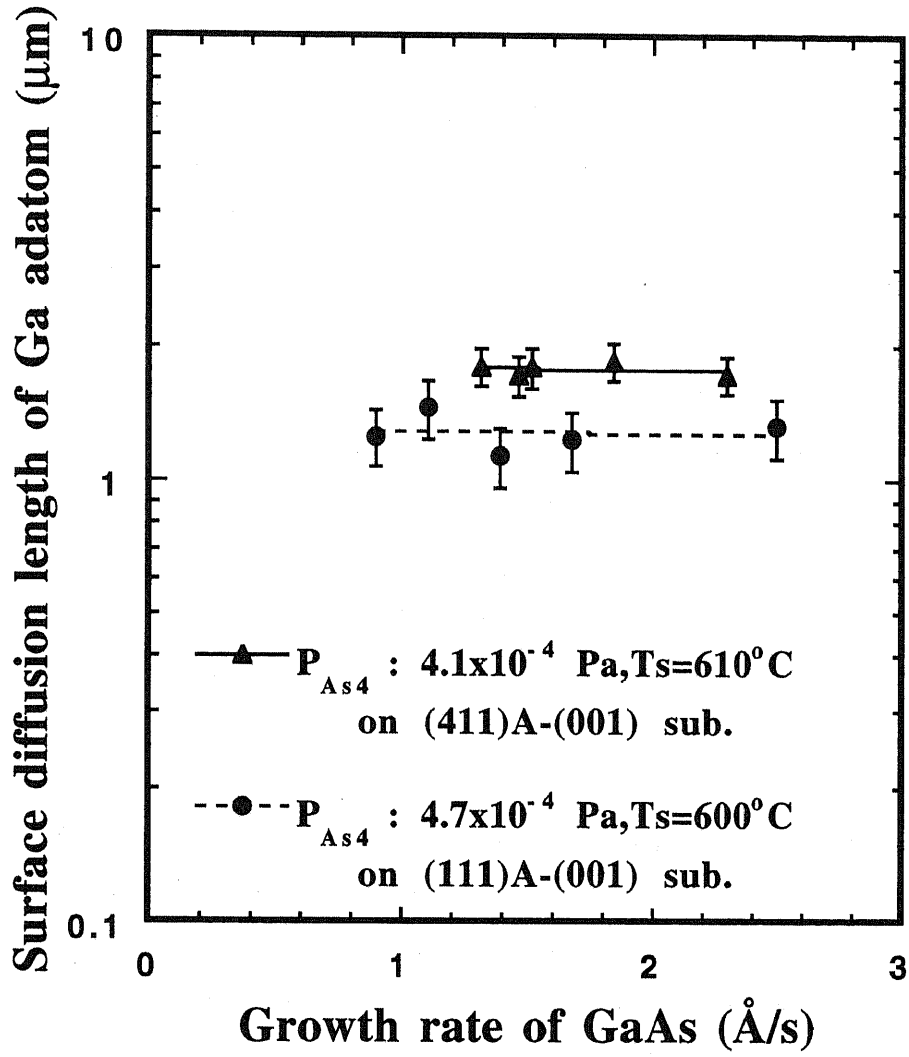

Figure 3.10. The Ga flux dependence of the surface diffusion length of Ga on the (001) GaAs surface.

§3.6 Inter-Surface Diffusion of In on (001) InAs Surface Using (111)A-(001) InAs NP Substrates

There is a strong interest in the growth of lattice mismatched system such as (In,Ga)As/GaAs because of the large energy gap difference and high electron mobility. Therefore, it is required to understand the In surface diffusion during the MBE growth. But it is difficult to observe the RHEED oscillation in the MBE of InAs on GaAs substrates because the surface becomes rough during the growth. According to this difficulty, the measurement of the surface diffusion length of In adatoms during MBE growth has to be done on InAs NP substrates, although it may be somewhat different from what was observed on GaAs NP substrates.

In this section, the inter-surface diffusion of In adatoms on InAs (111)A-(001) nonplanar substrates studied by μ-RHEED images is described. The results obtained in this work are compared with those of Ga on GaAs nonplanar substrates and the growth mechanism is discussed.

3.6.1 Experimental Process

MBE growth of InAs in the present work was carried out on the (111)A-(001) mesa-etched InAs (001) substrate in which grooves were cut along the [110] direction. The NP substrate was prepared by conventional photolithography methods and chemical etching using $HF:H_2O_2:H_2O$ (1:2.5:40 in volume) solution at the room temperature.

After the conventional chemical degreasing, the substrate was brought into the growth chamber of the μ-RHEED/SEM MBE system. The growth temperature was measured by pyrometer and the growth rate of InAs on the flat surface was set at 1.8Å/s. In order to investigate the growth temperature and the arsenic pressure dependence of In surface diffusion length, the growth temperature was changed from 400°C to 500°C and the arsenic pressure was varied from 3.1×10^{-4} Pa to 7.9×10^{-4} Pa. During the growth, the RHEED pattern of (2x4) reconstruction was observed showing that the arsenic-stabilized surface was always maintained.

3.6.2 Migration of In Between (111)A and (001) InAs Surfaces

Fig.3.11 shows the SREM images of the InAs growth rate on the (001) surface near the edge. It can be seen that when the arsenic pressure is relatively low, the growth rate $R_L(x)$ takes a positive value indicating that the In adatoms migrate from the (111)A sidewall to the (001) surface. This behavior is similar to that observed in MBE of Ga on GaAs (111)A-(001) NP substrates. But, when the arsenic pressure is increased, $R_L(x)$ becomes negative. This means that the lateral flux of In migrates from the (001) surface to the (111)A sidewall, while it has not been observed in the GaAs growth on the (111)A-(001) GaAs substrates. The change in migration direction of In lateral flux as described above was found to depend on the growth temperature and the arsenic pressure as shown in Fig.3.12. It is clear that when the growth temperature is high, or the arsenic pressure is low, $R_L(x)$ takes a positive value indicating that the lateral flux of In occurs from the (111)A sidewall to the (001) surface. But, when the growth temperature is low, or the arsenic pressure is high, the migration direction of In is reversed. These results indicate that the inter-surface diffusion of In adatoms between the (111)A sidewall and the (001) surface depends strongly on the growth conditions.

From the proposed model, it can be easily understood that the direction of the lateral flux is determined by the difference of the lifetimes of In incorporation on each surface. When the lifetime on the (111)A sidewall is longer than that on the (001) surface, the lateral flux will flow from the sidewall to the (001) surface. But the lateral flux will migrate from the (001) surface to the sidewall, when the lifetime on the (001) surface is longer than that on the sidewall. According to the experimental results, the direction of the lateral flux depends strongly on the growth conditions. This means that the lifetimes of In incorporation on each surface have different dependency on the growth conditions.

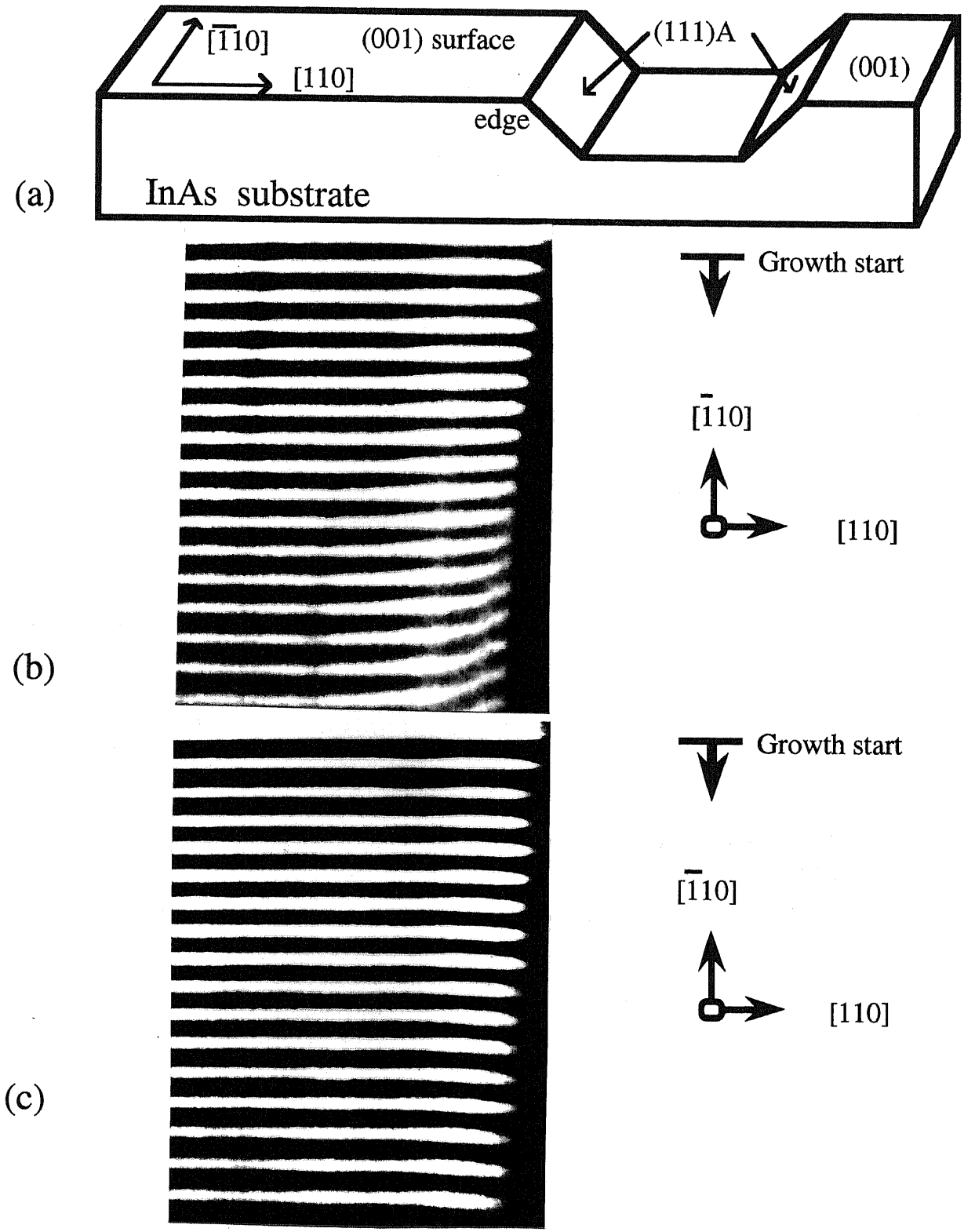

Figure 3.11. SREM images of the InAs growth rate on the (001) surface near the edge. Ts=450°C. (a) Schematic illustration of the NP substrate (b) P_{As4}=3.9x10^{-4} Pa, (c) P_{As4}=5.8x10^{-4} Pa

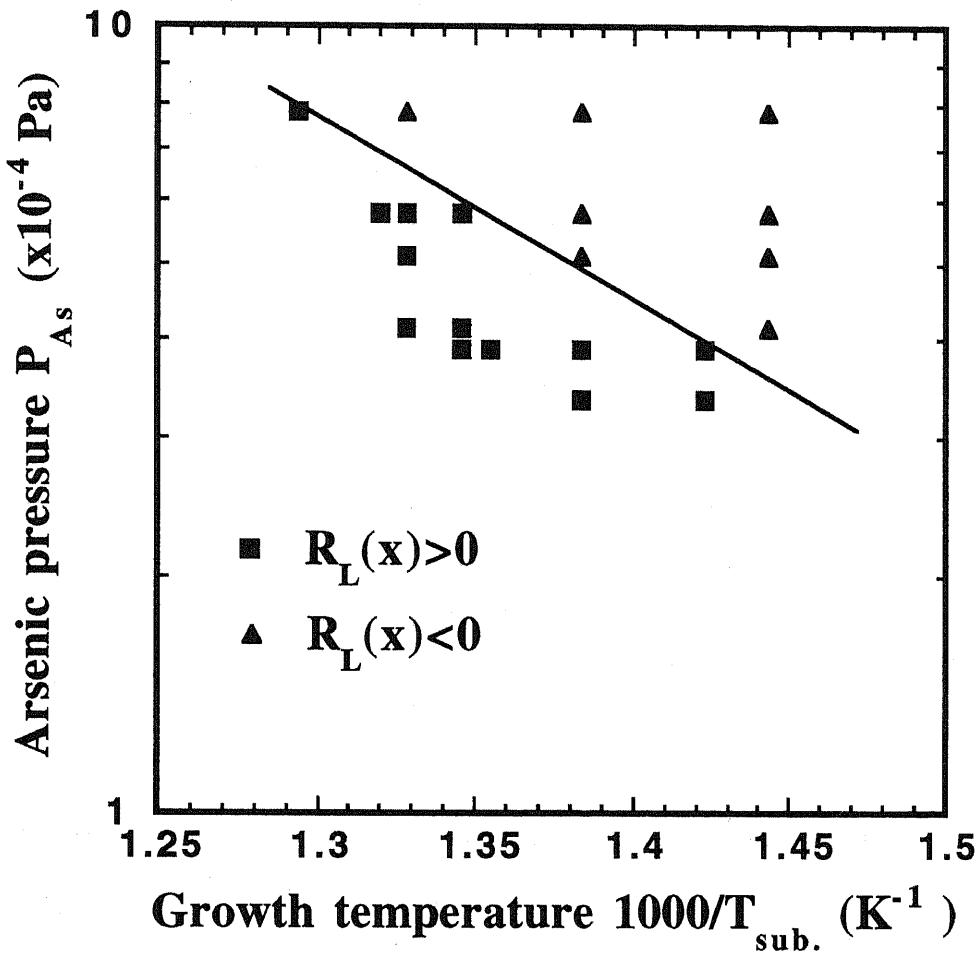

Figure 3.12. The growth temperature and the arsenic pressure dependence of the In lateral flux direction.

3.6.3 Surface Diffusion Length of In on the (001) InAs Surface

As described in §3.2, the growth rate changes exponentially with the distance from the edge and the gradient of the growth rate distribution refers to the converse of the surface diffusion length until incorporation into the crystals. Fig.3.13 shows the growth temperature dependence of the In diffusion length on the (001) surface. It can be seen that the In diffusion length depends on the growth temperature exponentially and the gradient is almost unchanged even if the arsenic pressure is changed. The activation energy for the In surface diffusion on the (001) InAs surface calculated from the dependencies is about 0.81eV which seems to be a little larger than what was calculated for Ga adatoms on GaAs (001) surface (about 0.7eV, Hata et al.1990).

Like the surface diffusion length of Ga on GaAs surface, the surface diffusion length of In on InAs (001) surface also depends strongly on the arsenic pressure as shown in Fig.3.14. The surface diffusion length of In adatoms on the (001) surface increases with the decrease of the arsenic pressure and the dependency is almost proportional to the reverse of the arsenic pressure as that of Ga. Comparing with the data of Ga on GaAs (001) surface, the surface diffusion length of In on InAs (001) seems to be longer than that of Ga on GaAs (001) surface within the same arsenic pressure range although the growth temperature of InAs is much lower than that of GaAs.

In the experiments, it is interesting to note that when the growth temperature and the arsenic pressure were fixed, the surface diffusion length did not change even if the In flux from the K-cell was varied as shown in Fig.3.15. In other words, the surface diffusion length of In on the (001) InAs surface is independent of In flux as that of Ga described in §3.5. This result, together with the results of Ga, may give important information to the incorporation and the detachment processes of Ga (In) and As at step edge as will be discussed in the next section.

From the above experimental results, it is clear that the surface diffusion behavior of In adatoms on the (111)A-(001) NP substrate is quite similar to that of Ga on GaAs (n11)A-(001) except for the change in migration direction of In lateral flux. This change implies that the lifetime of the In incorporation into each surface depends strongly on the growth conditions. According to the proposed model, it can be understood that the direction of the lateral In flux is changed because of the different dependencies of In lifetime on the growth temperature and the arsenic pressure on the (001) surface and the (111)A sidewall.

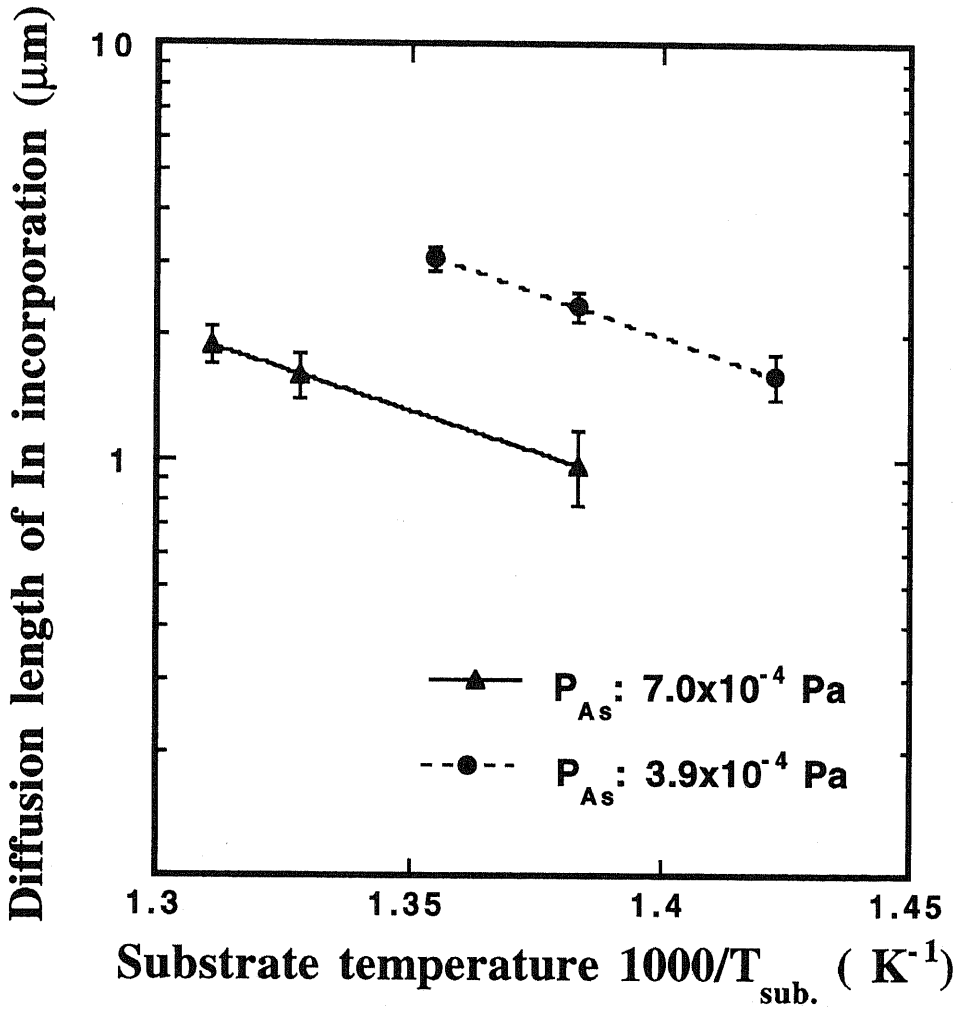

Figure 3.13. Surface diffusion length of In incorporation as a function of growth temperatures.

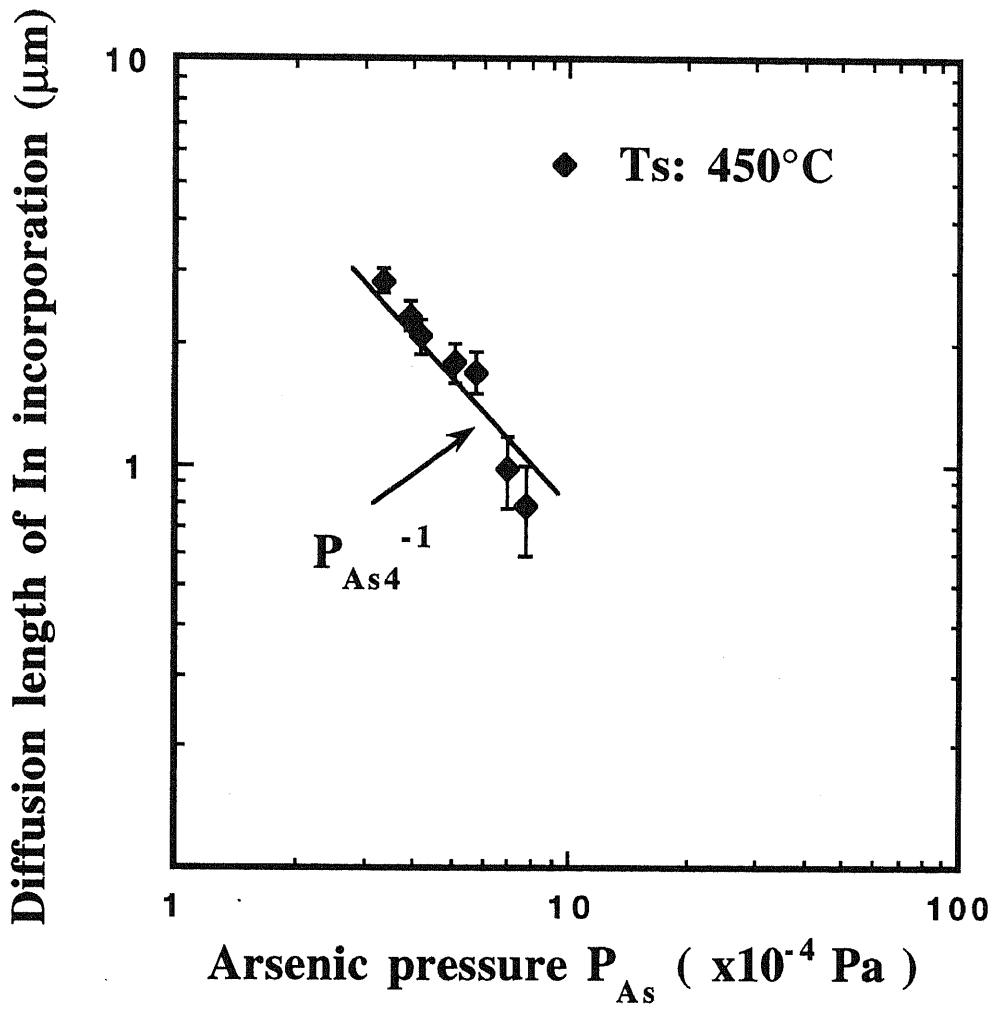

Figure 3.14. Surface diffusion length of In incorporation vs. arsenic pressures.

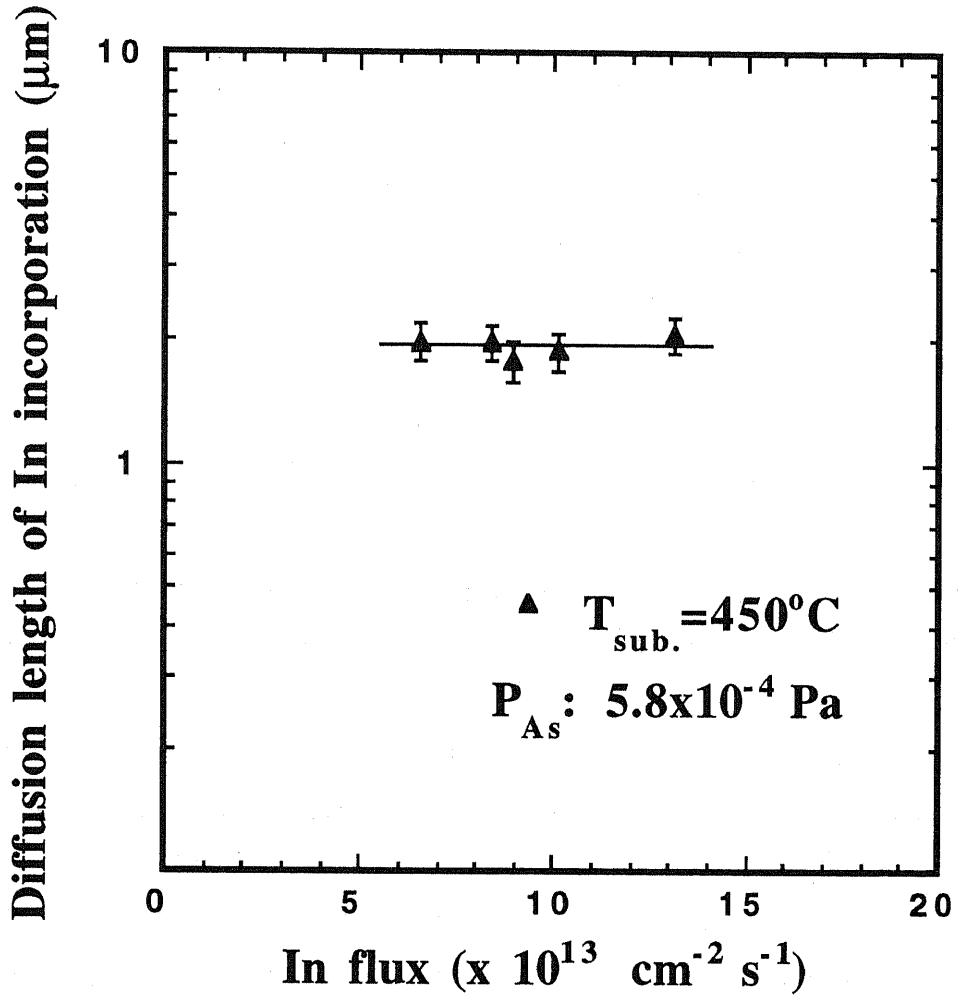

Figure 3.15. The In flux dependence of the surface diffusion length of In on the (001) InAs surface with (111)A sidewalls.

§3.7 Discussion

The diffusion length described here is defined as the distance until incorporation into the crystal. The values obtained in the experiments are about 100 times longer than what was obtained on the vicinal substrates by observing the disappearance of RHEED oscillations (Neave et al.1985). The drastic difference in the diffusion length is supposed to come from the difference in the ratio of As to III adatoms surface flux entering the step edge. In the conventional case, the As flux entering into the step is much larger than that of III atoms, because the usual MBE growth is under the arsenic rich condition. But, in the case of NP substrates, the lateral flux is very strong (Nishinaga et al.1991). Therefore, it is considered that much more III atoms due to the lateral flux hit the step edge than As_4 molecules do. As a result, the entering III adatoms will not be incorporated into the steps unless arsenic atoms come into these steps and fix the III atoms at the position. The unincorporated atoms will go cross many steps until they are incorporated into the crystal. This is quite similar to the MEE growth mode (Horikoshi et al.1989).

The above theoretical consideration is supported by the experimental studies. It was found that the surface diffusion lengths of III adatoms show strong dependence on the arsenic pressures. This gives a direct evidence to the consideration that the III adatom flux entering the steps is larger than that of arsenic flux and the incorporation probability is controlled by the arsenic pressure. Another experimental fact, which shows that the diffusion length is independent of the III flux itself, also gives a proof to the theoretical assumption. Since fluxes entering the steps have already been in the III adatom flux rich state, the change of the III flux will not affect the incorporation probability of III adatoms. With this mechanism, one can understand why the diffusion length obtained in the experiments is very long and depends strongly on arsenic pressure.

From the experimental results, the diffusion length of Ga(In) on the (001) surface is almost independent of the Ga(In) flux. This phenomenon can be understood by considering the above theoretical assumption and the actual reaction process of As_4 on the (001) surface. In the case of GaAs (Foxon et al.1974,1975), it was reported that the desorption of As_4 is expressed by the second order reaction with respect to the incident As_4 pressure at low arsenic surface concentrations. Hence, during the growth, two As_4 molecules will collide and be divided into

eight As atoms due to the second order reaction. But only one As atom is incorporated into the step (kink), the others will desorb as of As_2 or As_4 molecules as shown in Fig.3.16.

As described above, since the surface flux entering the step edges is in the Ga(In)-rich condition and arsenic atoms play an important role in the growth, the growth rate is thought to be determined not only by the Ga(In) flux but also by the arsenic pressure. Here, InAs is taken as an example. Therefore, the growth rate is considered to be proportional to the product of In and As fluxes which can be written as

$$R_{InAs}(x) \propto N_{In}(x) \times P_{As_4}^2, \tag{3.8}$$

where $N_{In}(x)$ is the surface density of In adatoms and P_{As_4} is the arsenic pressure. The factor 2 refers to the second order reaction of As_4.

According to the definition of the growth rate in eq.(6), the formula can be got as:

$$\tau_{In} \propto P_{As_4}^{-2}, \tag{3.9}$$

where τ_{In} is the lifetime of the In until incorporation into the crystal. From this result, it can be understood why the surface diffusion length of the In on the (001) InAs surface is independent of In flux, if the diffusion coefficient is thought to be independent of In pressure. From eq.(3.9), it is concluded that the surface diffusion length of In is proportional to $(P_{As_4})^{-1}$. The same conclusion would be also suit for the GaAs growth. From the arsenic pressure dependencies of the diffusion length of Ga in Fig.3.9 and In in Fig.3.14, the experimental values actually lie almost on $(P_{As_4})^{-1}$ line within the experimental error.

From the above discussions, the image of the MBE growth process becomes quite clear in the case of the NP substrates. The difference of the adatom stoichiometry entering the steps is thought to be the explanation for the drastic difference of the diffusion length of incorporation between the conventional plane substrates and the NP substrates.

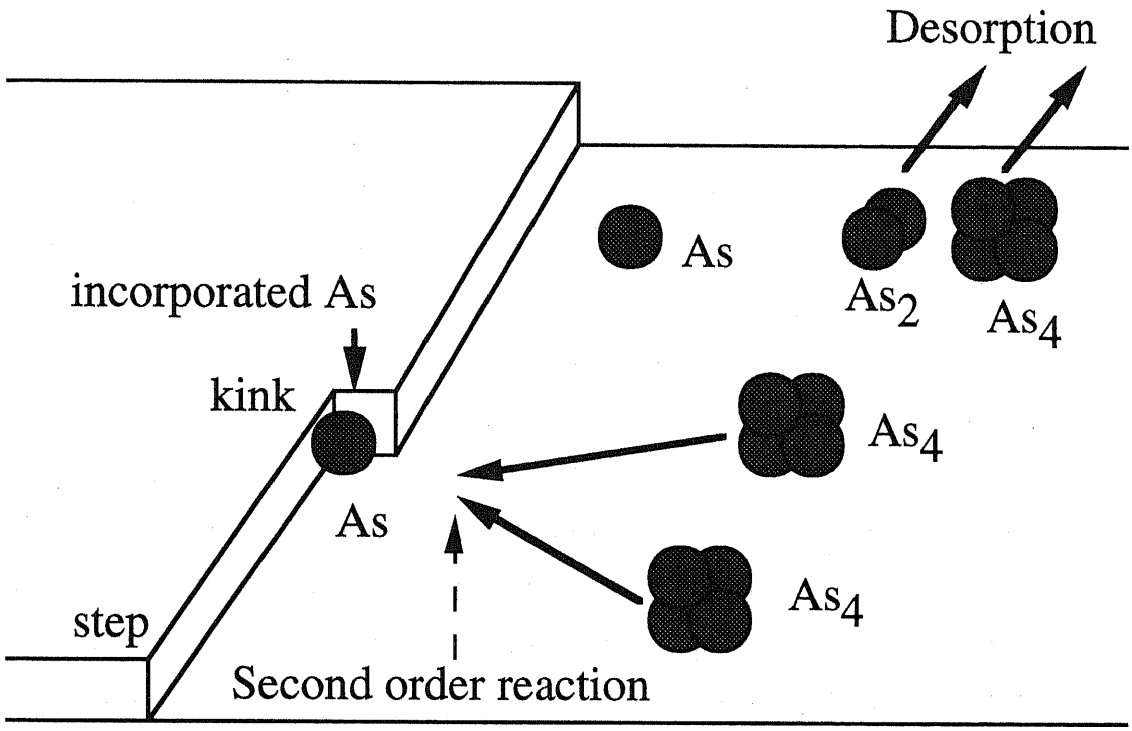

Figure 3.16. Schematic illustration of the chemical second reaction process of As_4 on the surface

§3.8 Summary

Firstly, a simple model, assuming one-dimensional surface diffusion equation, is proposed. The lifetime of Ga adatoms until incorporation into the crystal on each surface is introduced in this model. The surface chemical reaction processes are also taken into account for the understanding of the experimental results.

Then the dependence of surface diffusion of Ga adatoms on arsenic pressure during MBE growth on NP substrates with (111)A and (411)A sidewalls are studied by the μ-RHEED/SEM MBE system. The surface diffusion length of Ga adatoms shows strong dependence on arsenic pressure, while it is almost independent of Ga flux from the sidewall and the K-cell. The results can be explained well by the proposed model.

The inter-surface diffusion of In adatoms between the (111)A and the (001) surface on the InAs (111)A-(001) NP substrate is also investigated by μ–RHEED. The surface diffusion length of In adatom incorporation on the (001) InAs surface is found to be longer than that of Ga on the GaAs (001). It turns out that the diffusion length depends strongly on the growth temperature and the arsenic pressure, while it is independent of In flux as Ga does. Furthermore, it is observed that the migration direction of In lateral flux between the (111)A and the (001) InAs surface is changed depending on the growth conditions. This behavior is different from that of Ga adatoms on GaAs (111)A-(001) NP substrates.

At last, from the results obtained, the great contradiction of the surface diffusion length between the conventional plane substrate and the NP substrate is explained by considering the different condition of the adatom stoichiometry entering the step in both cases.

Chapter 4 Inter-Surface Diffusion of Ga Adatoms Between (111)B-(001) GaAs Surfaces

§4.1 Introduction

Surface diffusion is one of the most important processes during MBE growth and sometimes it plays a major role in determining the growth process. With the development of the growth and characterization techniques, it is possible now to measure the surface diffusion length. Among them, μ-RHEED/SEM MBE system is most powerful, since it directly gives the diffusion length of incorporation as described in chapter 3. It was reported that on the (111)B-(001) mesa-etched substrates, the growth rate $R_L(x)$ of GaAs on (001) surface takes the negative values as an exponential function of the distance from the edge due to the lateral flux of Ga adatoms from (001) surface to the (111)B sidewall (Hata et al.1990), i.e. $R_L(x)<0$. In their studies, the surface diffusion lengths of Ga adatoms on the (001) surface along the [$\bar{1}$10] direction was estimated to be about 8μm at 560°C, which is much longer than that along [110] direction. Koshiba et al.(1992) reported that on the ridge NP substrates with (111)B sidewalls, the growth rate $R_L(x)$ takes the positive value, which means that the lateral flux of Ga flows from the (111)B sidewall to the (001) surface. The diffusion length they obtained was about 1μm, which almost the same as that along [110]. But there have been no reports until now concerning the arsenic pressure dependence of surface diffusion length and the migrating direction of Ga adatoms on (111)B-(001) mesa-etched substrates.

On the other hand, it is difficult to obtain the surface diffusion coefficient from the present experiments, because there is no reliable data for the lifetime, although the surface diffusion length has already been obtained. Nishinaga et al.(1988) reported that the surface diffusion coefficient of (001) GaAs surface is 5×10^{-9} cm^2/s at 580°C by studying the disappearance of the RHEED intensity oscillation. Ohno et al.(1994) proposed that the surface diffusion coefficient of (001) GaAs surface varies from 10^{-11} cm^2/s to 10^{-6} cm^2/s at different temperature by the first parameter-free calculations. These studies described above concern the

surface diffusion coefficient on (001) GaAs surface, however, there is no such data of (111)B GaAs surface.

In this chapter, detailed studies on the arsenic pressure dependence of surface diffusion of Ga adatoms on (111)B-(001) mesa-etched GaAs substrates are performed for the first time by the method of μ-RHEED as described in chapter 3. The inter-surface migrating of Ga adatoms from or to the (111)B sidewalls and the arsenic pressure dependence of the surface diffusion length of Ga atoms on (111)B and (001) GaAs surfaces are investigated. The growth mechanism is also discussed by the model proposed in chapter 3. From the experimental data and the proposed model, the ratio of surface diffusion coefficients of (111)B and (001) GaAs surfaces is calculated for the first time.

§4.2 Experimental Methods

4.2.1 Substrate Preparations

MBE growth of GaAs in the present work was carried out on the (111)B-(001) mesa-etched GaAs substrates where the grooves were along [110] direction. The mesa-etched GaAs substrates were prepared by conventional photolithography methods and chemical etching. In the experiments, two kinds of NP substrates were used in order to measure the diffusion lengths both on the (001) surface and the (111)B surface. Therefore, the NP substrates with the top (001) surface and the (111)B sidewall were etched in the H_3PO_4:H_2O_2:H_2O (8:1:1 in volume) solution at 80°C for 5 seconds, while the NP substrates with the top (111)B surface and the (001) sidewall were etched in the NH_4OH:H_2O_2:H_2O (4:1:20 in volume) solution at 0°C for 7 min. After the conventional chemical degreasing, the substrates were introduced into the chamber of μ-RHEED/SEM MBE system.

4.2.2 MBE Growth

In the present work, exactly the same technique as described in chapter 3 was employed. The incident electron beam was in [110] direction at a glancing angle about 1° and the distribution of growth rates on the (001) or (111)B surfaces near the edge of the (111)B or (001) sidewalls was derived by measuring the intervals of the stripes using the image processor.

The growth temperature for the diffusion length measuring on the (001) surface was set at 600°C and the growth rate of GaAs was about 1.0 Å/sec on (001) flat place. In order to investigate the As_4 pressure dependence of the Ga surface diffusion, the As_4 pressures were varied from 2.5×10^{-4} Pa to 1.33×10^{-3} Pa during the growth and the RHEED patterns were kept on (2x4) reconstruction showing the arsenic stabilized surface.

For the measurement of the diffusion length of Ga on the (111)B surface, the growth rate of GaAs was set about 1.0 Å/sec. During the growth, the growth temperatures were changed from 500°C to 550°C. The measurements of $\lambda_{(111)B}$ were difficult to carry out at the same temperature with that of $\lambda_{(001)}$, because the RHEED oscillations on (111)B surface was unable to detect at this temperature.

§4.3 Surface Diffusion of Ga on the (001) Surface Along [$\bar{1}$10] Direction With (111)B Sidewalls

4.3.1 Inter-Surface Diffusion of Ga Between (001) and (111)B Surfaces

Fig.4.1(b) and (c) show the typical images of SREM during the MBE growth on the (001) surface near the edge of (111)B sidewalls in the experiments. From Fig.4.1(b), it can be seen that at the high arsenic pressure, horizontal stripes according to the RHEED intensity oscillations appear in the image of the upper (001) surface after the start of the MBE growth and the intervals between the stripes near the edge of the (111)B sidewalls are wider than that on the (001) surface far away from the edge. This is the same results as reported by Hata et al.(1990), i.e. $R_L(x)<0$, which correspond to the decreasing in growth rate of GaAs on the (001) surface near the edge.

But it was found in the experiments that when arsenic pressures were lowered down under a critical point of about 4.0×10^{-4}Pa, the shape of stripes near the edge of (111)B sidewalls shows the opposite phenomenon as shown in Fig.4.1(c) comparing with the case at the high arsenic pressure. The intervals between the stripes near the edge of the (111)B sidewalls are narrower than that on the (001) surface far from the edge suggesting the increase in the growth rate of GaAs on the (001) surface near the edge, i.e. $R_L(x)>0$, although the absolute narrowness is not so large.

Fig.4.2 illustrates the growth rate distributions of GaAs on the (001) surface near the edge under various arsenic pressures. It can be seen that the increase and the decrease in the growth rate show the exponential dependence on the distance from the edge and the gradients of the $\log R_L(x)$ increase with the increase of the arsenic pressures, suggesting that the surface diffusion length of Ga adatoms on the (001) surface depends strongly on the arsenic pressures.

The increase and the decrease in the growth rate of GaAs imply that the direction of the inter-surface migration of Ga adatoms on such substrates depends strongly on the arsenic pressures. According to the model proposed in chapter 3, It is considered that the difference of the lifetime of Ga adatom until incorporating into the crystals on the (001) surface and the (111)B sidewall determines the directions of the lateral flux. From the above experimental results, it is expected that the lifetime on each surface depends strongly on the arsenic pressure. When the lifetime on the (111)B sidewall is longer than that on the (001) surface, the Ga

adatoms migrate from the (111)B sidewall to the (001) surface resulting in the increase of the growth rate of GaAs on the (001) surface near the edge, i.e. $R_L(x)>0$. However, it leads to the decrease of the growth rate of GaAs, $R_L(x)<0$, when the incorporation time on the (001) surface is longer than that on the (111)B sidewall. Furthermore, the arsenic pressure dependence of the lifetime is expected to be quite different to each other, which will be described in §4.6. Therefore the competitions of the lifetime on each surface under various arsenic pressures result in the change of the direction of the surface migration of Ga adatoms on (111)B-(001) mesa-etched substrates.

4.3.2 Arsenic Pressure Dependence of the Diffusion Length

The relations between the surface diffusion length and the arsenic pressures during the MBE growth derived from the distributions of the growth rate on the (001) surface near the edge of (111)B sidewalls are shown in Fig.4.3. It is clear that the surface diffusion lengths of Ga adatoms on the (001) surface along $[\bar{1}10]$ direction vary from about 0.25 μm to 1.2 μm within the arsenic pressure range. It is necessary to point out here that the surface diffusion length of Ga adatoms seems to be independent of the direction of Ga adatoms migrating from or to the (111)B sidewall. Hata et al.(1990) reported that the surface diffusion length of Ga adatoms along the $[\bar{1}10]$ direction is about 8 μm at 560°C which is about 8 times longer than that along the [110] direction. In the present results, it shows that the surface diffusion length of Ga adatoms along the $[\bar{1}10]$ direction is almost the same as that along the [110] direction, which has been reported in chapter 3. This result illustrates the isotropy of the surface diffusion length on the (001) surface along $[\bar{1}10]$ and [110] directions within the same arsenic pressure range.

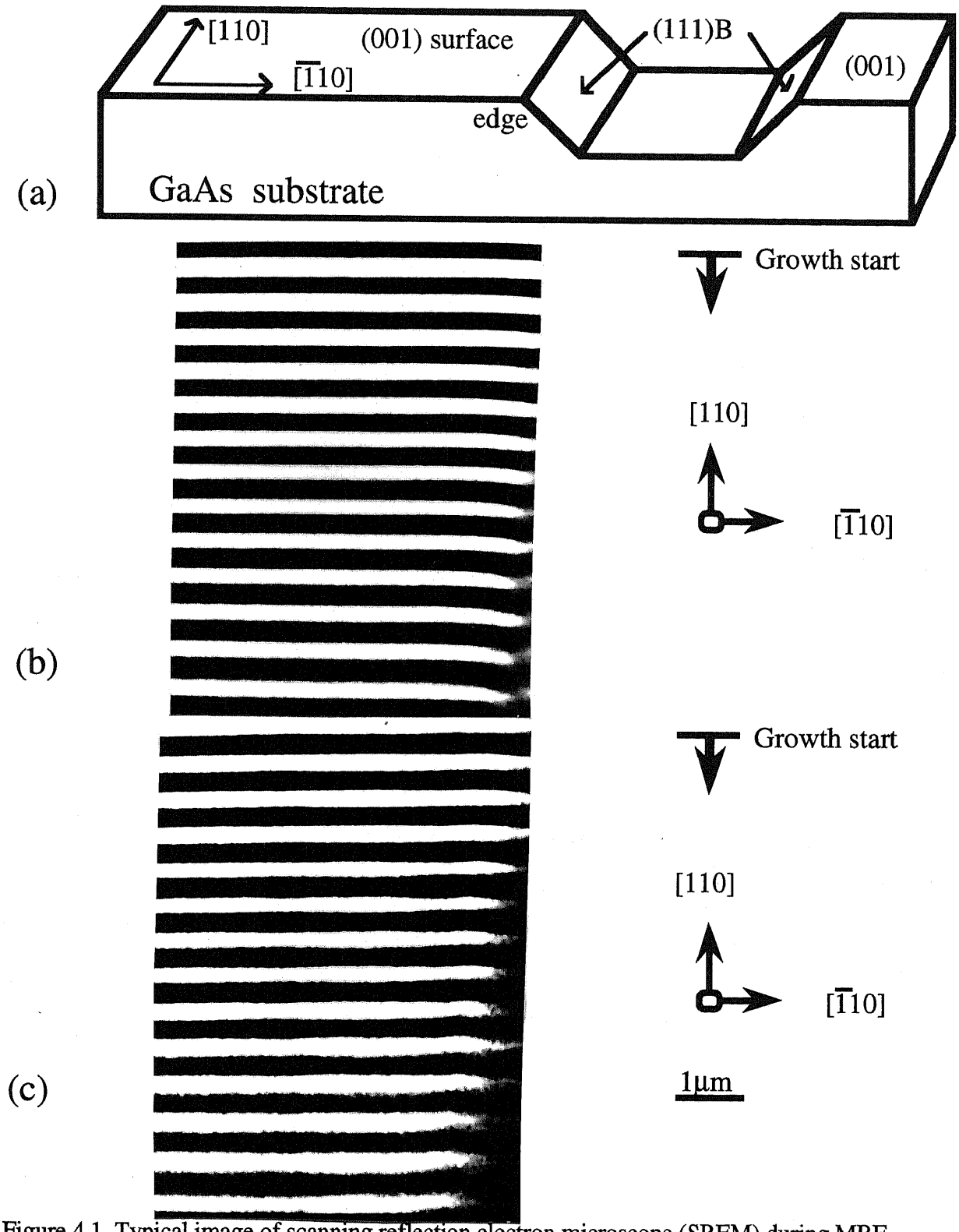

Figure 4.1. Typical image of scanning reflection electron microscope (SREM) during MBE growth on (001) surface near the edge of (111)B sidewalls. (a) a schematic illustration of the substrate, and the SREM image showing the decrease in the growth rate of GaAs (b)at high As_4 pressure, (c) at low As_4 pressure.

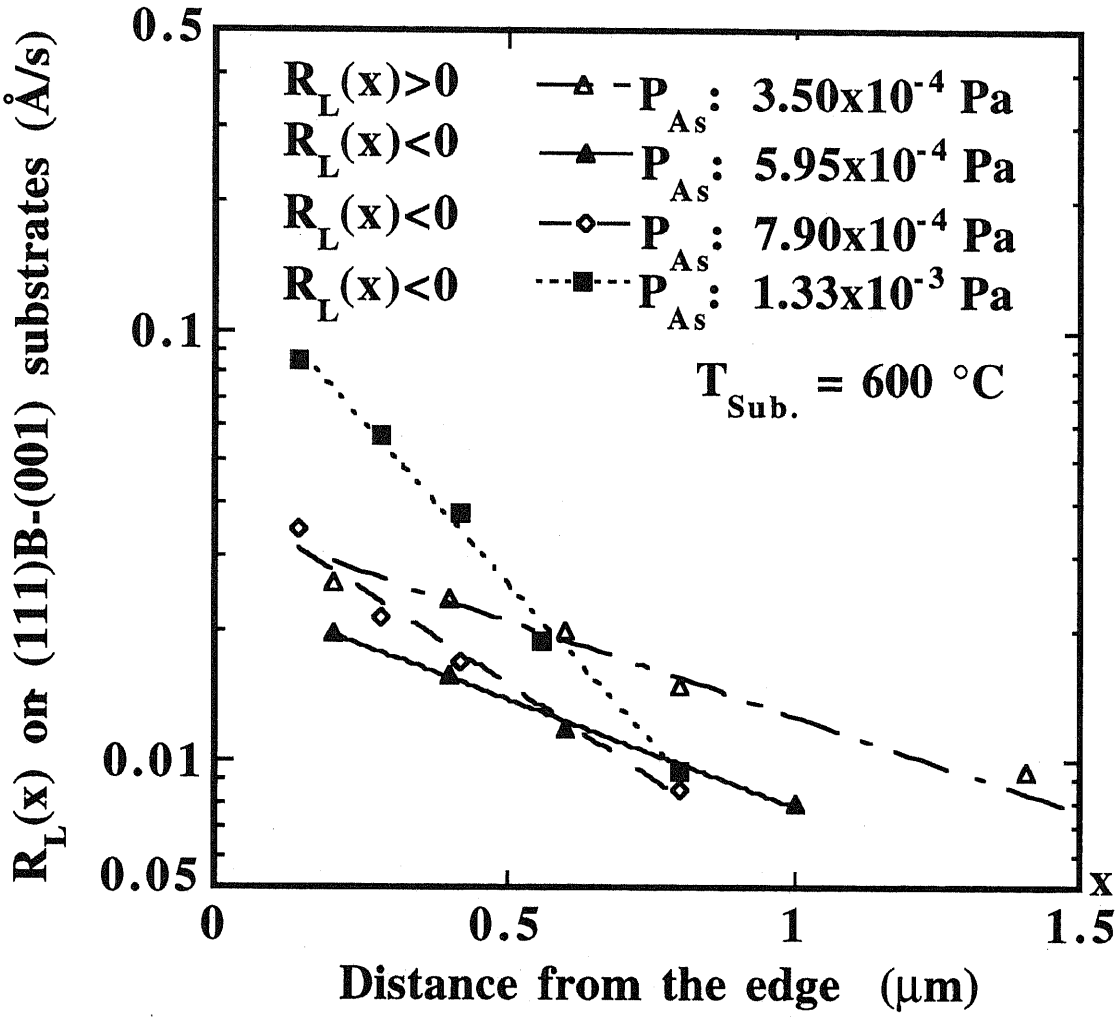

Figure 4.2. The distributions of the growth rates on the (001) surface near the edge as a function of the distance from the edge of (111)B sidewalls.

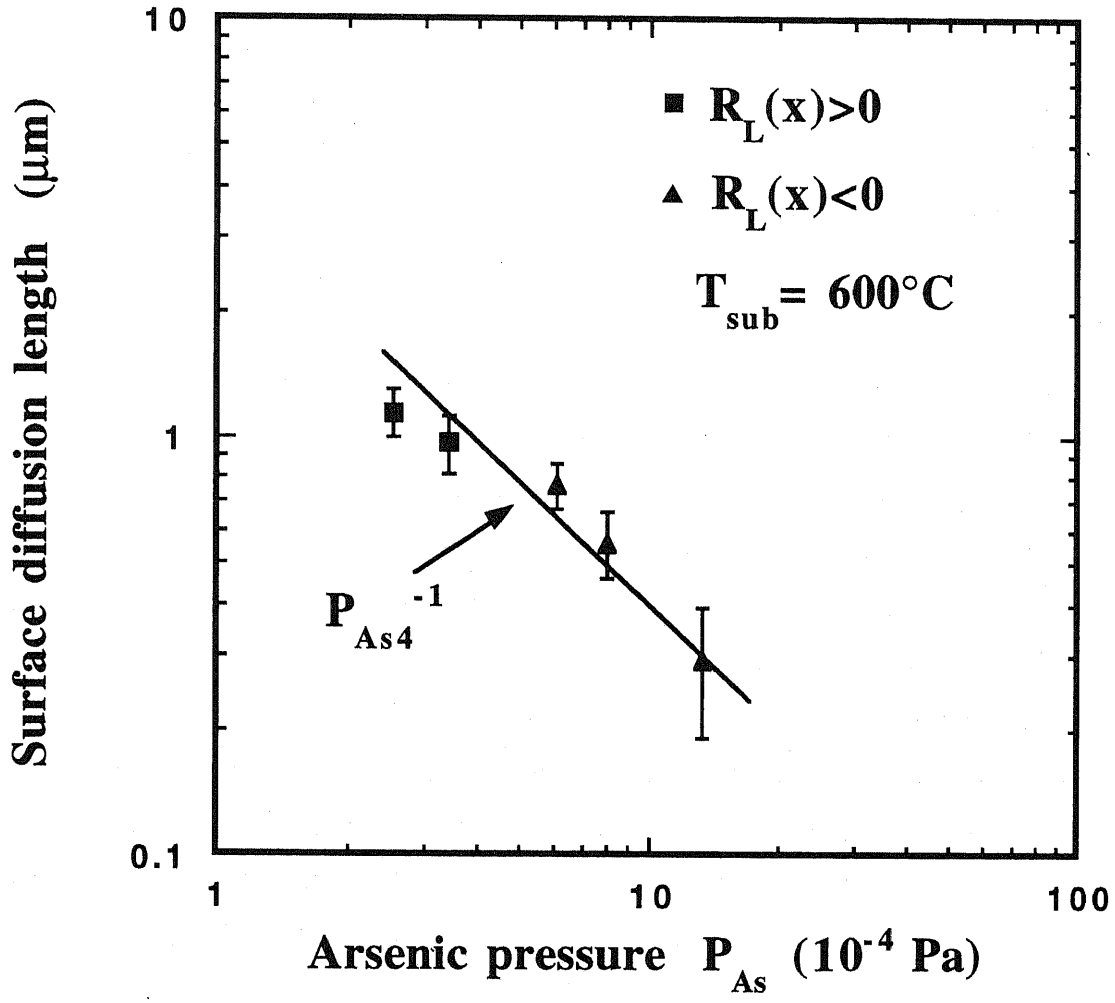

Figure 4.3. The dependence of the surface diffusion length of Ga adatoms on arsenic pressures under (2x4) surface reconstruction condition.

§4.4 Diffusion Length of Ga on the (111)B Surface

The experiments were carried out in μ-RHEED/SEM MBE system. The method of the surface diffusion length measurement was the same as described above. Fig.4.4 shows the arsenic pressure dependence of surface diffusion length of incorporation λ on the (111)B GaAs surface. The growth temperature is 545°C and the $\lambda_{(001)}$ on the (001) surface is also shown in the same figure. It is clear that $\lambda_{(111)B}$ is much longer than $\lambda_{(001)}$ in the same arsenic pressure range, although the growth temperature for $\lambda_{(111)B}$ measurement is lower than that for $\lambda_{(001)}$. Furthermore, the arsenic pressure dependence of surface diffusion length is different on the (001) and the (111)B surface, where the $\lambda_{(111)B}$ depends much more strongly on arsenic pressure than $\lambda_{(001)}$. This agrees very well with what we theoretically predicted in the section 4.3.1. The measurements of $\lambda_{(111)B}$ were difficult to carry out at the same temperature with that of $\lambda_{(001)}$ is because at this temperature, the RHEED oscillations on (111)B surface was unable to detect. Therefore, the temperature dependence of $\lambda_{(111)B}$ was also measured as shown in Fig.4.5, in order to extrapolate the results of $\lambda_{(111)B}$ to the same temperature as that of $\lambda_{(001)}$ for the calculation of the ratio of surface diffusion coefficient on the (111)B and the (001) surfaces. There is a transition of surface reconstruction near 520°C. When the temperature is higher than 520°C, the reconstruction shows the $\sqrt{19}x\sqrt{19}$, which refers to the Ga-stabilized surface. When the temperature is lower than 520°C, 2x2 reconstruction is observed indicating the arsenic stabilized surface condition. At the transition temperature, the reconstruction shows the change from 2x2 to $\sqrt{19}x\sqrt{19}$. Under the different surface reconstruction, the temperature dependence of the $\lambda_{(111)B}$ is different, as illustrated in Fig.4.5. This result is the same as already reported by Nomura et al.(1994)

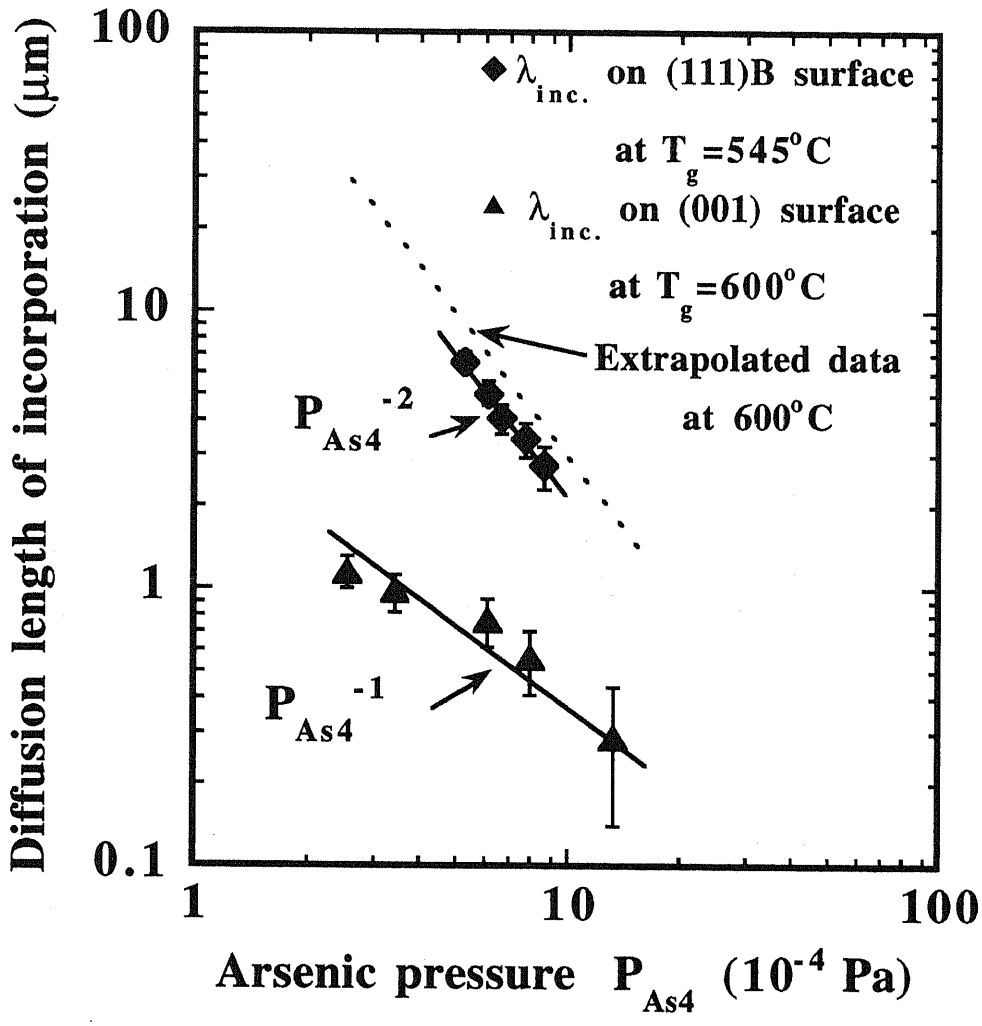

Figure 4.4. Arsenic pressure dependencies of surface diffusion length of Ga incorporation on (001) surface at 600°C and (111)B at 545°C. The dotted line is the extrapolated data at 600°C from the experimental data at 545°C.

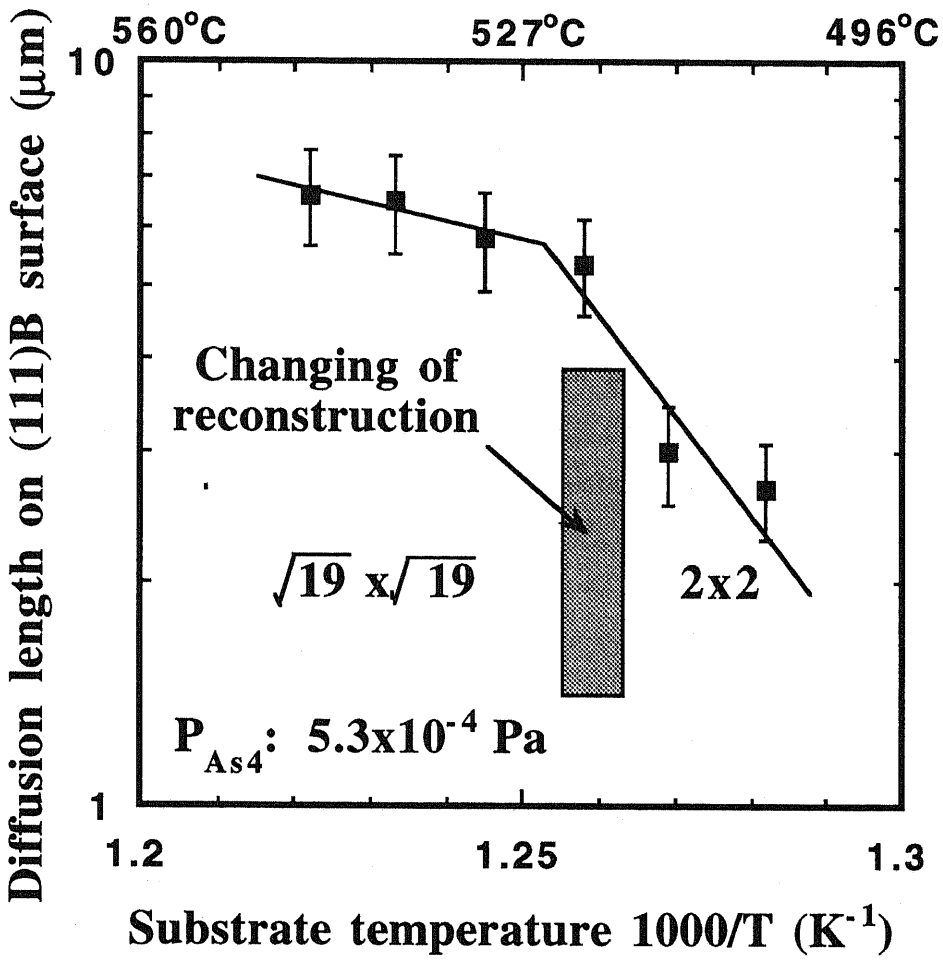

Figure 4.5. Growth temperature dependence of surface diffusion length of Ga incorporation on (111)B surface under 2x2 and $\sqrt{19}$x$\sqrt{19}$ surface reconstruction conditions.

§4.5 Determinations of the Ratio of the Surface Diffusion Coefficient of (111)B and (001) Surfaces

By solving one dimensional diffusion equation as described in chapter 3, one gets $R_L^{(001)}$, a component of the growth rate on the (001) surface caused by a lateral flux from or to the (111)B surface, as

$$R_L^{(001)}(x) = \frac{R_V^{(001)}(\lambda_{(111)B}^2 \cos\theta - M\lambda_{(001)}^2)}{(M\lambda_{(001)} + \lambda_{(111)B})\lambda_{(001)}} \exp(-\frac{x}{\lambda_{(001)}}), \qquad (4.1)$$

where M is $D_{(111)B}/D_{(001)}$ with $D_{(111)B}$ and $D_{(001)}$ respectively the surface diffusion coefficients on (111)B and (001) surfaces. $R_V^{(001)}$, θ, $\lambda_{(001)}$ and $\lambda_{(111)B}$ are the growth rate on the (001) surface by the direct flux from Knudsen cell, the angle between (001) and (111)B surfaces, surface diffusion length of incorporation on the (001) and the (111)B GaAs surface, respectively. Therefore, the ratio of surface diffusion coefficient M can be determined by using eq.(4.1) and the experimental data.

$$M = \frac{\lambda_{(111)B}(R_V^{(001)}\lambda_{(111)B}\cos\theta - R_L^{(001)}(0)\lambda_{(001)})}{\lambda_{(001)}^2(R_L^{(001)}(0) + R_V^{(001)})}, \qquad (4.2)$$

where $R_L^{(001)}(0)$ is the growth rate at the edge due to the lateral flux.

It is assumed that the arsenic pressure dependence of the diffusion length on the (111)B is the same at different growth temperature, if the reconstruction is kept without changing. From Fig.4.5, it is clear that when the growth temperature is 600°C, the reconstruction of (111)B surface is $\sqrt{19}$x$\sqrt{19}$. Therefore, the temperature dependence of $\lambda_{(111)B}$ under $\sqrt{19}$x$\sqrt{19}$ in Fig.4.5 should be used, when the $\lambda_{(111)B}$ is calculated at 600°C from the value at 545°C. The extrapolated data (dotted line) is shown in Fig.4.4. In the calculation, the experimental data of $R_V^{(001)}$, $\lambda_{(001)}$ and $R_L^{(001)}(0)$ are also used, while the data of $\lambda_{(111)B}$ at 600 °C is extrapolated by using the data at 545°C as shown in Fig.4.4.

Fig.4.6 shows the arsenic pressure dependence of the surface diffusion coefficient ratio M. It is interesting that the value of M is as large as 140, and is almost independent of arsenic pressure. Namely, the surface diffusion coefficient on (111)B surface is nearly 140 times

larger than that on (001) surface at 600°C. It is also interesting that M does not show arsenic pressure dependence when the reconstruction is kept unchanged. This probably means that the surface diffusion coefficient is independent of arsenic pressure under the same surface reconstruction condition, since it is very difficult to assume two diffusion coefficients for different faces have identical arsenic dependency. This is a direct experimental data about the arsenic pressure dependence of surface diffusion coefficient.

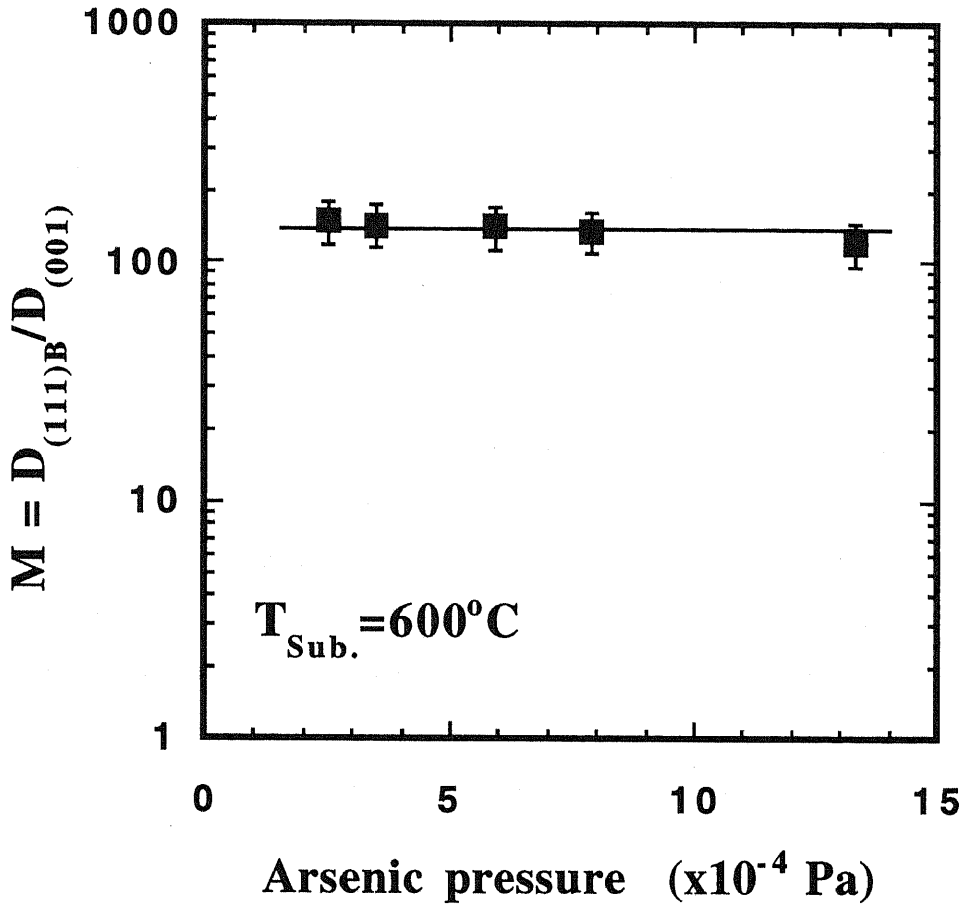

Figure 4.6. Arsenic pressure dependence of the ratio M of surface diffusion coefficient of (111)B and (001) GaAs surfaces.

§4.6 Discussions

From the experimental results, it is found that the arsenic pressure dependence of the surface diffusion length on the (001) and the (111)B surfaces is different from each other, where the diffusion length on the (111)B surface shows the stronger dependence than that on the (001) surface. The results agree quite well with what is expected by the proposed model. As discussed in §4.5, the surface diffusion coefficient seems to be independent of the arsenic pressure. Therefore, the lifetime of incorporation will strongly depend on the arsenic pressure and the dependence can be derived from the relationship between the surface diffusion length of incorporation and the arsenic pressure.

In the present experiments, it is impossible to get the absolute value of the surface diffusion coefficient because there is no reliable data for the lifetime of incorporation. Hence, results by different experiments should be refereed in order to estimate the value of the lifetime of incorporation. It was reported that the value of the critical Ga supersaturation is estimated to be 0.3 ML during the conventional MBE growth on the (001) GaAs surface, by time-resolved RHEED intensity measurements method (Karpov et al.). This result is very important because it means that the surface adatom density is 30% of the site density of the surface, when the 2D growth mode takes place during the MBE growth. By use of this data and the eq.(6), it can be estimated that the lifetime of incorporation on the (001) surface under the present growth condition is in the 10^{-2} s ~ 10^{-1} s order. In other words, the surface diffusion coefficient takes the value in the 10^{-8} cm^2 s^{-1} order using the diffusion length of incorporation in the present work.

In order to verify the theoretical prediction for the inter-surface diffusion between the (001) and the (111)B surfaces as described in §4.3, it is necessary to calculate the arsenic pressure dependence of the lifetime of incorporation on the (001) and (111)B surfaces. Here, the surface diffusion coefficient of the (001) GaAs surface is chosen to be $2x10^{-8}$ cm^2 s^{-1} according to the above discussion, although the absolute value may be somewhat different from the real one. Fig.4.7 shows the calculated results of the arsenic pressure dependence of the lifetime of incorporation on the (001) and (111)B surfaces. In the calculation, the value of the surface diffusion coefficient on the (111)B surface is taken as 140 times larger than that on the (001) surface as described in §4.5 and the diffusion lengths of incorporation described in §4.3 and §4.4 are used.

From Fig.4.7, it is clear that the arsenic pressure dependence of the lifetime of incorporation on the (001) surface is different from that on the (111)B surface. In the high arsenic pressure region, the lifetime on the (111)B is shorter than that on the (001) one, resulting in the lateral flux migrating from the (001) surface to the (111)B one. On the other hand, the lifetime on the (111)B is longer than that on the (001) one in the low arsenic pressure region, which causes the lateral flux migrating from the (111)B surface to the (001) one. This conclusion agrees very well with what is supposed from the model. Furthermore, the cross point of the two lifetime curves is near the 4.8×10^{-4} Pa of the arsenic pressure, which also agrees with the experimental results in §4.3.

From the above discussions, it is clear that the proposed model can explain the experimental results very well and the experimental results also proofs the theoretical predictions. This means that the proposed model is quite successful in explaining the MBE growth behavior on the NP substrates

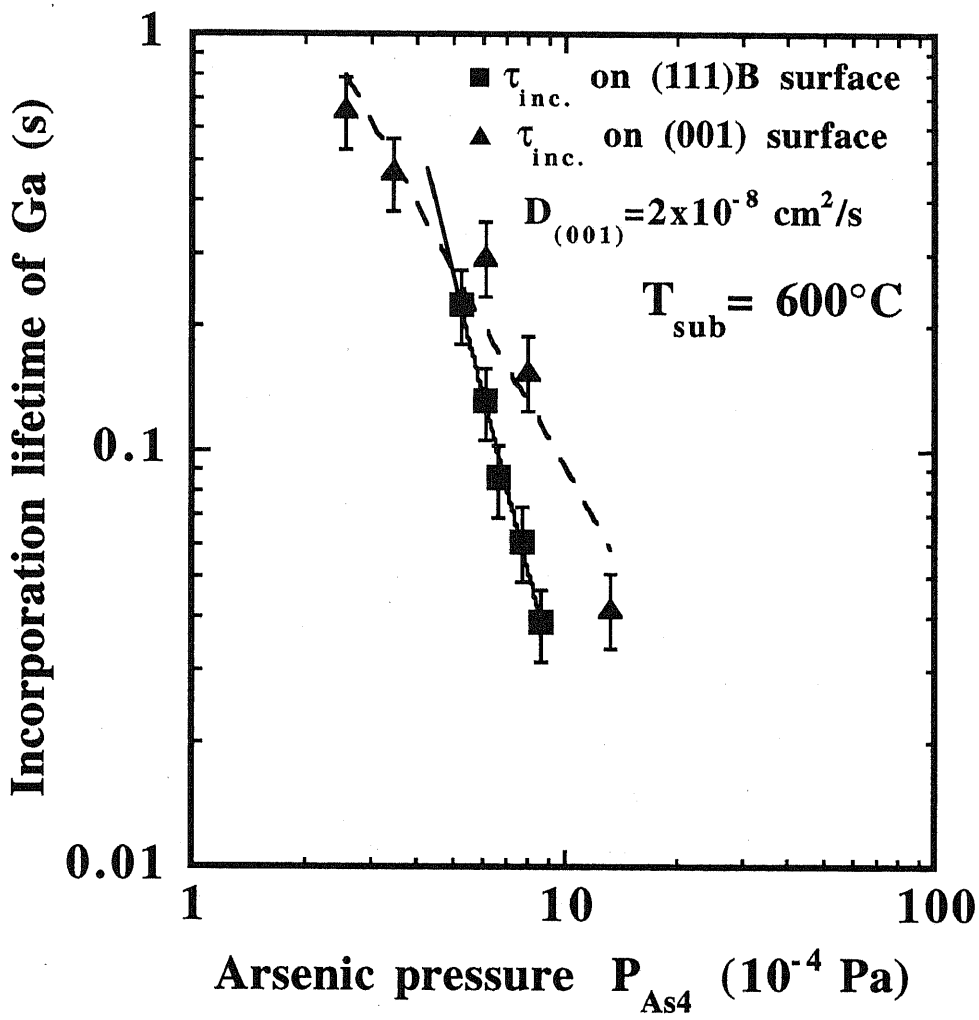

Figure 4.7. Arsenic pressure dependence of the Ga lifetime of incorporation on the (001) and (111)B surfaces.

§4.7 Summary

Arsenic pressure dependence of Ga surface diffusion in MBE growth on (111)B-(001) mesa-etched substrates was investigated by μ-RHEED.

It was observed for the first time that the direction of the lateral migration of Ga adatoms from or to the (111)B sidewall depends on the arsenic pressures on such substrates. Furthermore, the surface diffusion length of Ga adatoms on the (001) surface along [$\bar{1}$10] direction was found to vary with arsenic pressures strongly and as that along [110] direction, however it is independent of the direction of lateral migrations of Ga adatoms. The diffusion length shows isotropy both along [$\bar{1}$10] and [110]. According to the proposed model, it suggests that the lifetime of Ga adatoms until incorporating into the crystal on each surface depends on arsenic pressures strongly.

The surface diffusion length on the (111)B surface were measured, which is longer than that on the (001) surface within the same arsenic pressure range. It was found that the temperature dependence of the diffusion length is quite different at the $\sqrt{19}$x$\sqrt{19}$ and 2x2 surface reconstructions on the (111)B surface. Also, the arsenic pressure dependence of the diffusion length on the (111)B surface is different from that on the (001) surface. This result agrees very well with what was predicted theoretically.

The ratio of surface diffusion coefficients on the (111)B and the (001) GaAs surfaces were investigated. The results indicate that the surface diffusion coefficient on (111)B surface is nearly 140 times larger than that on (001) surface at 600°C. Furthermore, the ratio shows almost no dependence of arsenic pressure, which may imply that the surface diffusion coefficient itself is independent of arsenic pressure under the same surface reconstruction condition.

Chapter 5 Fabrications of GaAs/AlAs Quantum Wire Structures at the Bottom of V-grooves

§5.1 Introduction

Semiconductor quantum-wire (QWR) heterostructures has attracted much interest, since they are expected to exhibit novel and useful properties due to two-dimensional (2D) quantum confinement (Sakaki et al.1980; Arakawa et al.1985,1986; Kapon et al.1989), where these properties can not be realized by conventional superlattices (SL) and quantum wells (QWs). So far a variety of schemes have been proposed and attempted to fabricate QWRs with very narrow size. Among them, the formation of QWRs by directly growing on V-grooved substrates is shown to be one of the most powerful ways to fabricate QWRs without surface damages. Metaloganic Chemical Vapor Deposition (MOCVD) is now mainly used for fabricating QWR structures and QWR lasers on V-grooved substrates (Kapon et al.1989; Tsukamoto et al.1992,1993; Bhat et al.1990; Lee et al.1993; Christen et al.1992; Walther et al.1992), since AlGaAs has the resharpening effect, whereas GaAs tends to grow thicker at the bottom of the V-grooves during the MOCVD growth. The narrowest width of the QWR until now by MOCVD was reported to be about 70Å (Tsukamoto et al.1993). On the other hand, it was found that AlAs, instead of AlGaAs, has the resharpening effect during the MBE growth on the V-grooved substrates, and it has shown the possibility of fabricating multiple or single GaAs/AlAs QWRs on such substrates as described in chapter 2. Although some works have been reported so far on the MBE fabrication of QWRs on V-grooves (Kojima et al.1990; Sugaya et al.1993), there have been no reports on the successful fabrication of QWRs by MBE with very narrow width less than 100 Å to date.

In this chapter, the fabrication results of GaAs/AlAs multiple and single QWRs on V-grooved substrates by MBE are reported. Cross sectional HRSEM, TEM, low-temperature PL and CL are used to characterize the narrow QWRs formed at the bottom of the V-grooves.

§5.2 Quantum Well Tapering and Quantum-wire Structures

The concept of lateral band-gap patterning by epitaxial growth of QWs on NP substrates is illustrated in Fig.5.1, which shows a schematic cross section of a heterostructure grown on a NP substrate. Thin epilayers grown on the different surfaces show lateral thickness variations due to the different flux intensities arriving on each surface and the inter-surface migration between adjacent surfaces. The extremely thin QW structures on each facet will induce the strong transverse confinement energy $E_{conf.}$, which leads to lateral variation in the valence and conduction band edges (Kapon et al.1987).

For infinitely deep QW potential wells, the lateral (y direction) variation in the confinement energy can be given by

$$E_{conf.}^{c,v}(y) = \frac{\hbar^2 \pi^2 n^2}{2m_{c,v}^{*} t^2(y)} \tag{5.1}$$

where n=1,2,3 ··· is the transverse index of the QW energy subband, $m_{c,v}^{*}$ is the carrier effective mass for the conduction (c) and valence (v) bands and t(y) is the lateral thickness distribution.

Therefore, the effective band-gap variation can be expressed by

$$E_{eff}(y) = E_g + E_{conf.}^{c}(y) + E_{conf.}^{v}(y) \tag{5.2}$$

where E_g is the band gap of the bulk semiconductor.

From the above discussion, the lateral variation of the epilayer thickness will result in effective band-gap modulation and induce the lateral confinement of charge carriers. In other words, the thicker QW can trap the charge carriers and the thinner QW works as effective lateral barriers, as shown in Fig.5.1.

Fabricating semiconductor QWR structures at the bottom of V-grooves is just a application of the above discussions. As illustrated schematically in Fig.5.2, when the QW structures are grown on the V-grooved NP substrates, the thickness of the QW at the bottom is thicker than that on the sidewalls due to the different flux intensities arriving on each surface and the inter-surface migration between adjacent surfaces. This induces the lateral confinement

in the bottom QW. Therefore, the quantum confinements both in the vertical and the transverse directions yield 2D carrier confinement, and thus quasi-1D structures (QWR) can be realized in this way.

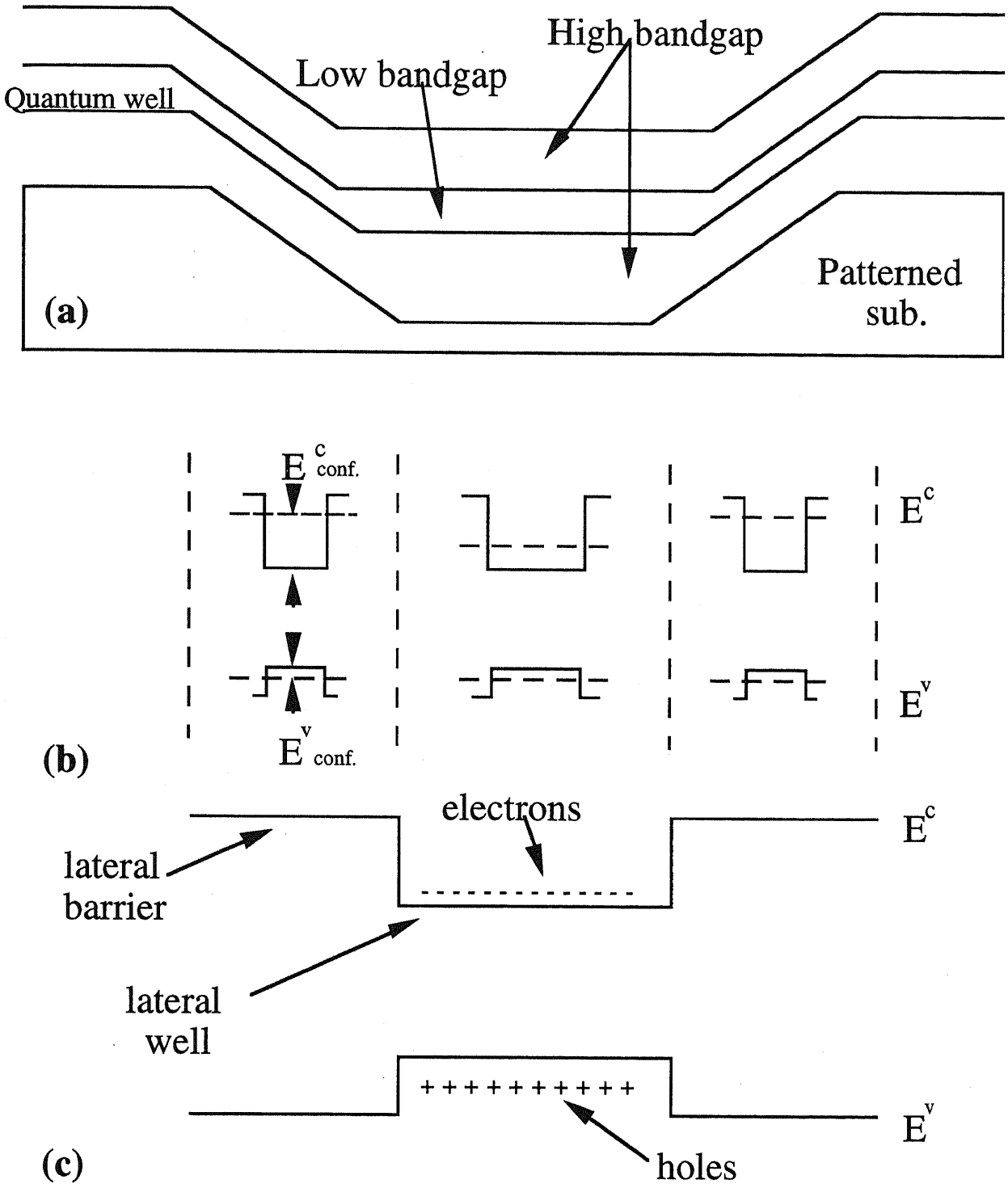

Figure 5.1. Lateral band-gap patterning by epitaxial growth of QWs on NP substrates: (a) schematic cross section, (b) confinement energy for different QW thickness and (c) lateral variation in conduction and valence bands.

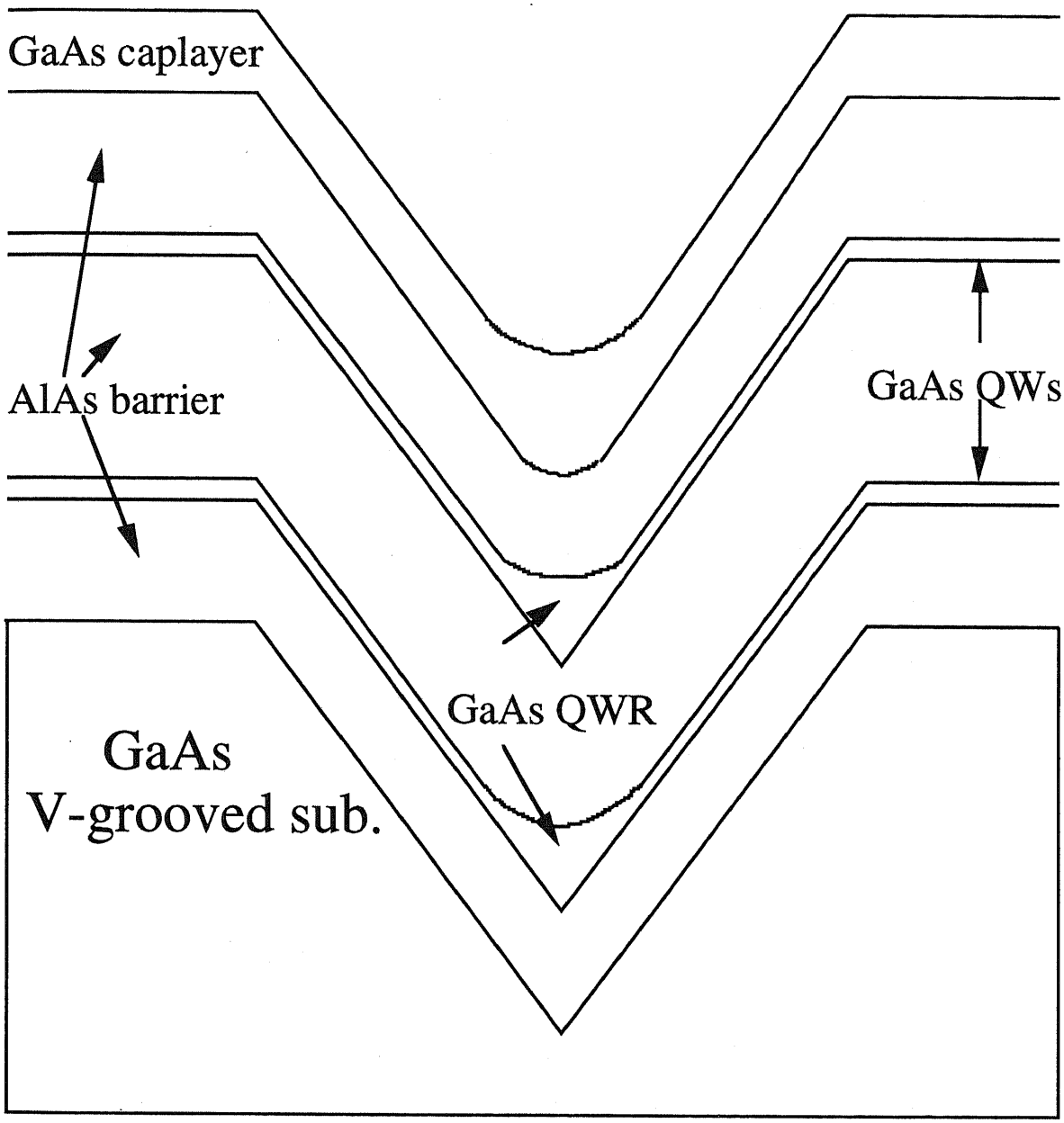

Figure 5.2. Schematically illustration of the double QWR structures at the bottom of V-grooves.

§5.3 Multiple GaAs/AlAs QWR Fabrications

5.3.1 MBE Growth

From the results described in chapter 2, the MBE growth of AlAs was found to have a resharpening effect while the growth of GaAs shows a fast filling at the bottom of the V-groove. In order to use this different growth behavior for the fabrication of multiple crescent-shaped quantum-wires at the bottom of the V-groove, GaAs/AlAs multiple quantum-well (QW) structures were grown by MBE. The period of the V-grooves is 100 μm with the flat (001) part between two grooves. The width and the depth of the grooves are nearly 14 μm and 9 μm, respectively. The sample structures are described as follows: first, a 0.5 μm AlAs buffer layer was grown on the V-grooved substrate in order to make the concave part of V-grooves sharp. Then four 80 Å-thick GaAs quantum wells were grown with 1000 Å-thick AlAs barrier layers. The 1000 Å-thick AlAs barrier layers are also expected to have the effect of resharpening the concave part of the V-grooves. Finally, a 200 Å-thick GaAs cap layer was grown. The thickness of each layer described here is the same as on the (001) plane surface. The growth temperature was set at 580°C and the rotation speed was chosen to be 4 rpm during the growth.

5.3.2 Cross Sectional HRSEM Observations

Fig.5.3 shows a cross-sectional photograph of the grown sample, which was taken without stain etching in reflected electron mode of a HRSEM (Hitachi S-5000). It can be seen that the concave part is very sharp and the GaAs layer (white line) shows the crescent shape with size about (140-160 Å)X(400-500Å) at the bottom of V-groove. Since the thickness of GaAs quantum-wells grown on the flat part of the (001) surface is only 80Å, the nearly 150Å-thick GaAs layers at the bottom of the V-groove must result from the migration effect of the Ga adatoms from the (111)A sidewall to the bottom. This is very similar to the results of the experiments which were done by Kapon et al.(1989,1992) by MOCVD to fabricate the GaAs/AlGaAs quantum-wire structures. However, there are advantages of MBE in controlling the surface diffusion by changing the growth conditions and hence the fabrication of fine quantum structures is expected.

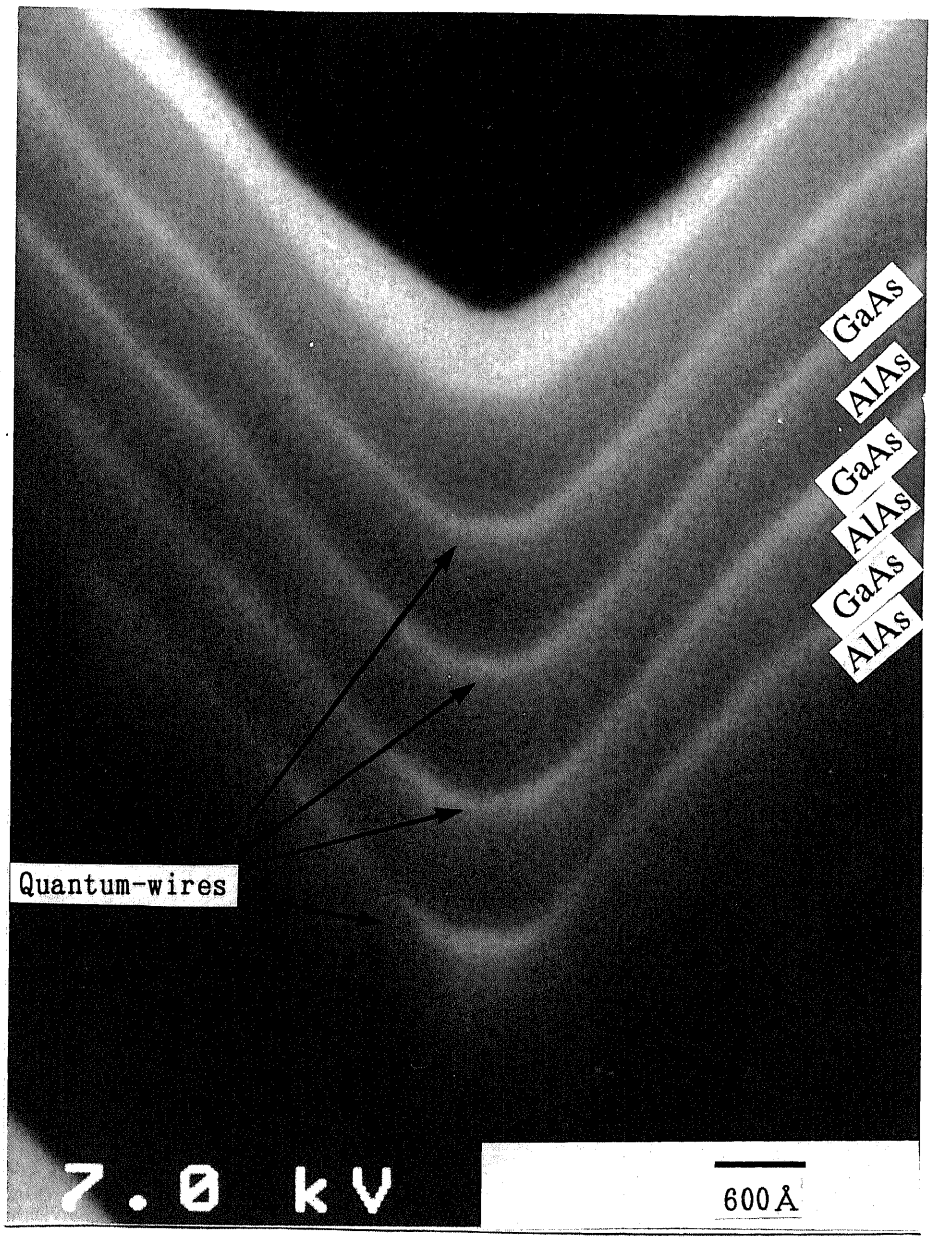

Figure 5.3. HRSEM images of multiple GaAs/AlAs quantum-wires structures at the bottom of the V-grooves. In the SEM picture, bright lines are the GaAs layers and the dark regions are the AlAs.

5.3.3 Low-Temperature CL Characterization

In order to characterize such GaAs/AlAs quantum-wire structures at the bottoms of V-grooves, a cathodoluminescence (CL) measurement was made at 16K. Acceleration voltage was 10 keV and beam current was 0.1nA. Fig.5.4(a) shows the spatially and spectrally resolved CL images along with a secondary electron (SE) image of one groove in the planar observation direction. The weak bright region at 755nm (1.647eV) originates from the 47Å-thick quantum wells (QWL) grown on the (111)A sidewalls. The thickness of the QWL is reduced by 59% because of the reduction of the beam flux on the (111)A sidewalls. The bright region at 775 nm (1.604 eV) is due to the luminescence from the 80 Å-thick quantum wells grown on the (001) surface outside the groove. In addition, a streaky bright line at the bottom of the groove can be seen at 795 nm (1.564 eV) corresponding to the luminescence from the crescent-shaped multiple GaAs quantum-wires (QWR) as expected. The uniform emission along the axis of the wires indicates that the surface diffusion of Ga adatoms from the (111)A sidewall to the bottom results in the uniform formation of wire structures. At 815 nm (1.525 eV), two bright lines appear in the image at the edge between (111)A sidewalls and the (001) surface, which are due to the exponential thickness change of GaAs at the edge. From the observations above, it is shown that the GaAs quantum-wire structures are actually formed at the bottoms of the V-grooves. Fig.5.4(b) shows the CL spectrum (at 16K) of the sample, which agrees well with the images described above. This study demonstrates the feasibility of MBE in successfully growing the GaAs/AlAs wire structures with such a small size, which are now grown mostly by MOCVD.

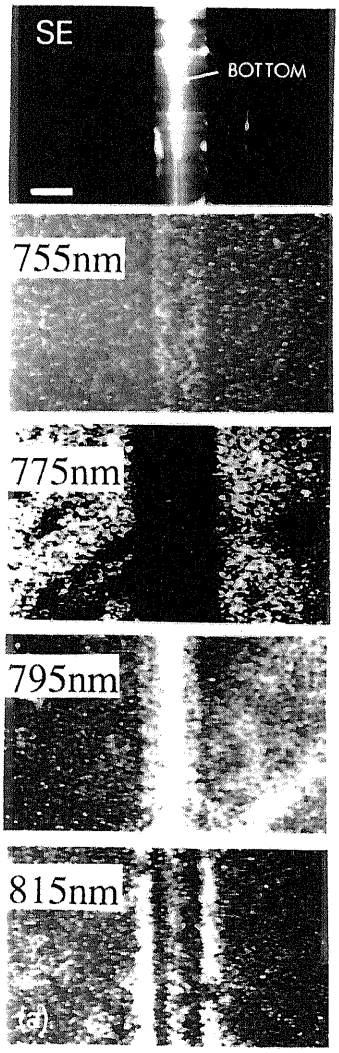

(a)

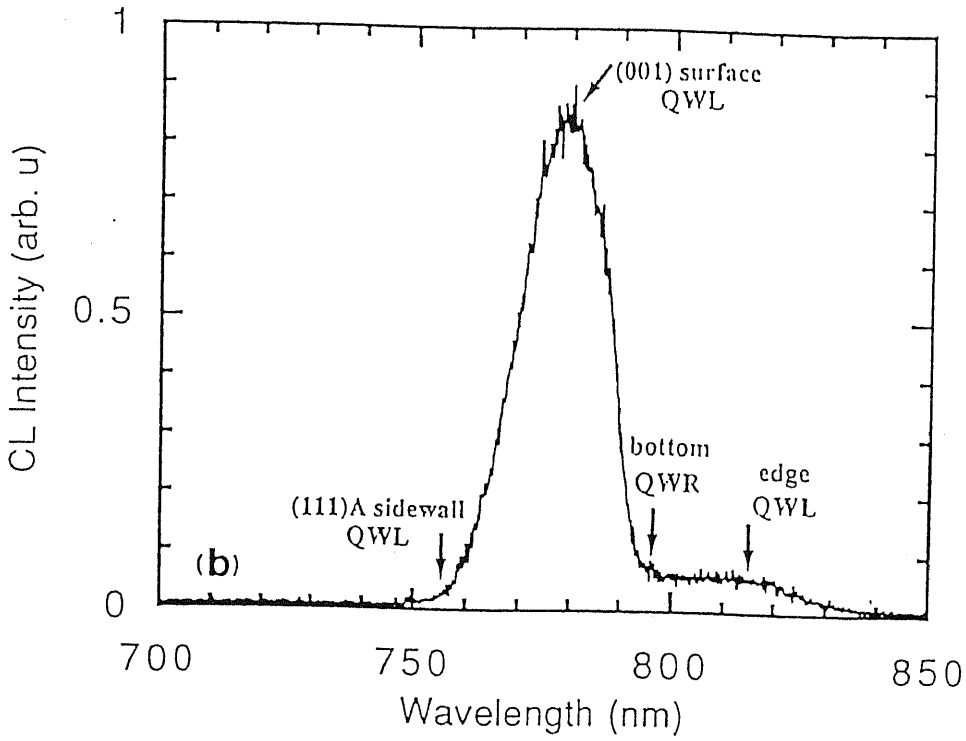

(b)

Figure 5.4. (a) Secondary electron image and cathodoluminescence images (plane view), (b) Cathodoluminescence spectrum of the structure. The mono-chromatic image at 795 nm corresponds to luminescence from the quantum-wire structure. The luminescence band appears to be a few microns in width. This wide width is probably due to carrier trapping from the quantum well formed on the (111)A sidewall to the wire, since the ground state of the quantum wire is considerably lower than that of the quantum wells on the sidewall. Beam voltage: 10 keV; beam current: 0.1 nA; T=16K.

§5.4 Fabrication of Very Narrow Double QWRs

As described in §5.3, it has been succeeded in fabricating QWRs by MBE at the bottom of V-grooves. It is well known that MBE has the advantage of controlling the growth processes very precisely by easily changing the growth conditions. Therefore, successful fabrications of QWR structures with very small size (≤100Å) and good luminescence properties are expected. In the following, such kind of effort is tried and the results are reported.

5.4.1 MBE Growth

The fabrication of the QWRs was carried out with the methods as described follows. The V-grooved NP substrate with (111)A sidewalls was prepared by the same method as described in chapter 2 and the chemical etchant was H_2SO_4:H_2O_2:H_2O (8:1:1 in volume), where the grooves were along the [110] direction on a semi-insulating GaAs (001) substrate. The period of the V-grooves is 3 μm, with the width and the depth of the groove to be nearly 0.75 μm and 0.5 μm respectively, where the density of the grooves is higher than that used in §5.2. The QWR structures were grown as follows. First, about a 2000Å-thick AlAs layer was grown in order to obtain a very sharp corner at the bottom of the V-grooved GaAs substrate. Then, two periods of GaAs (42Å) / AlAs (750Å) heterostructures were grown. The growth was interrupted for 90 seconds at each GaAs/AlAs interface. The 750Å-thick AlAs layers were also expected to have the resharpening effect for the grooves. At last, a 110Å-thick GaAs caplayer was grown to protect the grown structures. The values of the thickness described here refer to those on the flat (001) surface far from the grooves. The growth rates of GaAs and AlAs were 1.4 Å/s and 1.33 Å/s, respectively, and the growth temperature was set at 580°C. During the growth, the rotation speed was chosen to be 4 rpm.

5.4.2 Cross Sectional RHSEM Observation

A cross sectional image of the fabricated structures was observed by high-resolution scanning electron microscopy (HRSEM) in the reflection mode as shown in Fig.5.4. It can be seen that the heterostructures are well fabricated as intended and the bottom of the grooves are extremely sharp due to the resharpening effect of AlAs. Since the thicknesses of the GaAs QW layers are too thin (≤50Å), it is impossible to see clearly the exact shape of the ultrathin GaAs layers at the bottom even by HRSEM. But one can estimate the shape of the ultra-thin GaAs layers by observing the shape of the GaAs caplayer at the bottom of the V-grooves. The GaAs caplayer at the bottom shows the well-defined crescent shape and the width of such a crescent-shaped layer is estimated to be less than 300Å from the HRSEM picture. In the growth of the caplayer, the GaAs thickness on the (001) flat part was 110Å. Therefore, assuming that the QWRs at the bottom have the same shape as that of the GaAs caplayer, the width of the QWRs is estimated to be about or less than 100Å, since the thickness of the quantum wells (QWs) on the flat part was 42Å, nearly 1/3 of that of GaAs caplayer. The value of 100Å for the width of the QWRs is reasonable compared with the HRSEM observation.

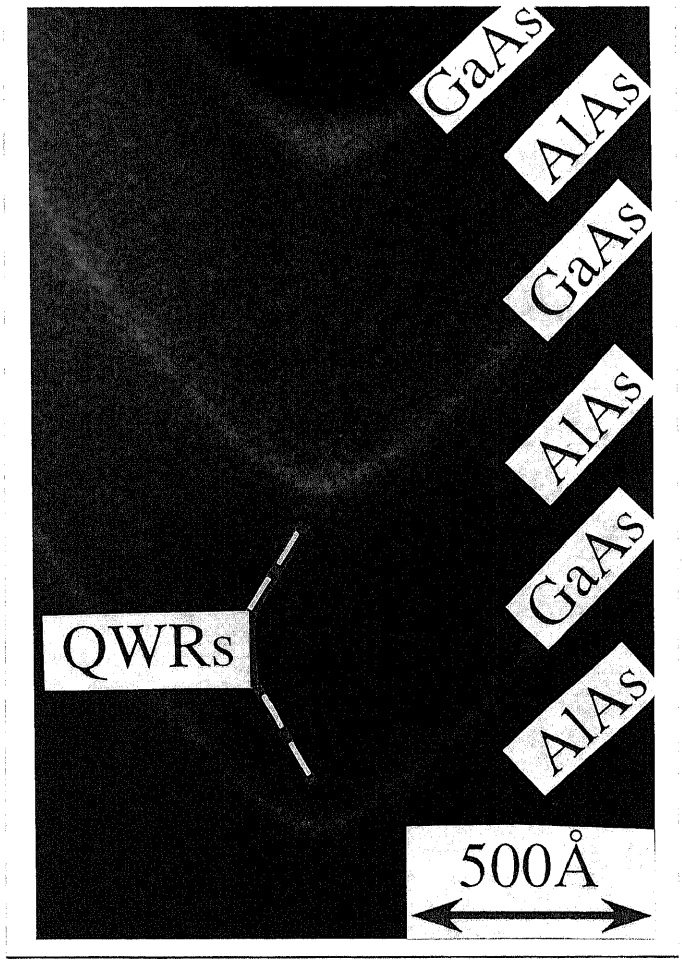

Figure 5.5. High-resolution SEM image of the cross section of the fabricated QWRs on the V-grooved substrates.

5.4.3 Cross Sectional TEM Observation

As described above, the size of the fabricated QWRs structures is very small and the exact shapes of the grown layer can not be clearly seen, although the HRSEM observation was carried out. In order to measure the accurate layer thickness on each surface for calculations and to determine the exact shape of the QWRs at the bottom of the V-grooves, cross sectional TEM observations were carried out. Cross sectional TEM picture of the QWRs structures at the bottom of the V-grooves is shown in Fig.5.6(a). From the picture, it can be seen that the thickness of GaAs at the bottom is thicker than that on the sidewalls, while the thicknesses at the bottom and on the (001) flat part between two grooves are more or less the same, comparing Fig.5.6(a) and Fig.5.6(b). The width of the QWRs at the bottom is observed to be less than 100Å from the TEM picture, which agrees very well with the results by the HRSEM observation as described above. Furthermore, the substrate and the grown layers seem to be quite good without any defects. This shows the advantage for the fabrication of the QWR structure on the NP substrate over other kind of methods.

From the TEM picture, the layer thickness at the bottom and the sidewall are measured to be nearly 42Å and 25Å, respectively. In the MBE growth, 42 Å-thick GaAs QW was grown on the flat place, which agrees well with the TEM results as shown in Fig.5.6(b). Almost no thickness difference between the bottom and the flat part means that the Ga flux migrating from the sidewalls to the bottom is very small under the present growth conditions, where the GaAs thickness on the sidewalls measured from the TEM picture follows the cosine law quite well. Since the width of the QWRs is very narrow and the GaAs thickness at the bottom is very thin, the strong lateral confinement is expected.

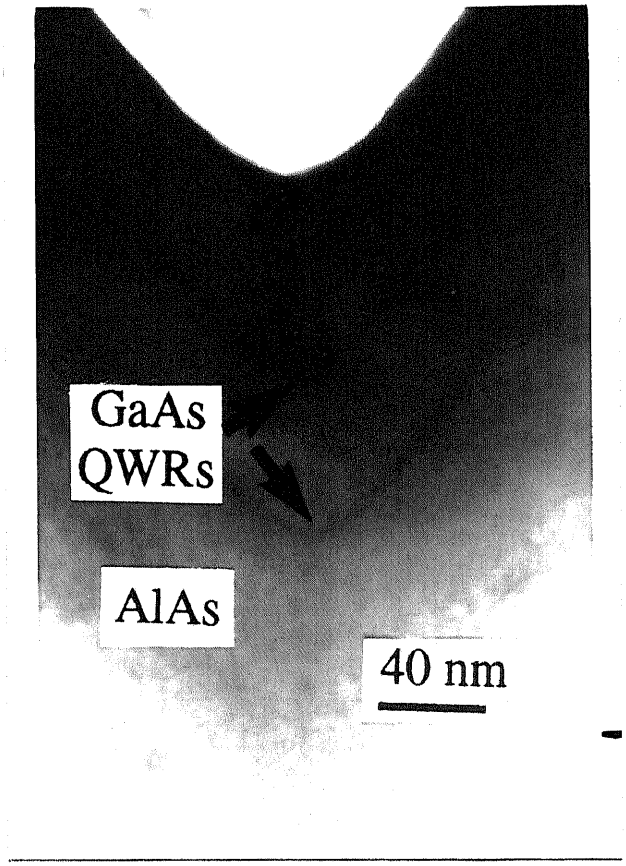

(a)

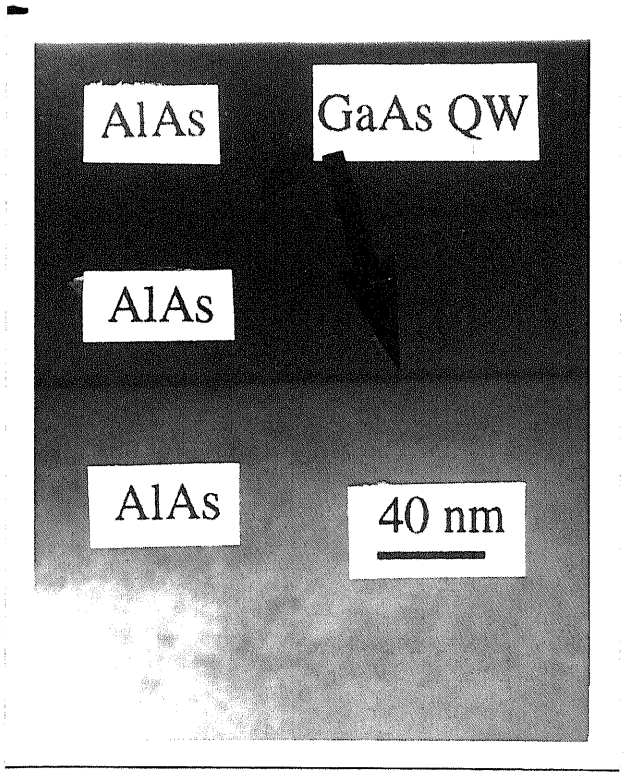

(b)

Figure 5.6. Cross sectional TEM picture of (a) the QWRs structures at the bottom of the V-grooves, and (b) QWs on the flat part between the two grooves.

5.4.4 PL Characterizations

5.4.4.a PL spectra of the sample at 77K

PL measurements at 77K were carried out and the result is shown in Fig.5.7. In the figure, three PL peaks are seen. The strongest peak at near 830 nm stands for the bandgap of GaAs bulk. A relatively strong peak at 736.5 nm (1.685 eV) is assigned to that from the QWs on the (001) surface. Since the thickness of the QWs on the (001) surface is 42 Å, the observed energy value of the QWs is in good agreement with the calculated values of the lowest energy gap in the QWs.

A peak at 717 nm (1.731 eV) is thought to be from the QWRs at the bottom of the V-grooves. This PL peak shows 46 meV blue shift from the PL energy of the (001) QWs, which is different from the results by MOCVD (Kapon et al., Tsukamoto et al.). From the TEM observation results, it shows that the thicknesses of the QWRs at the bottom and the QWs on the flat part are almost the same. Therefore, the blue shift of the peak from the QWRs can be realized reasonably due to the strong lateral confinement in the QWRs. This phenomenon is very interesting, because it gives a direct evidence to the strong lateral confinement in the QWRs structures. Furthermore, PL intensity from the QWRs is comparable to that of the (001) QWs, which also indicates the strong carrier confinement and the good luminescence property of the QWRs at the bottom. In the PL measurement, the peak from the (111)A sidewall QWs was not observed. There are two possible reasons for this phenomenon. One might be because that the peak intensity is very weak due to the ultra-thin sidewall QWs from the TEM observation. The other possibility might be due to the strong carrier capture process in the QWRs. Since the carrier capture in the QWRs is very strong, the carriers might migrate quickly from the sidewall to the bottom before they radiate. This also results in the weak PL peak from the sidewall QWs.

The effective width w of the QWRs is calculated in the effective-mass approximation using a finite-well model proposed by Kapon et al.(1989). The thickness of the GaAs QWs grown on the sidewalls and the maximum thickness at the bottom of the V-grooves are used to be 25Å and 42Å, respectively, from the TEM observation results. Using these values of the thickness and the observed PL energy of the QWRs, the effective width w of the QWRs at the bottom was calculated to be 80Å assuming $\Delta E_C/\Delta Eg=0.8$, and 60Å assuming $\Delta E_C/\Delta Eg=0.6$.

Here ΔEc and ΔEg are the energy differences in the conduction band edge and in the bandgap respectively between GaAs and AlAs. The value of $w \sim 70$Å is reasonable compared with the RHSEM and TEM observations, and as far as we know this is the smallest QWRs to date among the QWRs fabricated by MBE on V-grooved substrates.

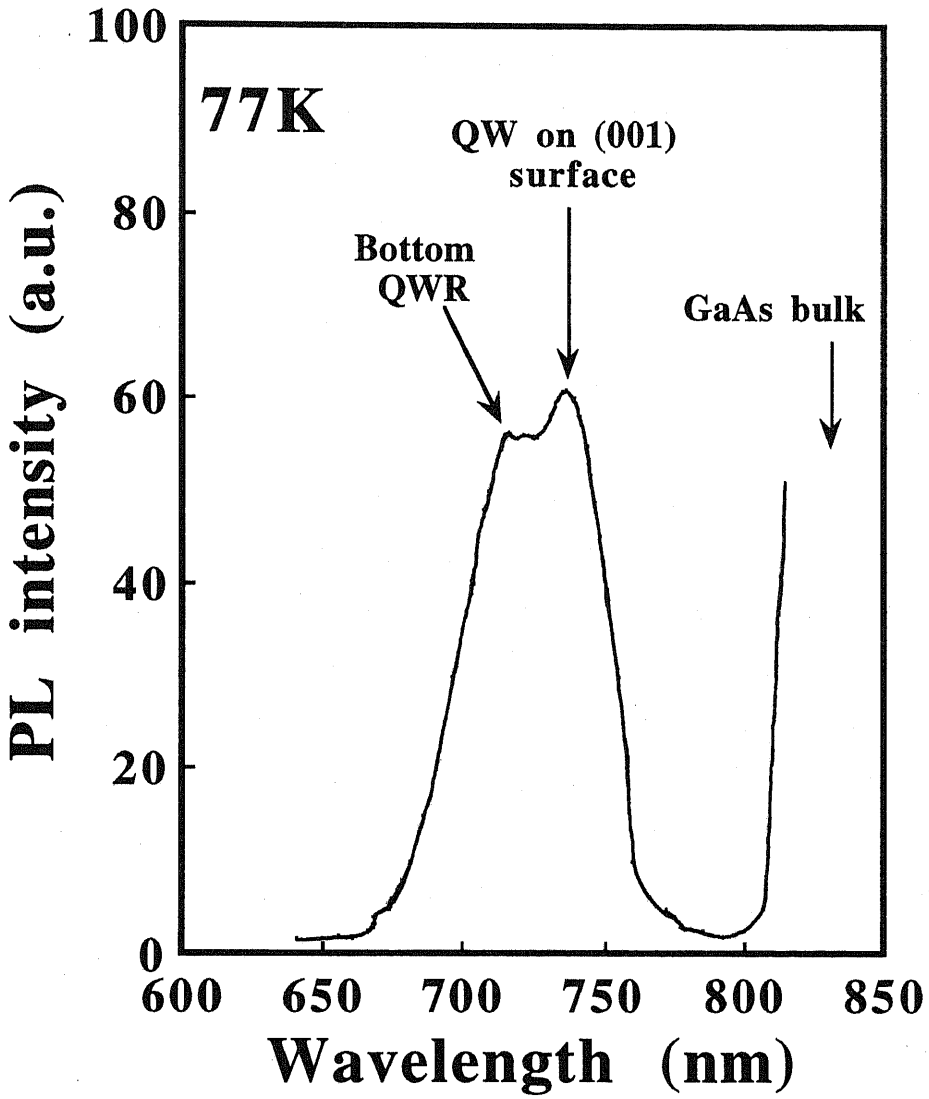

Figure 5.7. PL spectrum of the double QWRs structures at 77K

5.4.4.b Polarization Dependence of the PL Spectra

Fig.5.8 shows the polarization dependence of the PL spectra of the QWs and the QWRs structures at 77K. For the polarized PL measurement, the luminescence light was led to pass through a polarizer before a monochromater. The 77K PL spectrum of the QWRs, as plotted in Fig.5.8, shows strong polarization anisotropy with $(I_p-I_n)/(I_p+I_n)$ of about 22%. Here, I_p and I_n are the PL intensities of QWRs with the electric field **E** of the luminescence light parallel and normal to the wires, respectively. It is necessary to point out here that the PL intensities from the QWs on the (001) surface show almost no polarization dependence, which means that there is little influence from the monochromater in the present measurements. The strong polarization dependence confirms the existence of the QWRs and the anisotropy is considered to be related with the intrinsic radiation process in the QWRs due to the strong lateral confinement of carriers. To interpret the quantum confinement quantitatively from the result of the polarization-dependent PL, the theoretical calculations (Tanaka et al.1989,1990) which is based on the Kane's **k.p** perturbation theory and momentum matrix (Kane et al.1956) are used . From the measured polarization dependence of the PL, k_X/k_Z is calculated to be 0.75, where k_X and k_Z are the respective wave vector components of carriers in the lateral and vertical directions in QWRs. This result indicates that very strong lateral confinement is realized in QWRs. Since k_X and k_Z are approximately proportional to $1/L_X$ and $1/L_Z$, respectively, where L_X and L_Z are the lateral and vertical size of the QWRs, we got $k_X/k_Z \sim L_Z/L_X=0.6$, taking the L_X and L_Z values of 70Å and 42Å, respectively, as estimated from the TEM picture. This agrees with the result ($k_X/k_Z=0.75$) obtained from the polarization dependence of PL.

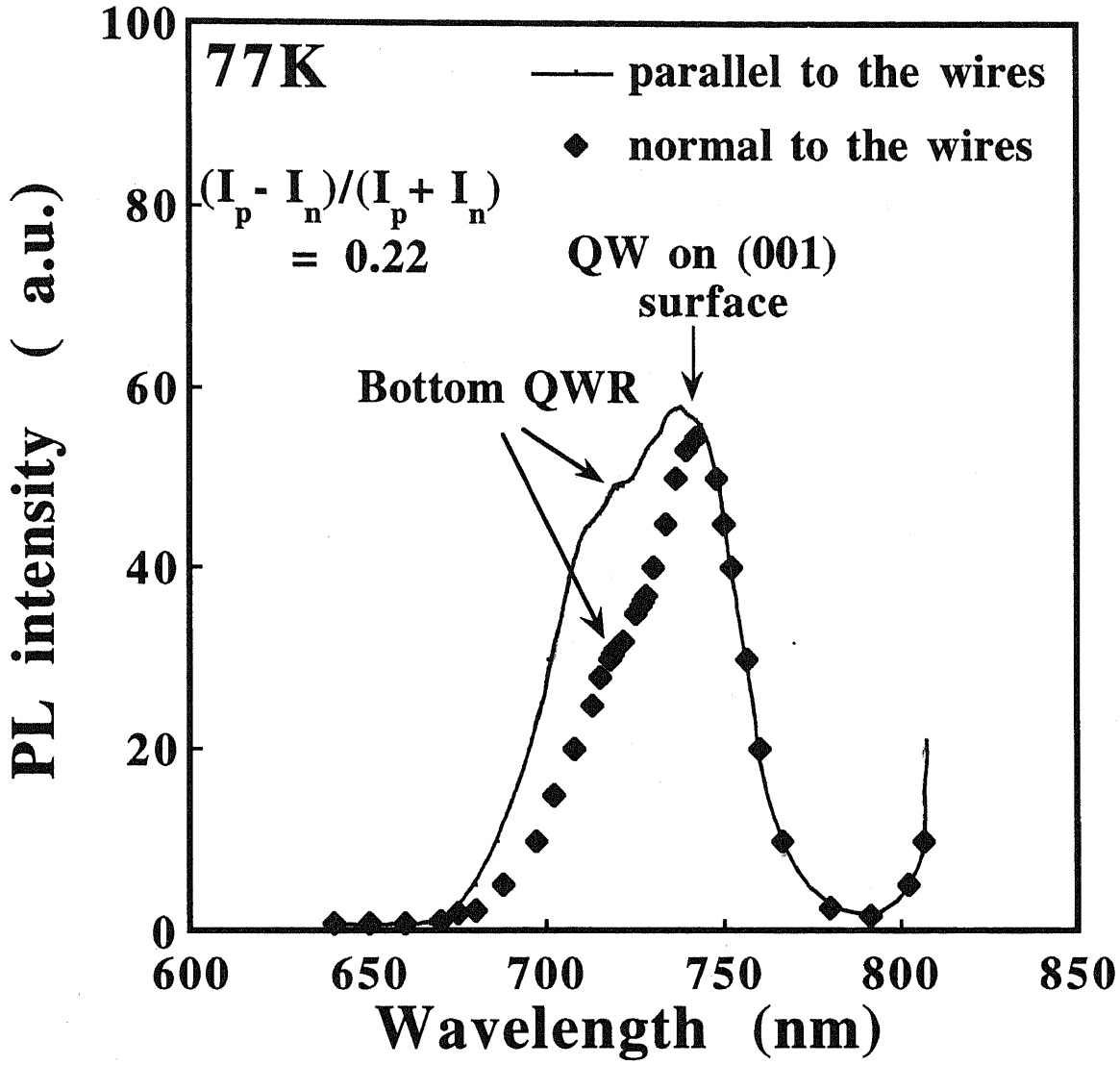

Figure 5.8. Polarization dependence of the PL spectrum of the sample at 77K. The solid and the dotted curves show the PL spectra with the electric field parallel and normal to the QWRs, respectively.

5.4.4.c Carrier Captures in the QWRs

In order to investigate the process of carrier capture in the QWRs, the temperature dependence of the PL intensity was measured. Fig.5.9(a) shows the PL spectra at various temperatures, and the intensity of PL from QWRs is shown as a function of temperature in Fig.5.9(b). The intensity of the incident laser light is about 1/5 of that shown in Figs.5.7 and 5.8, thus the noise of the signal are comparatively large. As shown in the Fig.5.9(b), the PL peak intensity from QWRs increases with increasing the temperature from 15K to 70K, taking a maximum at around 70K. Then it decreases with the increase of the temperature. The spectrum at 70K shows almost the same shape as that at 77K of Fig.5.7. This temperature dependence of the PL spectra suggests that photo-excited carriers migrate more efficiently at 70K than at lower temperature from the (111)A sidewall QWs to the QWRs at the bottom of the V-grooves. Although the PL peak from the sidewall QWs can not be observed in the present sample, it is believed that if there is a weak PL peak from the sidewall QWs, the intensity of the PL would decrease with the increase of the measuring temperature, which is similar to that reported in the fabrication by MOCVD (Walther et al.1992, Lee et al.1993).

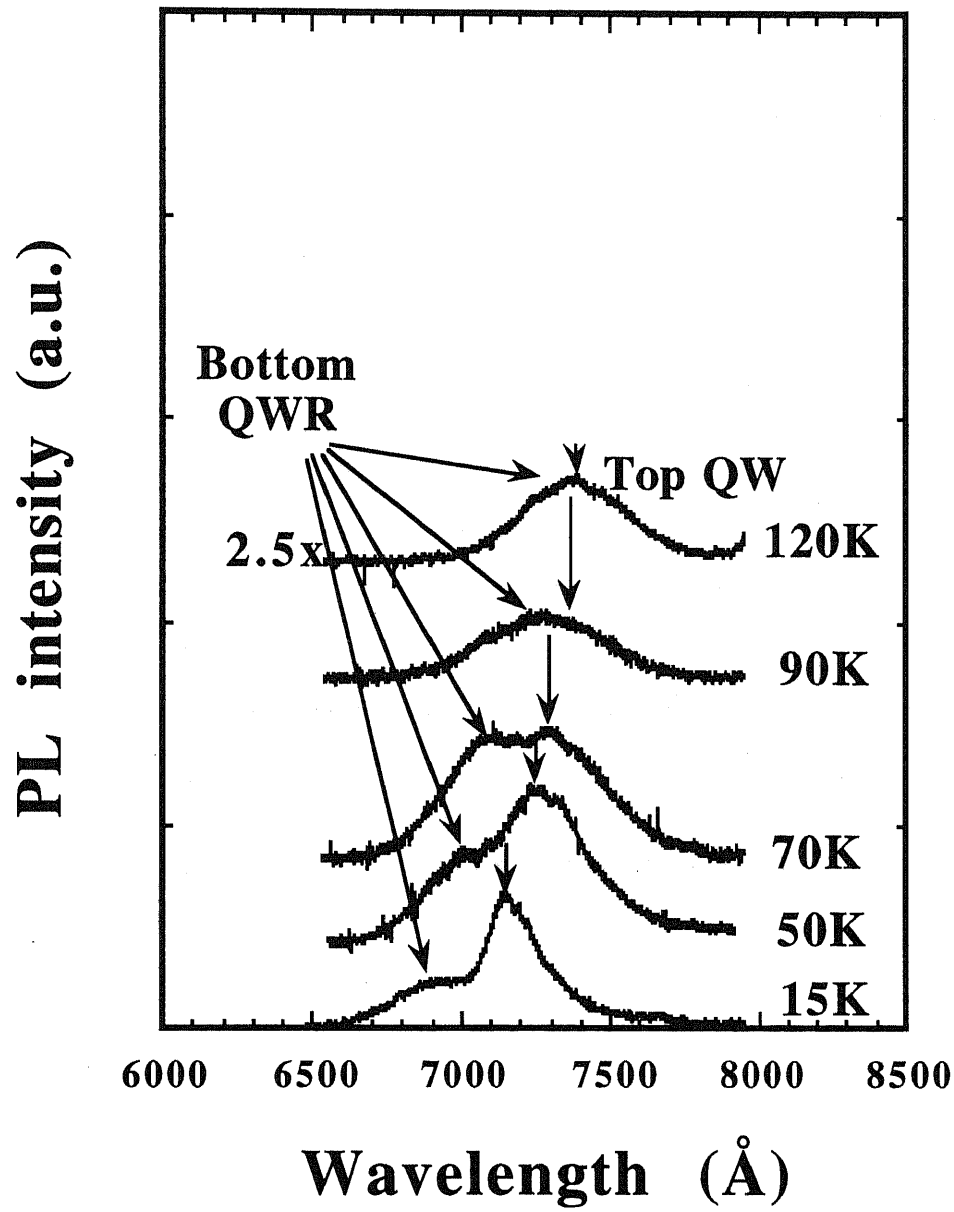
PL intensity (a.u.)
Bottom
QWR
Top QW
2.5x
120K
90K
70K
50K
15K
6000
6500
7000
7500
8000
8500
Wavelength (Å)

(a)

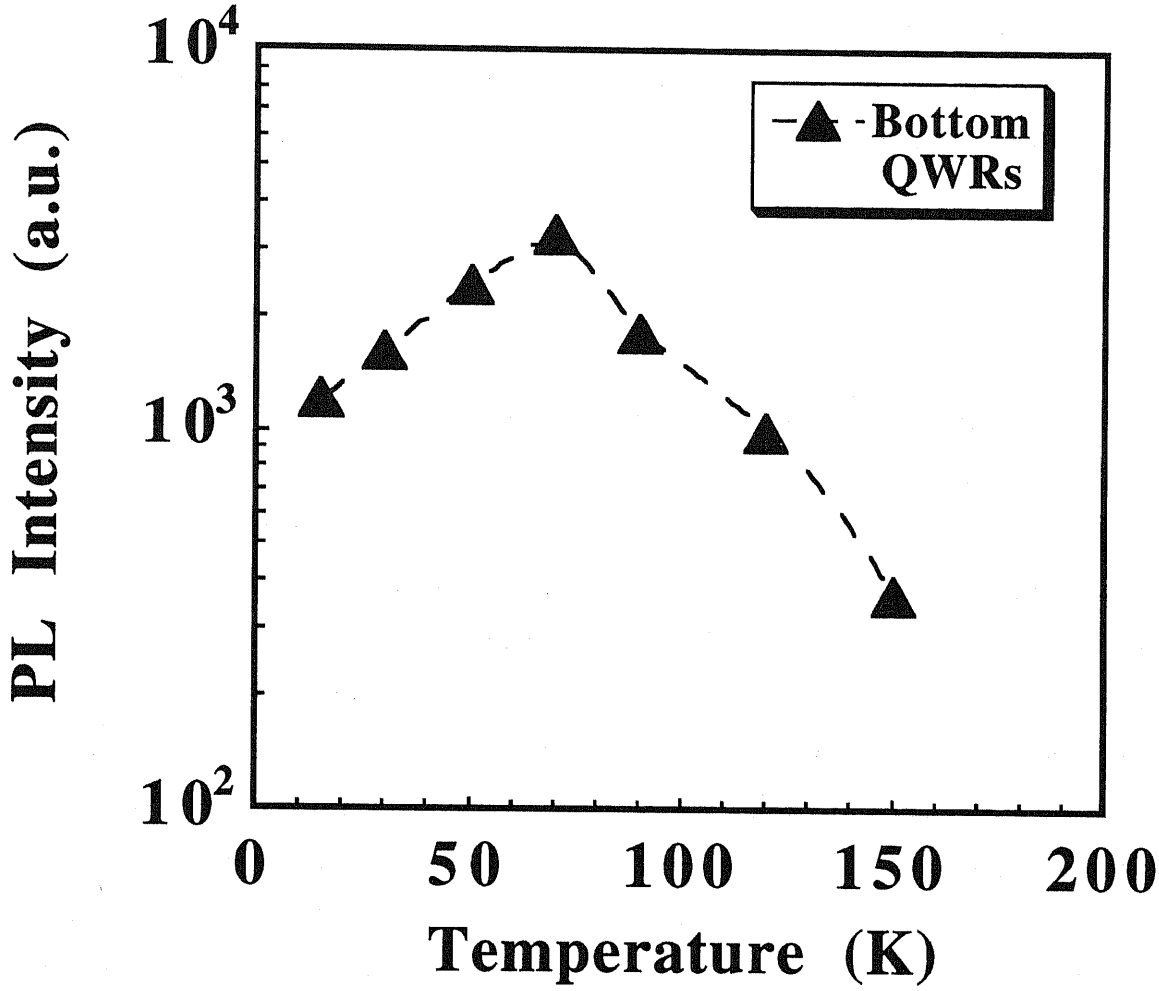

(b)

Figure 5.9. (a)Temperature dependence of the PL spectra of the QWRs structures.
(b) The PL intensity of the QWRs as a function of temperature .

§5.5 Single QWR Fabrication

From the above results, it is clear that the GaAs/AlAs QWRs can be successfully fabricated by MBE on the V-grooved NP substrates with very small size (≤100Å) and good luminescence properties. But the full width at half maximum (FWHM) of the QWR peak is quite large (~70 meV), as shown in Fig.5.7. This is thought to be due to the multiformity of the size and shape of the two QWRs. In order to investigate this phenomenon and improve the quality of the QWR, single GaAs/AlAs QWR structure was grown on the V-grooved NP substrate.

5.5.1 MBE Growth

The fabrication of the single GaAs/AlAs QWR was carried out with the same methods as described in §5.4. The period of the V-grooves is 3 μm, with the width and the depth of the groove to be nearly 1 μm and 0.65 μm, respectively, and the growth structures and process are described as follows. First, about a 3000Å-thick AlAs layer was grown in order to obtain a very sharp corner at the bottom of the V-grooved GaAs substrate. Then, GaAs (52Å) / AlAs (1000Å) heterostructures were grown. The growth was interrupted for 90 seconds at each GaAs/AlAs interface. At last, a 200Å-thick GaAs caplayer was grown to protect the grown structures. The values of the thickness described here refer to those on the flat (001) surface far from the grooves. The growth rates of GaAs and AlAs were 1.4 Å/s and 1.33 Å/s, respectively, and the growth temperature was set at 580°C. During the MBE growth, the rotation speed was chosen to be 4 rpm. A (001) flat substrate was also mounted beside the V-grooved NP substrate during the growth, which is used as a reference sample.

5.5.2 Cross Sectional TEM Observation of the QWR

Fig.5.10 shows the cross-sectional TEM picture of the fabricated single QWR structure at the bottom of the V-groove. It can be seen that the heterostructure is grown quite well and the interface is very sharp. At the bottom, the QWR structure is formed with the well-ordered crescent-shape. From the TEM picture, the thickness and the width of the QWR is measured to be 100Å and 350Å, respectively. Although the thickness (52 Å) of the single GaAs QW on the (001) surface is only 10Å thicker than the double QWs (42 Å) as described in §5.4, the shape of the single QWR at the bottom is quite different from the double QWRs. At the (001) flat place, the thickness of GaAs QW is 52 Å, however, the GaAs QW layer grown on the (111)A sidewall and at the bottom are measured to be nearly 28Å and 100Å, respectively, from the TEM picture. This is thought that during the growth at the present growth conditions, the inter-surface migration of Ga from the (111)A sidewall to the bottom is quite large, which is different from the case described in §5.4 . Also, no defects are found in the heterostructure from the TEM picture.

By the above TEM observation, it is sure that the single GaAs/AlAs QWR is well formed at the bottom of V-grooves with the size to be about 100Åx350Å.

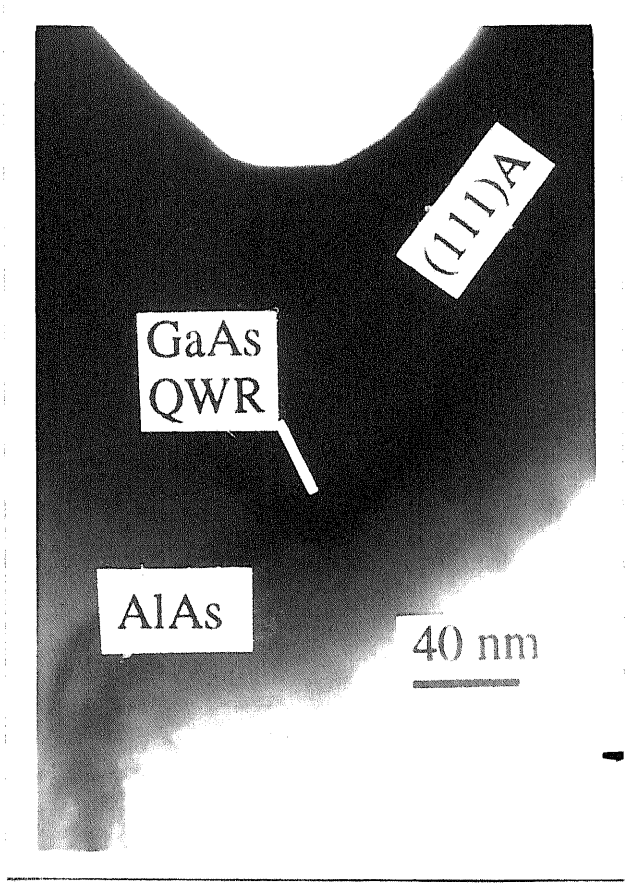

Figure 5.10. Cross sectional TEM picture of the single QWR structure at the bottom of the V-grooves.

5.5.3 Low-Temperature PL Characterization

PL measurement of the fabricated sample was carried out at 77K. Fig.5.11 illustrates the PL spectra of the QWR sample (solid line) and the reference planar sample (dotted line). It can be seen that two PL peaks occur at 750 nm and 825 nm on the reference sample, which refer to the 52 Å-thick QW on the (001) surface and the bandgap of GaAs bulk, respectively. On the other hand, PL spectrum from the V-grooved NP substrate shows three peaks. Peaks at 750 nm and 825 nm are thought to be from the same origin as that on the reference sample. The third peak at 790 nm is considered to be originated from the single QWR at the bottom. From the cross sectional TEM picture, the thicknesses at the bottom and on the sidewall are measured to be nearly 100Å and 28Å, respectively. Using the data of the thicknesses of the GaAs QW on the (111)A sidewall and at the bottom and the PL energy of the QWR, the effective width of the QWR is calculated to be about 300Å using the same calculation method as described in §5.4, which agrees very well with the TEM observation.

Furthermore, the PL intensity of the QWR is stronger than that of the QW on the flat (001) surface as shown in Fig. 5.11. This means that luminescence property of the QWR is quite good. The FWHM of the 77K PL spectrum of the single QWR structure is improved and decreases to a quite low value (~29 meV) comparing with the data of the double QWRs structures (~70 meV). This result indicates that the multiformity will affect the PL property of the QWR structure greatly.

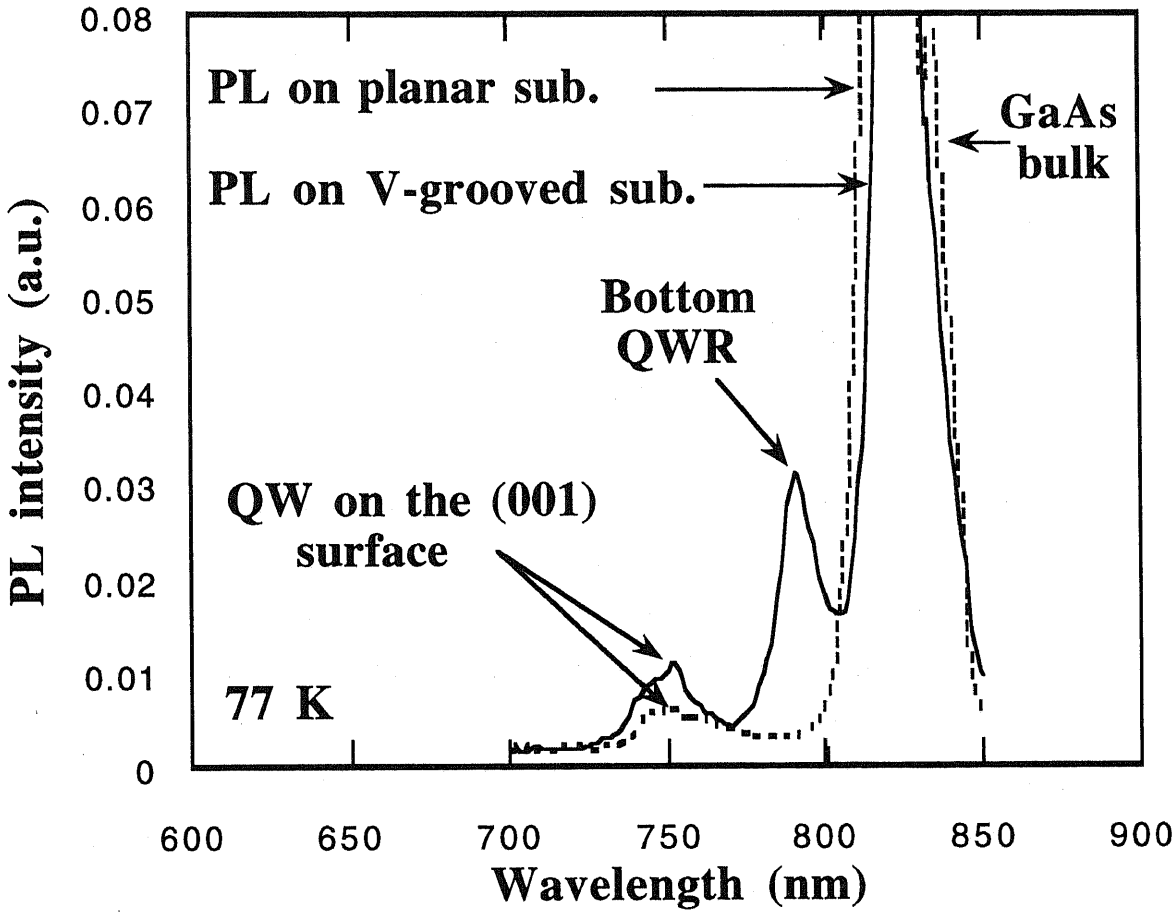

Figure 5.11. 77K PL measurements of the single QWR structure. The solid line shows the PL spectrum of the V-grooved substrate, while the dotted line shows the PL spectrum of the reference plane substrate.

§5.6 Summary

By use of the resharpening effect of AlAs at the bottom of the V-grooves, GaAs/AlAs multiple quantum-wires have been fabricated at the bottom of V-grooves by MBE. High-resolution SEM observations and CL measurements at 16K show that the multiple crescent-shaped GaAs quantum-wires with a size of about (140-160Å)X(400-500Å) have been successfully formed at the bottom of the V-grooves.

According to this fabrication method, very narrow double GaAs/AlAs QWRs have been successfully grown by MBE with good luminescence properties. Cross sectional observations by HRSEM and TEM confirm the formation of the QWRs of less than 100Å in width at the bottom of the V-grooves. In photoluminescence (PL) measurements at 77K, the QWRs show an intense well-resolved peak at 223 meV above the bandgap of GaAs, although the full width at half maximum (FWHM) of the QWRs peak is quite large (~70 meV) due to the multiformity of the size and shape of the two QWRs. The PL peak of the QWRs exhibits a strong polarization dependence, which is well explained by the lateral confinement of carriers. Furthermore, the temperature dependence of PL intensity shows strong carrier capture in the QWRs at ~70K. The calculated effective width of the QWRs is as narrow as ~70 Å which agrees well with the HRSEM and TEM observations.

Furthermore, single GaAs/AlAs QWR structure was grown to investigate the influence of the multiformity of the size and shape of the QWR on the FWHM of PL spectrum. Cross sectional TEM observation shows the excellent formation of the QWR structure at the bottom of the V-grooves with the size of about 100Åx300Å. Also, it is clear that the FWHM of the 77K PL spectrum of the single QWR structure decreases to a quite low value (~29 meV) comparing with the data of the double QWRs. Moreover, the PL intensity of the QWR is much stronger than that of the QW on the flat (001) surface. This means that luminescence property of the QWR is quite good and the inter-surface is very smooth.

The above results strongly demonstrate the feasibility of MBE for the fabrication of very narrow QWRs on V-grooved substrates, which could be employed for the future quantum effect devices.

Chapter 6 Summary

This thesis concerns the molecular beam epitaxial (MBE) growth of III-V semiconductor on nonplanar (NP) substrates. The contents are divided mainly into two parts. Part one is the study of the growth mechanism on such substrates. Part two relates to the fabrication and the characterization of quantum-wire (QWR) structures at the bottom of V-grooves, which is based on the results of part one. The results obtained in this study are summarized as follows.

First, in chapter 2, MBE growth of (Al,Ga)As and (In,Ga)As heterostructures on (111)A-(001) V-grooved substrates were carried out. By the cross sectional SEM observations of the grown layers on the various parts of the V-grooved substrates, the surface diffusion phenomena of adatoms (Ga, Al, In) were studied.

(411)A facet formations and the thickness change of GaAs grown layers on the (001) surface near the edge are observed, which relate to the inter-surface diffusion of Ga between the (111)A sidewall and the (001) surface. It is shown, in particular, that the growth of AlAs leads to a drastic sharpening at the bottom of the V-grooves (**resharpening effect of AlAs**). AlGaAs, however, has no such phenomena. Instead, it grows roughly on the (111)A surfaces and makes a new (001) surface at the bottoms as GaAs does.

Comparing the shape of the InGaAs layers grown at the bottom of V-grooves, it is found that the diffusion length of In adatom depends strongly on the growth temperature. Almost no growth of InAs on the (111)A sidewall shows the large diffusion length of In on the (111)A GaAs sidewall. Furthermore, the InAs layer at the bottom shows the formation of (311)A facets, which is different from the case of GaAs by forming (001) surfaces.

By using the different growth behaviors of each material at the bottom of the V-grooves, it is pointed out that fabrication of multiple GaAs/AlAs and (In,Ga)As/AlAs quantum-wires structures at the bottom of the V-grooves by MBE is possible.

Then, in chapter 3, a simple model, assuming one-dimensional surface diffusion equation, is proposed. The lifetime of Ga adatoms until incorporation into the crystal on each surface is introduced in this model. The surface chemical reaction processes are also taken into account for the understanding of the experimental results.

The dependence of surface diffusion of Ga adatoms on arsenic pressure during MBE growth on NP substrates with (111)A and (411)A sidewalls are studied by the μ-RHEED/SEM MBE system. The surface diffusion length of Ga adatoms shows strong dependence on arsenic pressure, while it is almost independent of Ga flux from the sidewall and the K-cell. The results can be explained well by the proposed model.

The inter-surface diffusion of In adatoms between the (111)A and the (001) surface on the InAs (111)A-(001) NP substrate is also investigated by μ–RHEED. The surface diffusion length of In adatom incorporation on the (001) InAs surface is found to be longer than that of Ga on the GaAs (001). It turns out that the diffusion length depends strongly on the growth temperature and the arsenic pressure, while it is independent of In flux as Ga does. Furthermore, it is observed that the migration direction of In lateral flux between the (111)A and the (001) InAs surface is changed depending on the growth conditions. This behavior is different from that of Ga adatoms on GaAs (111)A-(001) NP substrates.

By considering the different condition of the adatom stoichiometry entering the step in both cases, the great contradiction of the surface diffusion length between the conventional plane substrate and the NP substrate is explained.

In chapter 4, arsenic pressure dependence of Ga surface diffusion in MBE growth on (111)B-(001) mesa-etched substrates was investigated by μ-RHEED.

It was observed for the first time that the direction of the lateral migration of Ga adatoms from or to the (111)B sidewall depends on the arsenic pressures on such substrates. Furthermore, the surface diffusion length of Ga adatoms on the (001) surface along $[\bar{1}10]$ direction was found to vary with arsenic pressures strongly and as that along [110] direction, however it is independent of the direction of lateral migrations of Ga adatoms. The diffusion length shows isotropy both along $[\bar{1}10]$ and [110] directions.

The surface diffusion length on the (111)B surface were measured, which is longer than that on the (001) surface within the same arsenic pressure range. It was found that the temperature dependence of the diffusion length is quite different at the $\sqrt{19}x\sqrt{19}$ and 2x2 surface reconstructions on the (111)B surface. Also, the arsenic pressure dependence of the diffusion length on the (111)B surface is different from that on the (001) surface. This result agrees well with what was predicted theoretically.

The ratio of surface diffusion coefficients on the (111)B and the (001) GaAs surfaces were investigated. The results indicate that the surface diffusion coefficient on (111)B surface is nearly 140 times larger than that on (001) surface at 600°C. Furthermore, the ratio shows almost no dependence of arsenic pressure, which may imply that the surface diffusion coefficient itself is independent of arsenic pressure under the same surface reconstruction condition.

At last, in chapter5, by use of the resharpening effect of AlAs at the bottom of the V-grooves, GaAs/AlAs multiple quantum-wires have been fabricated at the bottom of V-grooves by MBE. High-resolution SEM observations and CL measurements at 16K show that the multiple crescent-shaped GaAs quantum-wires with a size of about (140-160Å)X(400-500Å) have been successfully formed at the bottom of the V-grooves.

According to this fabrication method, very narrow double GaAs/AlAs QWRs also have been successfully grown by MBE with good luminescence properties. Cross sectional observations by HRSEM and TEM confirm the formation of the QWRs of less than 100Å in width at the bottom of the V-grooves. In photoluminescence (PL) measurements at 77K, the QWRs show an intense well-resolved peak at 223 meV above the bandgap of GaAs, although the full width at half maximum (FWHM) of the QWR peak is quite large (~70 meV) due to the multiformity of the size and shape of the two QWR. The PL peak of the QWRs exhibits a strong polarization dependence, which is well explained by the lateral confinement of carriers. Furthermore, the temperature dependence of PL intensity shows strong carrier capture in the QWRs at ~70K. The calculated effective width of the QWRs is as narrow as ~70 Å which agrees well with the TEM observation.

Furthermore, single GaAs/AlAs QWR structure was grown to investigate the influence from the multiformity of the QWRs size and shape on the FWHM of PL spectrum. Cross sectional TEM observation shows the excellent formation of the crescent-shaped QWR at the bottom of the V-grooves. Also, it is clear that the FWHM of the 77K PL spectrum of the single QWR structure decreases to a quite low value (~29 meV) comparing with the above data. Moreover, the PL intensity of the QWR is much stronger than that of the QW on the flat (001) surface. This means that luminescence property of the QWR is quite good and the inter-surface is very smooth.

The techniques described above demonstrate the feasibility of MBE for the fabrication of very narrow QWRs on V-grooved substrates, which could be employed for the future quantum effect devices.

The experimental results and the discussions in this study concern only some aspects with the understanding of the MBE growth mechanism and the fabrication of QWRs structures. Many important topics, such as the absolute value of the surface diffusion coefficient, surface diffusion in the lattice mismatched material system, QWR laser fabrication by MBE, etc. are still remained. Therefore, new ideas and experimental methods are strongly expected for the purpose of the complete understanding of the MBE growth mechanism, together with the applications for the future devises.

References

Akiyama H., Koshiba S., Someya T., Wada K., Noge H., Nakamura Y., Inoshita T., Shimizu A. and Sakaki H., Phys. Rev. Lett. 72 (1994) 924.

Arakawa T., Tsukamoto S., Nagamune Y., Nishioka M., Lee J.H. and Arakawa Y., Jpn. J. Appl. Phys. 32 (1993) L1377.

Arakawa Y., Vahala K., Yariv A. and Lau K., Appl. Phys. Lett. 47 (1985) 1142

Arakawa Y., Vahala K., Yariv A. and Lau K., Appl. Phys. Lett. 48 (1986) 384.

Arakawa Y.and Yariv A., IEEE J.Quantum Electron, 22, 1887 (1986).

Arakawa Y., Solid-State Electronics 37 (1994) 523.

Arent D.J., Nilsson S., Galeuchet Y.D., Meier H.P. and Walter W., Appl.Phys. Lett. 55 (1989) 2611.

Arent D.J., Brovelli H. Jackel, Marclay E. and Meier H.P., Appl. Phys. Lett. 56 (1990) 1939.

Arthur J.R. and Jr., J. Appl. Phys. 39 (1968) 4032.

Bertram D., Spill B., Stolz W. and Gobel E.O. Solid-State Electronics 37 (1994) 591.

Bhat R., Kapon E., Werner J., Hwang D.M., Stoffel N.G. and Koza M.A., Appl. Phys. Lett., 56 (1990) 863.

Bhat R., zah C.E., Caneau C., Koza M.A., Menocal S.G., Schwarz S.A. and Favire F.J., Appl. Phys. Lett. 56 (1990) 1691.

Burton W.K., Cabrera N. and Frank F.C., Philos. Trans. R. Soc. London A 243 (1951) 299.

Cho A.Y., Surf. Sci. 17 (1969) 494.

Cho A.Y., J. Appl. Phys. 41 (1970) 782.

Christen J., Kapon E., Grundmann M., Hwang D.M. and Joschko M.and Bimberg D., Phys. Stat. Sol.(b) 173 (1992) 307.

Christen J., Grundmann M., Kapon E., Colas E., Hwang D.M. and Bimberg D., Appl. Phys.Lett.61 (1992) 67.

Christen J., Kapon E., Colas E., Hwang D.M., Schiavone L.M., Grundmann M., and Bimberg D., Surface Science 267 (1992) 257.

Clausen E.M., Jr., Kapon E., Tamargo M.C. and Hwang D.M., Appl. Phys.Lett. 56 (1990)776.

Colas E., Simhony S., Kapon E., Bhat R., Hwang D.M. and Lin P.S.D., Appl. Phys. Lett. 57 (1990) 914.

Colas E., Clausen E.M., Jr., Kapon E., Hwang D.M., Simhony S., Bhat R., Chen C.Y., Lin P.S.D., Schiavone L. and Gaag B.V., J. Crystal Growth 107 (1991) 243.

Colas E., Nihous G.C. and Hwang D.M., J. Vac. Sci. Technol. A10 (1992) 691.

Eberl K., Kurtenbach A., Grambow P., Lehmann A., Klitzing K.V., Heitmann D., Dilger M. and Hohenstein M., Solid-State Electronics 37 (1994) 535.

Eberl K., Grambow P., Lehmann A., Kurtenbach A., Klitzing K.V., Heitmann D., Dilger M. and Hohenstein M., Appl. Phys. Lett. 63 (1993) 1059.

Fafard S., Leonard D., Merz J.L. and Petroff P.M., Appl. Phys. Lett. 65 (1994) 1388.

Foxon C.T., Bondry M.R. and Joyce B.A., Surf. Sci. 44 (1974) 69.

Foxon C.T. and Joyce B.A., Surf. Sci. 50 (1975) 434.

Foxon C.T. and Joyce B.A., Surf. Sci. 64 (1977) 293.

Foxon C.T. and Joyce B.A., J. Crystal Growth 44 (1978) 75.

Fujii M., Yamamoto T., Shigeta M., Takebe T., Kobayashi K., Hiyamizu S. and Fujimoto I., Workbook of the 5th Int. Conf. Modulated Semiconductor Structures, (1991, Nara) p.149.

Fukui T., Saito H., and Tokura Y., Jpn. J. Appl. Phys. 27 (1988) L1320.

Guha S., Madhukar A., Kaviani K. and Kapre R., J.Vac.Sci.Technol. B8 (1990)149.

Haider N., Wilby M.R. and Vvedensky D.D., Appl. Phys. Lett. 62 (1993) 3108.

Harris J.J.and Joyce B.A., Surf. Sci. 103 (1981) L90.

Hasegawa Y., Egawa T., Jimbo T. and Umeno M., Jpn. J. Appl. Phys. 32 (1993) L997.

Hata M., Isu T., Watanabe A. and Katayama Y., J.Vac.Sci.Technol. B8 (1990) 692.

Hata M., Isu T., Watanabe A. and Katayama Y., Appl.Phys.Lett. 56 (1990) 2542.

Hata M., Isu T., Watanabe A., Kajikawa Y. and Katayama Y., J. Crystal Growth 114 (1991) 203.

Hata M., Watanabe A. and Isu T., J. Crystal Growth 111 (1991) 83.

Hayakawa T., Morishima M. Nagai M., Horie H. and Matsumoto K., Appl.Phys.Lett. 59 (1991) 2415.

Hayakawa T., Morishima M. and Chen S., Appl.Phys.Lett. 59 (1991) 3321.

Hersee S.D., Barbier E. and Blondean R., J. Crystal Growth 77 (1986) 310.

Hoenk M.E., Chen H.Z., Yariv A., Morkoc H. and Vahala K.J., Appl. Phys. Lett. 54 (1989) 1347.

Hoenk M.E., Nieh C.W., Chen H.Z. and Vahala K.J., Appl.Phys.Lett. 55 (1989)53.

Horikoshi Y., Yamaguchi H. and Kawashima M., Jpn. J. Appl. Phys. 28 (1989) 1307.

Ichikawa M. and Hayakawa K., Jpn. J. Appl. Phys. 21 (1982) 145.

Ichikawa M., Ohkura M. and Hayakawa K., Jpn. J. Appl. Phys. 21 (1982) 154.

Ichikawa M. and Hayakawa K., Jpn. J. Appl. Phys. 22 (1983) 527.

Ichikawa M., Doi T., Ichihashi M. and Hayakawa K., Jpn. J. Appl. Phys. 23 (1984) 913.

Inoue N., J. Crystal Growth 111 (1991) 75.

Inoue N., Tanimoto M., Kanisawa K., Hirono S., Osaka J. and Honma Y., J. Crystal Growth 127 (1993) 956.

Ismail K., Burkhardt M., Smith H.I., Karam N.H. and Sekula-Moise P.A., Appl. Phys. Lett. 58 (1991) 1539.

Isu T., Watanabe A., Hata M. and Katayama Y., Jpn. J. Appl. Phys. 27 (1988) L2259.

Isu T., Hata M., Watanabe A. and Katayama Y., J. Vac. Sci. Technol. B7 (1989) 714.

Isu T., Hata M. and Watanabe A., J. Crystal Growth 111 (1991) 210.

Isu T., Hata M., Morishita Y., Nomura Y., Goto S. and Katayama Y., J. Crystal Growth 120 (1992) 45.

Jones S.H., Seidel L.K., Lau K.M. and Harold M., J. Crystal Growth 108 (1991) 73.

Kane E.O., J. Phys. Chem. Solids, 1, 82 (1956) 249 .

Kapon E., Tamargo M.C. and Hwang D.M., Appl. Phys. Lett. 50 (1987) 347.

Kapon E., Harbison J.P., Yun C.P. and Stoffel N.G., Appl.Phys.Lett. 52 (1988) 607.

Kapon E., Hwang D.M. and Bhat R., Phys. Rev. Lett. 63 (1989) 430 .

Kapon E., Harbison J.P., Yun C.P. and Florez L.T., Appl.Phys.Lett. 54 (1989) 304.

Kapon E., Kash K., Clausen E.M., Jr., Hwang D.M. and Colas E., Appl.Phys.Lett. 60 (1992) 477.

Karam N.H., Mastrovito A., Haven V., Ismail K. and Smith H.I., J. Crystal Growth 107 (1991) 591.

Karpov S.Y., Myachin V.E. and Pogorelsky Y.V., to be published in J. Crystal Growth.

Kojima N., Mitsunaga K. and Kyuma K., Appl. Phys. Lett. 56 (1990) 154.

Komori K., Hamano A., Arai S., Miyamoto Y. and Suematsu Y., Jpn. J. Appl. Phys. 31 (1992) L535.

Kono T., Tsukamoto S., Nagamune Y., Sogawa F., Nishioka M. and Arakawa Y., Appl.Phys.Lett. 64 (1994) 1564.

Koshiba S., Nakamura Y., Noda T. and Sakaki H., Proc. 3rd Top. Meet. Crystal Growth Mechanism, Tokyo, 1992 p.233.

Koshiba S., Noge H., Ichinose H., Akiyama H., Nakamura Y., Inoshita T., Someya T., Wada K., Shimizu A., Nagamune Y., Tsuchiya M., Kano H. and Sakaki H., Solid-State Electronics 37 (1994) 729.

Koshiba S., Noge H., Akiyama H., Inoshita T., Nakamura Y., Shimizu A., Nagamune Y., Tsuchiya M., Kano H. and Sakaki H., Appl. Phys. Lett. 64 (1994) 363.

Lee M., Kim Y., Kim M., Kim S., Min S., Kim Y.D. and Nahm S., Appl. Phys. Lett. 63 (1993) 3025.

Liu D. and Lee C., Appl. Phys. Lett. 63 (1993) 3503.

Lopez M., Ishikawa T., Matsuyama I., Tanaka N. and Nomura Y., Solid-State Electronics 37 (1994) 563.

Lopez M., Ishikawa T. and Nomura Y., Jpn. J. Appl. Phys. 32 (1993) L1051.

Karam N.H., Mastrovito A., Haven V., Ismail K.P. and Smich H.I., J. Crystal Growth 107 (1991) 591.

McInlyre C.R. and Sham L.J., Phys. Rev. B 45 (1992) 9443.

Meier H.P., VanGieson E., Walter W., Harder C., Krahl M. and Bimberg D., Appl.Phys.Lett. 54, (1989) 433.

Meier H.P., Van Gieson E., Epperlein P.W., Harder C. and Walter W., J. Crystal Growth 95 (1989) 66.

Mirin R.P., Tau I.H., Weman H., Leonard M., Yasuda T., Bowers J.E. and Hu E.L., J. Vac. Sci. Technol. A10 (1992) 697.

Murray R., Roberts C., Woodbridge K., Barnes P., Parry G. and Norman C., Appl. Phys. Lett. 62 (1993) 2929.

Nagamune Y., Arakawa Y., Tsukamoto S., Nishioka M., Sakaki H. and Miura N., Phys. Rev. Lett. 69 (1992) 2963 .

Nagata S., Tanaka T. and Fukai M., Appl. Phys. Lett. 30 (1977) 505.

Nagata S. and Tanaka T., J. Appl. Phys. 48 (1977) 940.

Nakamura Y., Koshiba S., Tsuchiya M., Kano H. and Sakaki H., Appl. Phys. Lett. 59 (1991) 700.

Nakamura Y., Tsuchiya M., Motohisa J., Noge H., Koshiba S., and Sakaki H., Solid-State Electronics 37 (1994) 571.

Neave J.H. , Dobson P.J. , Joyce B.H. and Zhang J., Appl. Phys. Lett. 47 (1985) 100.

Nilsson S., Van Gieson E., Arent D.J., Meier H.P., Walter W. and Forster T., Appl.Phys.Lett. 55 (1989) 972.

Nishinaga T. and Suzuki T. J. Crystal Growth 115 (1991) 398.

Nishinaga T. and Cho K. Jpn. J. Appl. Phys. 27 (1988) L12.

Nomura Y., Morishita Y., Goto S., Katayama Y. and Isu T. Appl. Phys. Lett. 64 (1994) 1123.

Ohno T., Shiraishi K. and Ito T., Materials Research Society Symposium Proceedings Vol. 326 (Materials Research Society, Pittsburgh, 1994) p 27.

Ohtsuka M. and Miyazawa S., J.Appl.Phys. 64 (1988) 3522.

Ohtsuka M. and Suzuki A., J. Crystal Growth 95 (1989) 55.

Osaka J., Inoue N., Mada Y., Yamada K. and Wada K., J. Crystal Growth 99 (1990) 120.

Ozdemir M. and Zangwill A., J. Vac. Sci. Technol. A10 (1992) 684.

Pratt A.R., Williams R.L., Norman C.E., Fahy M.R., Marinopoulou A. and Chatenoud F., Appl. Phys. Lett. 65 (1994) 1009.

Rajkumar K.C., Madhukar A., Rammohan K., Rich D.H., Chen P. and Chen L., Appl. Phys. Lett. 63 (1993) 2905.

Ratsch C. and Zangwill A., Appl. Phys. Lett. 58 (1991) 403.

Saito H., Sugimoto M., Anan M. and Ochiai Y., Jpn. J. Appl. Phys. 32 (1993) L1034.

Saito H., Uwai K. and Kobayashi N., Jpn. J. Appl. Phys. 32 (1993) 4440.

Sakaki H., Jpn. J. Appl. Phys. 19 (1980) L735 .

Sakaki H., Surface Science 267 (1992) 623.

Schmitt-Rink S., Miller D.A.B. and Chemla D.S., Phys. Rev. B 35, 8113 (1987).

Shimomura S., Okamoto Y., Takeuchi M., Tamaoka E., Yuba Y., Namba S., Hiyamizu S., Shigeta M., Yamamoto T. and Kobayashi K., J. Crystal Growth 111 (1991) 1105.

Shimomura S., Wakejima A., Adachi A., Okamoto Y., Sano N., Murase K. and Hiyamizu S., Jpn. J. Appl. Phys. 32 (1993) L1728.

Shimomura S., Inoue K., Tanaka M., Tomita N., Adachi A., Fujii M., Yamamoto T., Watanabe T., Sano N., Murase K. and Hiyamizu S., Solid-State Electronics 37 (1994) 597.

Simhony S., Kapon E., Colas E., Hwang D.M. and Stoffel N.G., Appl. Phys. Lett. 59 (1991)2225

Smith J.S., Derry P.L., Margalit S. and Yariv A., Appl.Phys.Lett. 47 (1985) 712.

Sugaya T., Kaneko M., Okada Y. and Kawabe M., Jpn. J. Appl. Phys. 32 (1993) L1834 .

Suzuki T. and Nishinaga T., J. Crystal Growth 142 (1994) 49.

Suzuki T. and Nishinaga T., J. Crystal Growth 142 (1994) 61.

Takebe T., Fujii M., Yamamoto T., Fujita K. and Kobayashi K., J. Crystal Growth 127 (1993) 937.

Tanaka M. and Sakaki H., Appl. Phys. Lett. 54 (1989)1326.

Tanaka M., Motohisa J. and Sakaki H., Surface Scince 228 (1990) 408.

Tanaka T., Yamauchi T., Schulman J.N. and Arakawa Y., Jpn. J. Appl. Phys. 32 (1993) L1592.

Tokura Y. Saito H. and Fukui T., J. Crystal Growth 94 (1989) 46.

Tsukamoto S., Nagamune Y., Nishioka M. and Arakawa Y., J. Appl. Phys. 71 (1992) 533.

Tsukamoto S., Nagamune Y., Nishioka M. and Arakawa Y., Appl. Phys. Lett. 62 (1993) 49.

Tsukamoto S., Nagamune Y., Nishioka M. and Arakawa Y., Appl. Phys. Lett. 63 (1993)355 .

Turco F.S., Simhony S., Kash K., Hwang D.M., Ravi T.S., Kapon E. and Tamargo M.C., J.Cryst.Growth 104 (1990) 766.

Usami N., Mine T., Fukatsu S. and Shiraki Y., Solid-State Electronics 37 (1994) 539.

Walther M., Kapon E., Christen J., Hwang D.M. and Bhat R., Appl. Phys. Lett. 60 (1992) 521.

Watson G.P., Ast D.G., Anderson T.J. and Hayakawa Y., Appl. Phys. Lett. 58 (1991) 2517.

Wood C.E.C., Surf. Sci. 108 (1981) L441.

Yamada K., Inoue N., Osaka J. and Wada K., Appl. Phys. Lett. 55 (1989) 622.

Yang K., Schowalter L.J. and Thundat T., Appl. Phys. Lett. 64 (1994) 1641.

Publication Lists

Papers related to this thesis

[1] X.Q. Shen, M. Tanaka and T. Nishinaga, Proceedings of the 10th Record of Alloy Semiconductor Physics and Electronics Symposium, Nagoya, Japan, (1991) 65-72.

[2] X.Q. Shen, M. Tanaka and T. Nishinaga, Proceedings of the 11th Record of Alloy Semiconductor Physics and Electronics Symposium, Kyoto, Japan, (1992) 333-340.

[3] X.Q. Shen, M. Tanaka and T. Nishinaga, Proceedings of the 12th Record of Alloy Semiconductor Physics and Electronics Symposium, Izunagaoka, Japan, (1993) 367-372.

[4] X.Q. Shen and T. Nishinaga, Jpn. J. Appl. Phys. 32 (1993) L1117-L1119.

[5] X.Q. Shen, M. Tanaka and T. Nishinaga, J. Crystal Growth 127 (1993) 932-936.

[6] X.Q. Shen, M. Tanaka, K. Wada and T. Nishinaga, J. Crystal Growth. 135 (1994) 85-96.

[7] X.Q. Shen, D. Kishimoto and T. Nishinaga, Jpn. J. Appl. Phys. 33, (1994) 11-17.

[8] X.Q. Shen and T. Nishinaga, to be published in J. Crystal Growth.

[9] T.Nishinaga and X.Q. Shen, to be published in Appl. Surface Science.

[10] T.Nishinaga and X.Q. Shen, Journal of the Jpn. Association of Crystal Growth, Vol.21 No,1 (1994) 3-10. in Japanese

[11] X.Q. Shen, H.J. Chen, M. Tanaka and T. Nishinaga, Submitted to Appl. Phys. Lett.

[12] X.Q. Shen, D. Kishimoto and T. Nishinaga, Submitted to Jpn. J. Appl. Phys.

International conferences

Presentation related to this thesis

[1] X.Q. Shen, M. Tanaka and T. Nishinaga, 7th International Conference of MBE, 1992, Germany.

[2] T.Nishinaga and X.Q. Shen, 3rd International Symposium on Atomic Layer Epitaxy and Related Surface Processes. 1994, Japan.

[3] X.Q. Shen and T. Nishinaga, 8th International Conference on Vapor Growth and Epitaxy. 1994, Germany.